On the Role of Sensory Cancellation and Corollary Discharge in Neural Coding and Behavior

Armen Enikolopov

Submitted in partial fulfillment of the
requirements for the degree of
Doctor of Philosophy
in the Graduate School of Arts and Sciences

COLUMBIA UNIVERSITY

2018

ABSTRACT

On the Role of Sensory Cancellation and Corollary Discharge in Neural Coding and Behavior

Armen Enikolopov

Studies of cerebellum-like circuits in fish have demonstrated that synaptic plasticity shapes the motor corollary discharge responses of granule cells into highly-specific predictions of self-generated sensory input. However, the functional significance of such predictions, known as negative images, has not been directly tested. Here we provide evidence for improvements in neural coding and behavioral detection of prey-like stimuli due to negative images. In addition, we find that manipulating synaptic plasticity leads to specific changes in circuit output that disrupt neural coding and detection of prey-like stimuli. These results link synaptic plasticity, neural coding, and behavior and also provide a circuit-level account of how combining external sensory input with internally-generated predictions enhances sensory processing. In addition, the mammalian dorsal cochlear nucleus (DCN) integrates auditory nerve input with a diverse array of sensory and motor signals processed within circuity similar to the cerebellum. Yet how the DCN contributes to early auditory processing has been a longstanding puzzle. Using electrophysiological recordings in mice during licking behavior we show that DCN neurons are largely unaffected by self-generated sounds while remaining sensitive to external acoustic stimuli. Recordings in deafened mice, together with neural activity manipulations, indicate that self-generated sounds are cancelled by non-auditory signals conveyed by mossy fibers. In addition, DCN neurons exhibit gradual reductions in their responses to acoustic stimuli that are temporally correlated with licking. Together, these findings suggest that DCN may act as an adaptive filter for cancelling self-generated sounds. Adaptive filtering has been established

previously for cerebellum-like sensory structures in fish suggesting a conserved function for such structures across vertebrates.

Table of Contents

List of Figures

Acknowledgements

As in any significant undertaking, the work described in this dissertation is a product of the help and support granted me by many people.

Firstly, I owe more than words can express to my advisor Nate Sawtell, who has with patient eye and word supported me through my time in his lab. He took a chance when I joined his laboratory in 2012, and I am forever in his debt for that. Through these years his role as a mentor, advisor, and colleague has done much to shape not only the work here but myself.

Next, my thanks to Stuart Firestein, mentor and advisor before I joined the Sawtell Lab. My thanks as well to Larry Abbott, for thoughtful support as a coauthor in the conduction of the experimental work described herein.

Jointly, my thanks to my thesis committee, Larry Abbott, Dima Rinberg, Stuart Firestein, and Andres Bendesky. Vince Ferrera and Jian Yang were insightful and helpful as earlier members of the committee.

My thanks to Alex Koulakov, who bravely first introduced me to thinking about the mind and the brain and has continued to be a mentor and friend.

My thanks to Ron Prywes, John Hunt, and Sarah Kim Fein of the Biology department.

The motley bunch that has made up the Sawtell lab over the years I've been there has made the time there exciting. In particular the fellow grad students there when I first settled in 5th-floor-Hammer. Tim Requarth, through whom I first heard about weakly electric fish, and in whose apartment I first heard the tick-tick-tick of its amplified EOD. Karina Scalise, with whom I sat back to back for years and could always rely on for thoughtfulness and intellectual incisiveness, and Shobhit Singla, with whom I worked directly for two years thinking about auditory function, and beyond that when I moved to working on the mormyrid. And my thanks

go out to the other Sawtellites who joined the lab after my time, Kathryn Birchenbach, Abby Zedina, and perky Krista Perks. A special thanks to Rick Warren, who was inexplicably always willing to discuss my plans for building one Rube Goldbergian device or another, and Conor Dempsey, scientist and potter.

Members of the Firestein Lab, Jesse Brann, Xiaohong Huang, Tanner Mullen, Zita Peterlin, Shari Saideman, Dong-jing Zou, and Matt Valley, were all formative for my early thinking about neuroscience.

Anna Sarfaty, Rachel Rampil, and Nadine Piazza, lab managers over the years, allowed any of this work to actually get done. Thanks also to Alison Lowell, friend first, lab manager second.

Ella Batty was instrumental in thinking about behavior in mormyrid, and Melina Tsitsiklis performed early pilot work in that system.

My deepest thanks to friends and colleagues that have supported me intellectually and psychologically: Rebecca Brachmann Brian Depasquale, Piotr Evdokimov, Andrew Fink, Tim Machado, Mariano Gabitto and Cristina Fernandez, Irina Khokhlova, Amy Norovich, Pia O'Neill, David Pfau and the David Pfau Society, Nora Pyenson Carl Schoonover Ilya Schnitser.

Thank you to my brother Grisha, my sister Marina, my brother-in-law Greg, Nina and Sonia, both younger than this dissertation, and my mother and father, Natalia and Grigori, without whose support it is an understatement to say that none of this would be possible. Finally, thanks to my grandparents, the memory of whose own lives and work were in many ways my inspiration.

Chapter 1

Introduction

Historical motivations and background

As I sit to write the first sentence of this manuscript, I stare out at the water of Cold Spring Harbor. Some hundred feet out, a gull beats its wings and with measured pace flies across the field of my vision. My gaze is fixed, looking forward, but finally my eyes snap to attention and point directly at the bird. No difference in its motion is apparent to me through these two phases of my observation, yet a gulf exists between what I perceive and what my eyes detect. Not only the bird, but the world as well, flies across my retinas as my eyes saccade at five hundred degrees per second. As photoreceptors are concerned, the movement of the bird and movement of the world are indistinguishable. Yet the perception of the gull's movement is not perturbed, and the harbor beyond remains fixed in space.

The body in motion is its own enemy in this regard. Movement generates sensory input that, from the perspective of sensory receptors, is often indistinguishable from sensation caused by the outside world. Cancellation of the sensory consequences of an animal's own movement is thought to be an important and early responsibility of all sensory processing systems. Motion seen in the outside world must be distinguished from apparent movement imposed by movement of the eyes, the head, and the rest of the body. The smells and taste of one's own body must be ignored to pay attention to the world beyond. Mechanosensation generated through active touch must be distinguished from the body being touched, and reflexes triggered by touch must not be reactivated in turn by the reflexive motion. The sound of one's diaphragm moving and the lungs expanding as one takes in a breath, the pounding of blood shuttling through atria and ventricles, valves and arteries, the sounds of mandibular joints chewing and teeth grinding, tongues and lips licking, all of these must be filtered out, seen beyond, and these predictable inputs must be ignored in favor of the sensory novelty of the world outside. How might the distinction be

made? In principle, it should be possible – after all, the brain has access to both the sensory input and information about the motor act that generated it.

Human attention has been turned to these matters for thousands of years and constitutes some of the earliest written introspection about brain function. It's noteworthy that the first theories of vision were efference-driven. The pre-Socratic Alcamaeon of Croton (ca. 450 BCE) noted the spots of light and color, phosphenes, that result from a blow to the head and took them as evidence of an internal fire that resides in the eye (Celesia, 2012; Gross, 1999). This and the light seen in the eyes of some animals when observed in the dark, now known to be reflection from the tapetum lucidum present in the eyes of some (particularly nocturnal) animals, were the foundational evidence of the emission theory of vision. First proposed by Empedocles of Akragas (ca. 5th century BCE) and refined by others such as Plato, emission theory held that the eye is like a lantern, emitting an internal fire that leaves the eye to perform the task of seeing (Grüsser, 1995). Euclid in his *Optics* registered a complaint, noting that the distant stars were evident to us immediately on opening the eyes, without the delay necessary for the eye's fire to travel, as implied by theory. Though the early theorists were mistaken in some of the finer details, the idea of sensation resulting from self-generated motion can be thought of as forward-thinking, and is line with the subject of this thesis.

Aristotle observed the persistence of afterimages when looking at the sun and at rushing water and noted their movement relative to the static visual scene when the eyes were shifted (or as we now understand, the movement of the visual scene relative to the retinally-static afterimages) (Aristotle, 330 BCE). These observations were to continue to be the foundation of thought about sensory cancellation (though not recognized in that name) for some two thousand years. Descartes noted that these afterimages did not move when the eye was pressed in

darkness, yet shifted during active eye movement. The same procedures performed on natural images yielded the reverse – the visual scene remained static with active eye movements but moved when the eye was pressed.

In the 19th century, Hermann von Helmholtz noted the same. How could one distinguish between movement of the world and movement of one's retina? Between an eye moved voluntarily, where the world appears stable, and an eye moved involuntarily such as an eye pressed by another person, where the world appears unstable, the only difference is that of intention. Helmholtz considered the third case – what happened when there was intention but no movement. He reflected on the contemporary findings of Albrech von Graefe in patients with paralysis of the external rectus muscle of the eye. When these patients attempted to move an eye to the left, while their paralyzed eye remained still, their perceived vision jumped in the direction of the intended motion. Helmholtz deduced that a copy of the signal used to move the eye must be used to construct a prediction of the movement's sensory consequences, and the visual representation adjusted accordingly (von Helmholtz, 1925; Jeannerod, 1985; Grüsser, 1995).

The preceding history lesson is included because by the mid-20th century, Sherringtonian reflex theory held sway; motion as a response to sensation, rather than sensation as a response to motion, was at the center of thinking about how the brain functions. Sherrington summarized the views of Helmholtz (and others such as Bain, Lewes, and Mach, who supported similar ideas) as proposing "that during movement, e.g., a willed movement, the outgoing current of impulses from brain to muscle is accompanied by a 'sensation of innervation.' Where a movement is to be precise, we do become aware, in fact, acutely aware immediately in advance of the amount and direction it is to assume." Remarkably, Sherrington argued vociferously against this prescient view, hinting as it does towards corollary discharge and reafferent cancellation, predictive

coding, and forward models, ultimately concluding that it "remains unproven" (Sherrington, 1900; Matthews, 1982).

It was in this historical context that Erich von Holst and Horst Mittelstaedt performed a series of experiments investigating the optomotor reflex in the hoverfly *Eristaltis* (von Holst and Mittelstaedt, 1950). In response to a rotating environment, a stationary fly will itself begin to turn. The reflex is a stabilizing one, accounting for environmental perturbations such as wind that act on the animal. The authors questioned why the same reflex was not elicited during voluntary rotation in a stationary environment, where the movement of the environment across the retina was identical to that in the former case. In *Eristalsis*, it is possible to rotate the head by 180 degrees about its neck, which effectively inverts left-right motion. In this preparation, clockwise rotation of the environment produces retinal image movement that would normally result from rotation in the opposite direction. It was found that under these conditions, rotation of the environment initiates a continuous turning responses. Von Holst and Mittelstaedt interpreted this to mean that a copy of the motor signal used to initiate turning was routed to a sensory area and used to subtract the predicted self-generated sensory results of the voluntary motion from perceived motion (**Figure 1.1**). Inverting, or negating, the visual effects of motion meant that subtracting this prediction now yielded a sensory effect of twice the real amplitude rather than being cancelled, and initiated a kind of positive feedback loop, resulting in the turning behavior. They called this copied signal an efference copy, and lay the framework for our current thinking about the cancellation of self-generated sensory signals: in order to separate sensory information resulting from changes in the external world, "exafference," from self-generated sensory signals, "reafference," an efference copy was sent from motor to sensory areas and used to subtract reafference from the total sensory stream, leaving only exafference. The

authors expanded their work to centipedes and fish and presented a theoretical accounting for birds and mammals (von Holst and Mittelstaedt, 1950; von Holst, 1954).

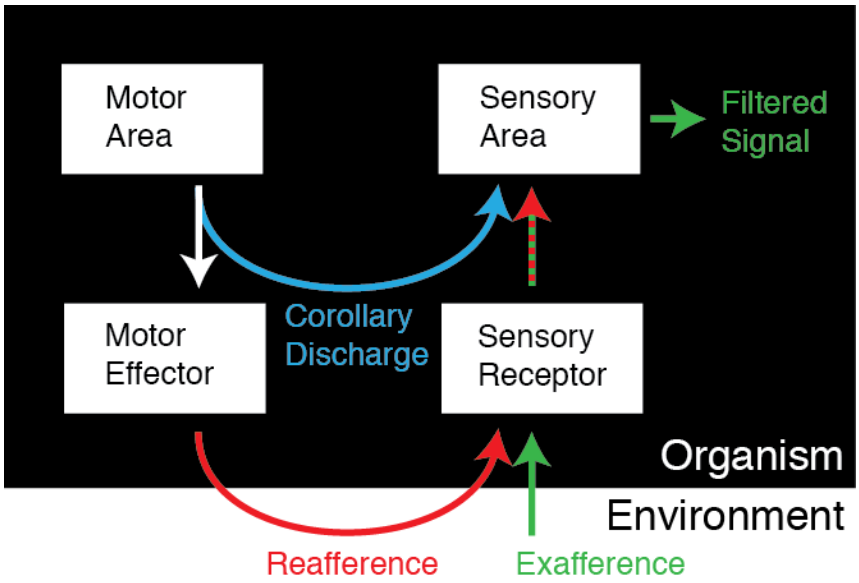

Figure 1.1 Schematic of reafference principal.
Motor areas generate motor commands that are sent to motor effectors such as muscles. Movement of those effectors generates sensory input (reafference) at sensory receptors which corrupts sensory information about the outside world (exafference). As a result, a signal containing both reafferent and exafferent input is sent to sensory processing areas. A copy of the original motor signal (corollary discharge, also called efference copy) is sent from the motor area to sensory processing areas, where it is subtracted from sensory input to yield a filtered signal devoid of reafference.

Contemporaneously, and in linguistic isolation from von Holst and Mittelstaedt, who had published in German, Roger Sperry developed a similar theory from his treatment of the analogous optomotor reflex in fish (Sperry, 1950). He showed that occluding one eye and inverting the other similarly resulted in a forced turning behavior. Lesioning the optic lobe removed the effect, which Sperry interpreted as evidence for a feedback on an upper motor signal to the visual system. He termed the signal a "corollary discharge" (CD). Despite minor

differences in conceptual implementation, the term is typically treated as synonymous with "efference copy" and will be used as such in the text to follow.

The ensuing decades have confirmed many of the predictions of von Holst, Mittelstaedt, and Sperry. Efferent feedback, or CD, has been found to be involved in many aspects of neural processing. Though they will mostly be discussed here with regard to their role in modifying, cancelling, or reinterpreting reafference, CD mechanisms also serve to pattern and sequence motor acts, as in the *Xenopus* case discussed below (Sillar and Roberts, 1988; Li et al., 2002), or ventral spinocerebellar activity which has been shown to be modulated during fictive locomotion, helping coordinate descending and spinal motor commands (Arshavsky et al., 1972, 1983; Lundberg, 1971), or recent work on skilled reaching (Azim et al., 2014). Additionally, CD has been shown to serve as a replacement for, or alternative to proprioceptive signals. In this case, CD has the benefit of being fast, occurring before the actual motor act, but suffers in that it provides information about the intended act, not the actual one, and ultimately relies on the fidelity of execution of the motor task by external effectors (Bell, 1989). For example, eye position may accurately be deduced from CD of input to the oculomotor system (Guthrie et al., 1983). More broadly, and combining the above, CD has been suggested, in theoretical accounts termed forward models, to play a role in ensuring accurate and timely movement despite delayed and noisy proprioceptive feedback (Miall and Wolpert, 1996; Shadmehr et al., 2010).

From the perspective of information theory, the information present in a signal is inversely proportional to its predictability. The extreme case of a totally predictable signal contains no information at all (Shannon, 1948; Shannon and Weaver, 1949). Many of the responsibilities of sensory systems can be viewed from the perspective of their role as generators of predictions about sensory input and the removal of those expectations from sensory inflow so

as to increase the sensory stream's information density (Barlow, 1990; Bullock, 1988; Bell et al., 1997a). Mechanisms of sensory prediction and cancellation have been studied in many systems, and these range from simple gating mechanisms that silence sensation during motion to the class of systems in which they have been studied in perhaps the closest detail, a class of circuits termed 'cerebellum-like'. This circuit architecture has been found across a wide range of taxa in neural structures involved in sensory processing.

In particular, over the last forty years, the cerebellum-like electrosensory lateral line lobe (ELL) of the mormyrid fish has yielded evidence from *in vivo*, *in vitro*, and modelling studies for the formation of a 'negative image' of predicted sensory input in a modifiable CD. The system in question suffers from a disruptive but predictable reafference. This negative image of the expected sensory response is summed with the actual response in principal cells of the circuit to produce a signal from which the confounding effects of reafference have been subtracted.

In the following section, I will present some examples of sensory cancellation mediated by CD, as well as some other roles for CD, specifically in systems other than those implementing cerebellum-like circuits. Following, I will discuss the general architecture of cerebellum-like circuits, their specific implementation in the mormyrid ELL, as well as in an analogous structure in the mammalian auditory system, the dorsal cochlear nucleus (DCN). In Chapter 2, the main focus of this dissertation and my doctoral research, I present evidence for the functional significance of negative images at both the neural coding and behavioral levels, neither of which has heretofore demonstrated. Chapter 3 presents work done in collaboration with others in the Sawtell laboratory that demonstrates that the DCN cancels self-generated sound. Finally, in Chapter 4, I will present concluding remarks and discuss avenues for further research.

Corollary Discharge and Cancellation in Reflexes

Reafferent input impinges on the ability of the central nervous system to process information about the outside world, and the problem exists in nearly all sensory systems. In order to optimize sensitivity, reliability, and precision, many systems take advantage of CD mechanisms, routing signals about motor actions to sensory processing areas, to cancel or modify such input. The function of CD across these systems varies. Some CD mechanisms act mainly at the periphery, generally targeting sensory receptors and serving to gate sensory input on and off in time with motion. Such systems are ubiquitous and are necessary in nearly all sensory systems to regulate sensory inflow and serve to generate transient inhibition of sensory networks (Crapse and Sommer, 2008a). CD mechanisms found in invertebrates are of this type, sometimes termed lower order CD, though they exist in vertebrates as well. Such examples will be considered in crayfish, frog, and cricket. *Drosophila* visuomotor coordination displays a related type of CD. Similar suppressive mechanisms can be found vertebrates, as demonstrated in work on mouse and primate auditory cortex and in primate saccadic suppression. Deficits in such systems have been linked to schizophrenia. Higher order CD engages more central processing areas and performs more nuanced computations, facilitating the contextual interpretation of sensory input, constructing stable internal representations of sensory input, and making more temporally-complex predictions about sensory reafference. Below, some examples other than those instantiated in cerebellum-like circuits are discussed.

Like many organisms, the crayfish *Procamarus clarkii* employs a mechanosensitive hair cell system in detecting the presence of prey and approaching predators. Mechanosensitive hair cells on its tail and appendages of its abdomen elicit a reflex termed the "tail-flip response" on sensing water current disturbances caused by potential predators (Edwards et al., 1999). This tail

flip propels the animal away from said predator. However, he rapid movement itself has the possibility of reactivating the same mechanosensitive hairs. This is problematic for the crayfish because mechanosensory afferents and interneurons desensitize through repeated stimulation, so responsiveness to self-generated water flow would desensitize the system to predator-generated water flow. Moreover, the tail flip reflex stands the chance of repetitive self-activating in a positive feedback loop.

The crayfish is able to maintain the sensitivity of this reflex though a CD mechanism. A class of corollary discharge interneurons (CDIs), the primary afferent depolarizing interneurons (PADIs), target mechanosensory afferent terminals and inhibits them in time with tail-flips. The mechanosenory pathway elicits tail-flip commands from motor neurons called giant escape command neurons, and these neurons send a corollary discharge to, and drive activity in, the PADIs (Kirk and Wine, 1984; Krasne and Bryan, 1973). A use of CD with remarkable functional similarity exists in the cockroach, where locomotion-associated CD mediates a hair-cell based escape response (Delcomyn, 1977).

A similar example of sensory gating via corollary discharge exists in vertebrates. In its larval tadpole stage, *Xenopous laevis* possesses a predator avoidance reflex that generates swimming locomotion away from the direction of a mechanosensory stimulus. Again, swimming itself generates a mechanosensory stimulus via water flow, and this reafference interferes with sensory tasks broadly, and more specifically, causes reactivation of the reflex. An identified population of interneurons termed the ascending interneurons has been shown to fire rhythmically during swimming, and to make glycinergic synapses onto interneurons of the mechanosensory pathway and elicit IPSPs. These ascending interneurons are driven by a motor central pattern generator (CPG), that is, a corollary discharge. In addition to modulating sensory

input, they also have a role in modulating the patterning of reflexive swimming itself (Sillar and Roberts, 1988; Li et al., 2002). Analogous phase-dependent gating of sensory input in reflexes exists in humans, such as in modulation of the reflexes of the ankle flexor and extensors during walking. (Duysens et al., 1990)

A particularly clear example is found in the cricket. The male Mediterranean field cricket *Gryllus bimaculatus* produces courtship calls by means of a set of rasp-like hooks on the outer edges of its forewings which are rubbed against each other in a process called stridulation. These rasps are located <10mm from the acoustic sensory organs of the cricket, and the resultant calls, which can continue for hours, exceed 100dB in volume. Externally generated and presented acoustic stimuli of this amplitude sharply desensitize auditory interneurons in the cricket (Poulet and Hedwig, 2003) but behavioral work shows that crickets can maintain auditory sensitivity (that is, detect the calls of conspecifics) when the call is generated by their own stridulations, rather than presented externally (Heiligenberg, 1969). How are crickets able to prevent being deafened when, and only when, they are the ones producing the sound? The problem is solved in this system by a single class of CDIs which make inhibitory connections onto both primary auditory afferents and auditory interneurons (Poulet and Hedwig, 2006). Critically, these CDIs inhibit the auditory system in time with the cricket's stridulations because they receive a signal from a mesothoracic CPG that is a relayed copy of the activation signal sent to the very motor neurons controlling wing rasp stridulations. Notably, the extent of inhibition is not affected by the amplitude of the call, which is to say that the mechanism simply gates the sensory system, effectively deafening the animal for the brief period of its call, but thereby ensuring continued sensitivity of the auditory system.

Recent work by the Maimon lab has focused on a role for corollary discharge in visuomotor processing in *Drosophila*. Reflexive visuomotor coordination, flight-, and gaze-stabilization in the fly has been considered in this context since von Holst and Mittelstaedt (von Holst and Mittelstaedt, 1950) (*Eristalis* is a hoverfly and performs particularly impressive feats of flight command and stabilization as it hovers during feeding). Flight in Drosophila consists of rapid and volitional turns of the body, termed body saccades, interleaved with periods of stable flight. During these periods of stable flight, the optokinetic reflex, or the optomotor response, corrects flight trajectory disturbances such as those caused by local air currents or injury, and repositions the head to maintain a stable visual field. Wide-field visual motion (that is, movement of the entire visual scene as opposed to specific elements of that scene) in a given direction elicits a corrective and compensatory motor response, so leftward rotation of the visual scene is followed by a motor response that "recenters" the animal by rotating it leftward, maintaining a consistent visual center. However, body saccades also cause wide-field visual motion, and the optokinetic reflex clearly needs to be disengaged by some means during volitional motion, or the animal would never get anywhere, trapped in a perpetual positive-feedback loop. Maimon et al have identified three classes of optic flow processing neurons (HSN and VS, which respond to optic flow in the yaw and pitch axes, respectively, as well as visual processing interneurons further upstream) that receive motor-related, putatively CD, inputs during these body saccades. HSN and VS neurons in particular are shown to mediate aspects of the optomotor response. Whole-cell patch clamp recordings show that these inputs are sufficient in timing and are of the correct sign and amplitude to cancel out reafferent visual input during body saccades. Moreover, while optic flow can exist in any of three axes, voluntary saccades mainly generate optic flow in the yaw axis. Fittingly, further work (Kim et al., 2017)

shows that the extent of saccade-related membrane polarization or depolarization in these cells correlates with the extent of their visual responsiveness to yaw. This implies, and the authors go on to show, that these neurons are able to encode multiple channels of exafferent input while selectively cancelling out reafference in one of them. This is particularly concordant with von Hostl and Mittlestaedt's formulation of the reafference principle (von Holst and Mittelstaedt, 1950) in that it does not blind (literally in this case) the sensory input entirely. Rather than operating like the gating mechanisms of the cricket auditory system or locust visual motion detection discussed above, the mechanism subtracts reafference while keeping exafferent input.

Higher order Corollary Discharge and Cancellation

Corollary discharge mechanisms have long been assumed, and more recently demonstrated, to play a role in mammalian auditory processing as well. The anatomical existence of motor inputs into auditory cortex has been reported for decades (Reep et al., 1987; Budinger and Scheich, 2009; Nelson et al., 2013). Earlier work in humans had implicated corollary discharge in perceiving self -generated speech (Creutzfeldt et al., 1989). In these experiments, extracellular single-unit recordings in the middle and superior temporal gyri showed that neurons which responded to speech presented through a speaker had weaker responses, or none at all, to speech generated by the patient himself. This was in line with earlier work in monkeys which had shown differential responses to self- and other-generated vocalizations in the superior temporal gyrus (Müller-Preuss and Ploog, 1981). Following those findings, it has been proposed that deficits in corollary discharge systems might underlie some of the positive symptoms of schizophrenia - most strikingly, auditory hallucinations (Feinberg, 1978). If, on hearing speech produced by oneself, no signal exists by which to recognize that the

sound just heard was self-generated, it might incorrectly be ascribed to an outside agent. That could be true of vocalized speech as well as subvocal, internal speech, or thought, which has been shown to be correlated to activity in motor cortical areas. This would explain not only the false perception of voices, but also feelings that the hallucinated voice has access to the hallucinator's thoughts – because, after all, it does.

To this end, a series of electroencephalography experiments (Ford et al., 2001a) looked at the N1 component of event-related potentials during listening and speaking tasks in healthy and schizophrenic subjects. Whereas healthy patients showed a smaller amplitude N1 during speaking than during listening, schizophrenic patients showed no difference (**Figure 1.2**) (it should be added that for schizophrenic patients, the amplitudes were actually both of the same size as control patients' listening-related N1 components, which seems to imply, confusingly, that schizophrenics ascribe both self- and other-generated speech to themselves, rather than ascribing both to external persons). A related set of experiments by the same group showed that inner speech suppressed N1 event-related potentials elicited by externally-generate sound for control subjects but not schizophrenic patients (Ford et al., 2001b). That said, attempts that have tried to specifically tie either of these effects to corollary discharge have so far failed (Ford and Mathalon, 2005).

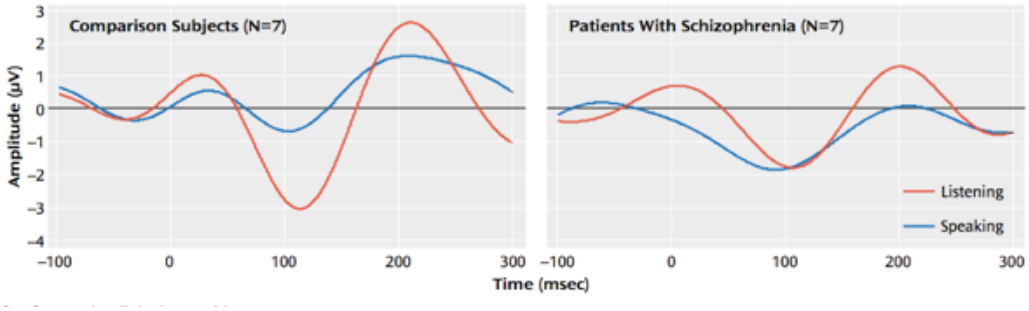

Figure 1.2 Differences in auditory perceiving of self and other in control and schizophrenic patients N1 component of event-related potentials at electroencephalographic site Cz, referenced to linked mastoids, for control (left) and schizophrenic (right) patients, in response to onset of vowel sounds spoken by the subject (blue), or played back after recording (blue). Note inability of this measure to discriminate between self- and other- generated speech, in schizophrenia patients compared to control subjects. (reproduced from (Ford et al., 2001a))

Looking more broadly at auditory cortex, findings such as the above, and confirmatory electrophysiology in monkeys demonstrating suppression of activity during vocalization in auditory cortex (Eliades and Wang, 2008), and reciprocally, during auditory attention tasks (Otazu et al., 2009), imply a processing role for corollary discharge in auditory cortex. The former finding is functionally similar to the discussed findings in crickets. Anatomical tracing studies have shown primary auditory cortex to receive input from several motor-related cortical areas, including the cingulate, primary motor, and secondary motor cortex. Recent work has identified a circuit modulating sound-evoked activity in AC1 involving a corollary discharge from secondary motor cortex (Schneider et al., 2014). Locomotion has also been shown to suppress auditory responses, and *in vivo* intracellular recording has demonstrated that this is due to an increase in inhibition (rather than a decrease in excitation). Cortical inhibition is mediated almost entirely by local interneurons, and it was found that this is a type of feed-forward inhibition in which projection neurons in secondary motor cortex activate a set of parvalbumin-

positive interneurons in auditory cortex. These inputs are active during locomotion and serve to suppress both spontaneous and sound-evoked synaptic activity (Nelson et al., 2013; Schneider et al., 2014). This is in some contrast to findings in visual cortex, where locomotion has been found to facilitate visual responses (Fu et al., 2014). The inhibition seems to be broad, and it is postulated that this may serve to enhance sensitivity to specific auditory inputs by suppressing responses to self-generated sound arising from locomotion. This is in keeping with other work that shows that activity in auditory cortex is suppressed during behaviors that require increased auditory processing (Eliades and Wang, 2008; Otazu et al., 2009).

Corollary discharge figures in theories of predictive coding. Predictive coding has been postulated to exist in primary visual cortex to explain non-classical visual responses in V1. In such a scheme, CD of motor commands fed back to early sensory areas could be used to generate an experience-dependent prediction of sensory input, in particular reafference. A recent study has identified such a mechanism in mouse V1 (Leinweber et al., 2017). Secondary motor cortex and neighboring Broadmann area 24b were shown to target most V1 neurons in layer 2/3. Imaging activity in axons of these inputs in V1 shows correlation with locomotion as well as visual flow resulting from said locomotion. Training the mice on a left-right inverted 2D environment reversed the correlation of neural activity with behavior to match visual flow. The exact nature of what can be, or is, done with these signals is currently unclear. Possibly, Leinweber et al. postulate, they exist to cancel out self-generated optic flow.

Returning to the question of the visual processing during motion, consider that saccadic movements of the eyes or head should cause visual blur given their speed, but noticeably, do not. In fact, we seem to pay little attention to visual input during saccades at all. This is easily demonstrated by looking in the mirror and trying to catch your eyes in motion as you shift your

focus from one reflected eye to the other – you only ever see yourself staring right back (though the observation that from a moving train, railroad ties are only visible during saccades in the direction of travel, which effectively stabilize the scene, demonstrates that the suppression is not complete) (Krekelberg, 2010). This dampening of the sensation of motion, saccadic suppression, is known to use a gating-type CD mechanism to suppress movement-detection neurons during voluntary and optokinetic saccades in the analogous case of locust (Zaretsky and Rowell, 1979) (though the neuronal class directly responsible for this suppression has yet to be identified), but there has long been disagreement as to whether CD was present in saccadic suppression in vertebrates, and primates in particular, with the alternative being mechanisms based on visual or proprioceptive signals (Battaglini et al., 1996; Ross et al., 2001). Clues to a role for CD have existed for some time - one way to distinguish between visual and non-visual effects is to compare suppression during true saccades and "simulated" saccades, achieved by rapidly deflecting a screen at saccade-like speeds. Psychophysical studies demonstrate that for some visual stimuli, real saccades are accompanied by a loss in contrast sensitivity of about one order of magnitude relative to "simulated" saccades for a brief time window surrounding the saccade (Diamond et al., 2000). That the onset of sensitivity loss precedes the saccades argues for a CD rather than a proprioceptive input.

Neural correlates of saccadic suppression have been found throughout the visual system (for a recent review, Krock and Moore, 2014). Earlier physiological studies were in conflict – some argued for a passive, visually-driven mechanism for suppression (Fischer et al., 1981; Wurtz, 1969), while other findings, such as the identification of cells in primate V1 that respond to external motion, but not retinal motion induced by saccades (Battaglini et al., 1986), argued for an active, CD-driven role. The reality seems, as is often the case, that both types of

mechanisms exist – passive and active mechanisms are both at play. A number of findings over the past decade and a half have confirmed neural saccadic suppression with an 'extraretinal' source, some supporting CD over proprioceptive mechanisms based on a timing argument (proprioception cannot initiate suppression before the actual saccade, as is sometimes seen) (Ibbotson and Krekelberg, 2011; Krock and Moore, 2014). Finally, recent work claims to have identified such a corollary discharge pathway (Berman et al., 2016). Suppression in the middle temporal visual area (MT) was found to depend on corollary discharge signals from motor superior colliculus (SCi) which could be inactivated with lidocaine injection. The authors present a putative pathway, as the path from SCi to MT is not direct, but it should be noted that these results are based on findings in one monkey. Behaviorally-studied deficits in saccadic suppression have been noted in schizophrenia patients (Crawford et al., 1995).

Following saccades, the visual system must not only suppress sensory input during the saccade, but must also maintain the perception of a stable physical world that is pieced together from very unstable retinal images, and retinotopic input must somehow be shifted to account for the new image resulting from each saccade. The hypothesis laid out by Helmholtz a century and a half ago has found support in work on vision in humans and non-human primates. Goldberg and others have demonstrated that neurons in several cortical and subcortical visual areas undergo a process called remapping which mediates the perceptual stability of attended objects by shifting retinotopic representations to account for saccadic shifts of gaze (Hall and Colby, 2011; Ross et al., 2001; Sun and Goldberg, 2016). Through this, a continuously accurate representation of visual space is maintained. Moreover, this process is performed anticipatorily, implicating corollary discharge mechanisms – neurons in the lateral intraparietal cortex (LIP) (Duhamel et al., 1992) were shown to respond in anticipation of saccades which will bring an

existing, out-of-receptive-field stimulus into their receptive field. Further work has demonstrated similar remapping in frontal eye fields (FEF) (Umeno and Goldberg, 2001), and the superior colliculus (SC) (Walker et al., 1995). These interconnected areas all receive both visual signals and signals related to saccadic eye movements (Barash et al., 1991; Bruce and Goldberg, 1985; Wurtz and Goldberg, 1972). Areas V2, V3a (Nakamura and Colby, 2002), and V4 (Neupane et al., 2016), and potentially V1 (Knapen et al., 2016, though this is a weak effect examined with fMRI) have also demonstrated remapping.

The first corollary discharge pathway described in primate is in the visual system. Sommer and Wurtz demonstrated that a corollary discharge from SC is conveyed through the mediodorsal nucleus of the thalamus (MD) to FEF (Sommer and Wurtz, 2002, 2006). Having confirmed that spatiotemporal patterns of the eye saccade CD match responses in cortical neurons, the authors used the $GABA_A$ antagonist musimol to temporarily inactivate MD. This treatment eliminated FEF remapping. Recent work has demonstrated a functional role for this CD pathway. Inactivation of MD induced an impairment of perceptual localization of visual stimuli following contralateral saccades (Cavanaugh et al., 2016). Corollary discharge then, is responsible for a complex reinterpretation of incoming sensory information based on known motor inputs which has the functional consequence of filtering out reafferent changes to visual input.

The above examples demonstrate that corollary discharge is used in many systems to make predictions about incoming sensory information, and in particular to deal with the problem of cancelling or separating reafferent sensory input from informative exafferent input about the external environment. The lower order CD mechanisms typically serve in peripheral gating roles. Higher order CDs are able to accomplish more nuanced modulation of sensory inflow.

Many of the mechanisms discussed above, especially those using generalized suppression schemes, are incapable of dealing with complex reafference. Those that 'blind' the sensory organs effectively throw the baby out with the bathwater, at least for the duration of the gating. Moreover, they are not flexible enough to account for reafference which changes due to external environmental state (Bell, 1989). Cancellation mechanisms that can deal with periodic but brief events, such as cricket stridulations, cannot sufficiently deal with reafference of long time duration, because gating off of a sensory system during reafference that is always present effectively incapacitates the sensory system in question. The weakly electric mormyrid fish, whose ampullary receptor afferents display an extended response to its own electric organ discharge (EOD) for 100ms stretches typically 5 times per second, is one such example among many – broadly inhibiting the ampullary receptor during the EOD response would render it nearly useless, since the reafference is nearly always 'on'. The early conceptual groundwork of Sperry, von Holst and Mittelstaedt predicted a more nuanced approach, whereby a corollary discharge, once sent from motor to sensory processing areas, could be sculpted to create a negation of the predicted reafference, thereby allowing its cancellation. Further, we will consider a class of circuits that have been shown to perform just such a calculation.

Cerebellum-like circuits

The early experimental and conceptual work of Sperry, von Holst and Mittelstaedt was a means of moving away from the then-dominant reflex theory of motion activation. In doing so, they posited and presented evidence for a system which would be capable not simply of silencing the sensory organs during reafference, but rather of sculpting a predicted and plastic negative image of the signal-corrupting reafference so that it could, by addition, be cancelled out. These

ideas have found their strongest support in work since the 1970s on cerebellum-like circuits. In these systems, nearly all of the predictions for such systems made by von Holst / Mittlestaedt / Sperry have been borne true, and a considerable literature has worked out the circuitry and physiology of mechanisms which allow the formation of such negative images. A notable body of theoretical work has also expanded our understanding of the capabilities and limitations of these circuits in constructing negative images.

With the possible exception of hagfish and lampreys, the brains of all craniates possess a cerebellum (Bell et al., 2008). In addition, in many craniates (birds and reptiles excluded) one may find other structures that share similarities in anatomy, gene expression, and function with the cerebellum. These have been termed cerebellum-like structures. These exist among many disparate taxa and significantly different neural systems, and while their particular implementation varies widely across these, the basic circuit architecture that defines them is easily recognized.

These include the electrosensory lobe (ELL) of mormyrids and the dorsal cochlear nucleus (Oertel and Young, 2004) of most mammals, already mentioned. Additionally, the ELL is present in another class of weakly electric fish, the gymnotids. Further, most basal aquatic vertebrates possess a medial octavolateral nucleus (MON) which is used to process mechanosensory input from the lateral line, auditory, and vestibular systems. Excluding the bony fish, most animals that have an MON also have a dorsal octavolateral nucleus (DON) that processes electrosensory input. The optic tectum of teleosts is thought by possess a cerebellum-like circuit in its margin layer, and the insect mushroom body has also suggested to share features with these systems (Farris, 2011) (for an in-depth review, Bell, 2002).

In the following section I will describe the general anatomical, developmental, pharmacological and genetic features shared by cerebellum-like circuits, and how these lead to their integration of sensory information with a wide array of motor CD and sensory input. Having introduced an architectural schema for these systems, I will discuss their specific implementations in the DCN and the mormyrid ELL. Further I will describe the physiological mechanisms that allow the creation of negative images in these circuits. Note that in the immediately following section, the term 'cerebellum-like structure' excludes the cerebellum proper, except when otherwise noted.

Anatomy common to cerebellum-like circuits

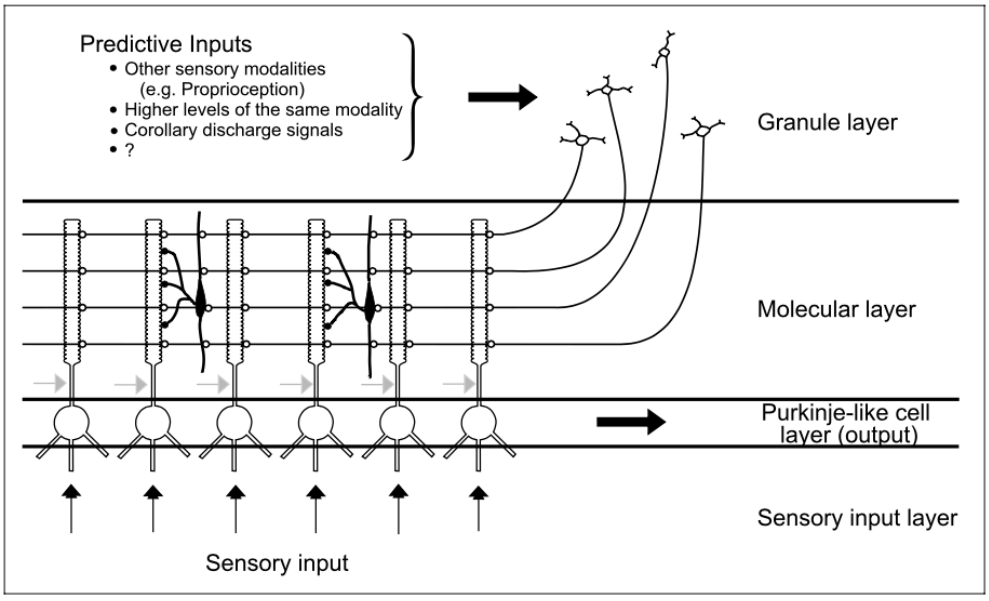

Figure 1.3: Schematic of major anatomical features of a cerebellum-like circuit.
Principal cells receive input from peripheral sensors in a sensory input layer or of principal and Purkinje-like cells. Sensory afferents terminate on basal dendrites of those cells at proximal apical dendrites (gray) or basal dendrites (black), sometimes via interneurons. Principal cells extend widely-arborized spiny dendrites into a molecular layer consisting of axons from granule cells residing in a granule cell layer or sometimes a non-laminar structure (figure reproduced from (Bell et al., 1997a)).

Common identifying features are shared across the class of circuits termed cerebellum-like (Bell, 2002; Bell et al., 2008; Requarth and Sawtell, 2011; Warren and Sawtell, 2016) (**Figure 1.3**). The molecular layer can perhaps be considered the defining feature of cerebellum-like circuits. It contains fine parallel fibers (PFs) that span the breadth of the layer, all oriented in approximately the same direction. PFs arise from a mass of granule cells (GCs) that is typically located outside the cerebellum-like structure proper, though in the case of the DCN and the cerebellum they are considered part of the structure itself, residing in several masses, the granule cell domains, on the periphery of the DCN, and in the granule cell layer beneath the molecular layer in the cerebellum. In some cerebellum-like structures, the parallel fibers also include the axons of Golgi cells. Unipolar brush cells, a class of excitatory interneurons, are also present in some structures as well (Floris et al., 1994; Mugnaini et al., 2011). These appear to play a key role in generating delayed responses in granule cells, discussed below (Kennedy et al., 2014). GCs are densely packed and typically represent the majority of neurons in the CNS (cerebellar GCs account for approximately 2/3 of all human neurons (Llinas et al., 2004)). Their small size has prevented in vivo recordings until only recently (Chadderton et al., 2004; Kennedy et al., 2014). In the cerebellum, the DCN, and the eminentia granularis, which gives rise to parallel fibers of the ELL and MON, granule cells have a classic granule cell shape, consisting of small cell bodies with several thin, radially-extending dendrites which terminate in claw-like post-synaptic structures (Bell, 2002).

The inputs to GCs, mossy fibers (MFs) originate in a broad array of other brain areas and typically carry information that is in some way predictive of the primary sensory input that the structure is responsible for. In that way they provide information which can be used to predict changes in sensation in that modality. These inputs can be corollary discharge but can also be

sensory input from other modalities such as proprioception, or can consist of feedback from higher order areas dealing with the same sensory modality.

PFs synapse onto the spines of principal neurons and onto stellate cells (Montgomery et al., 1995). This is similar to the parallel fiber inputs onto Purkinje cells and local interneurons in the cerebellum. The principal cells are cells with spine-covered dendrites. They fall into two classes – first, large excitatory output neurons which project to higher brain areas, and the second, Purkinje-like in many structures, that make local inhibitory connections onto other cells of the same class as well as onto the output principal neurons. The cell bodies of these two classes of cells are typically in a layer below the molecular layer but are sometimes in the molecular layer itself.

Cerebellum-like structures, potentially including the cerebellum, are sensory processing structures, and they integrate some type of peripheral sensory input with potentially predictive inputs about that modality. That peripheral input comes in via afferents of primary sensory neurons such as electroreceptors and targets deeper layers of the structure, where the afferents synapse onto principal and Purkinje-like cells, either directly or through local interneurons, some of which may be inhibitory and allow for a sign-flip of the incoming signal, allowing excitatory signals from the periphery to be represented as inhibitory signals in the circuit. The afferent inputs onto output and Purkinje-like cells occur at basilar dendrites or at proximal apical dendrites. Typically, the peripheral inputs make connections in a manner that preserves a mapping of the sensory modality in its representation in cells of the cerebellum-like structure, be it a tonotopic representation of frequency-space, as in the DCN, or a somatotopic representation of the skin surface, as in the ELL.

Other commonalities of cerebellum-like structures

That such similarities exist between structures in widely disparate taxa has naturally led to thinking about the source of these similarities, and the extent to which the formation and patterning of these structures is controlled by similar underlying genetic mechanisms. Though they are to some extent the result of convergent evolution (Bell, 2002; Bullock et al., 1983), it seems that there may exist a kind of genetic framework that can be activated to produce cerebellum-like structures.

Indeed, work in chick has shown that implantation of fibroblast growth factor 8 (FGF8)-containing beads into the neural tube of chick embryos at the prospective location of caudal diencephalon or midbrain produced ectopic growth of cerebellum-like structures (Martinez et al., 1999). FGF8, a growth factor family broadly involved in development, cell growth, and morphogenesis (O'Leary et al., 2016), acts in this case via a suppressive effect on Otx2. This role for Otx genes (Otx1 and Otx2 are murine homologs of the Drosophila orthodenticle (otd) gene) in patterning the cerebellum and cerebellum-like structures is further supported by the finding that Otx1-/-;Otx2+/- mice develop both ectopic cerebellar tissue and enlarged cerebella that replace the entire mesencephalon (Acampora et al., 1997).

Gene expression patterns are shared between cerebellum-like structures and cerebellum to varying degrees. The DCN cartwheel cell in particular shares much in common with cerebellar Purkinje cells, at least three different mutations resulting in cell-type-specific degeneration of both Purkinje and cartwheel cells (Berrebi et al., 1990). GluRdelta2, related to ionotropic glutamate receptors and necessary for long-term depression (LTD) at the cerebellar PF-Purkinje cell synapse (Yawata et al., 2006), is also expressed in most cerebellum-like circuits. Beyond mammalian cerebellar Purkinje cells (Yuzaki, 2003), its expression has been established in

mammalian DCN, (Petralia et al., 1996) , in the molecular layers of the cerebellum, in MON and OTML (and not in other brain regions) in zebrafish (Mikami et al., 2004) and mormyrids, as well as the ELL of the mormyrid (Sawtell and Bell, 2013).

Other genes that are expressed in the cerebellum or cerebellum-like circuits only in adulthood are expressed only during development in circuits. Functional NMDA receptors, for example, are expressed in principal cells of the adult DCN (Manis and Molitor, 1996) as well as principal cells of the ELL in both adult mormyrids (Grant et al., 1998a) and gymnotids (Berman et al., 2001), but are expressed in cerebellar Purkinje cells parallel fiber synapses only during development (Dupont et al., 1987), though they are present at climbing fiber synapses (Piochon et al., 2007) (Bell et al., 2008; Sawtell and Bell, 2013).

Dorsal Cochlear Nucleus

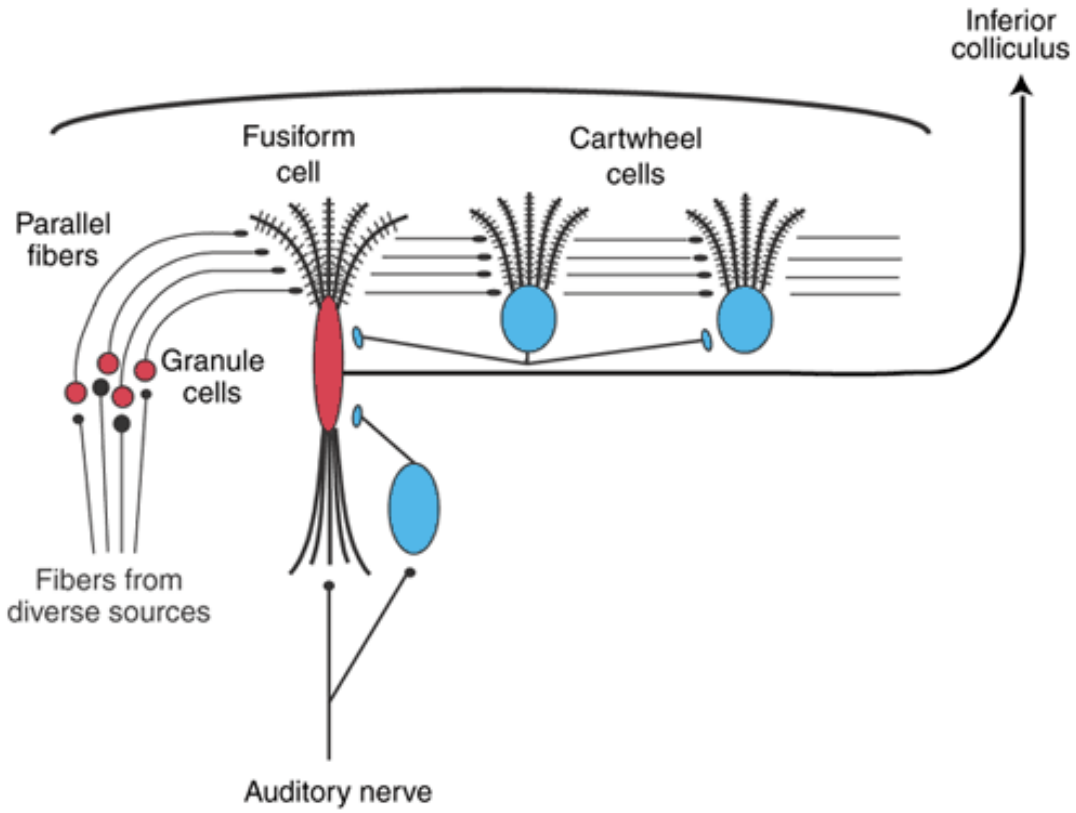

Figure 1.4 Simplified schematic of circuitry of the Dorsal Cochlear Nucleus.
Peripheral auditory input enters the DCN via the auditory nerve, synapsing onto basal dendrites of fusiform cells. Mossy fibers convey a wide range of proporioceptive, vestibular, motor corollary discharge, and high-order auditory inputs onto granule cells. Granule cells send parallel fibers into a molecular layer, where they synapse onto the spiny arborized dendrites of glutamatergic fusiform cells and Purkinje-like glycinergic and GABAergic cartwheel cells. Fusiform cells send the output of the DCN to inferior colliculus via the dorsal acoustic stria. Cartwheel cells excite each other but inhibit fusiform cells. Several other cell types are not shown. (reproduced from (Nelson, 2004))

The mammalian DCN is a brainstem structure that acts in parallel with the ventral cochlear nucleus (VCN) as the first stage for central processing of auditory sensory input (**Figure 1.4**). While the VCN serves largely as a relay and computation area for purely auditory input, extracting higher-order features from the Fourier-transformed auditory output of the cochlea, the DCN integrates auditory input with a wide array of other inputs in order to contextualize and perhaps selectively filter self-generated modulations of audition. Together,

these may give upstream auditory areas access to two channels of auditory information – one (the VCN) representing reafference and exafference together, and the other, from the VCN, a filtered channel containing only exafference.

DCN's shares many similarities with other cerebellum-like structures, as first noticed by de Nó (Lorente de Nó, 1933, 1979). It is a laminar structure that receives peripheral inputs via the auditory nerve, which in turn carries information, as part of the 8th cranial nerve (the vestibulocochlear nerve) from the spiral ganglion of the cochlea. The spiral ganglion contains spiral ganglion cells which innervate inner hairs of the cochlea. These inner hair cells are laid out along the length of the basilar membrane of the cochlea, and the tonotopy extracted and imposed by the acoustico-mechanical structure of the basilar membrane is maintained through to the spiral ganglion, the axons of those neurons which form the auditory nerve itself, and finally to the tonotopically organized connections it makes onto cells of the DCN and VCN (Cant, 1992; Young and Davis, 2002).

Auditory nerve fibers innervate the deep layer of the DCN, where they make synapses onto the smooth basal dendrites of glutamatergic fusiform cells (FCs) and giant cells, together the output cells of the DCN, as well as inhibitory glycinergic interneurons called vertical, or tuberculoventral cells. As mentioned, the inputs onto these cells classes are tonotopically arranged, such that there is a medio-lateral gradient in the DCN from low to high pitch, but the exact organization of inputs onto one class versus another, as well as the connectivity between them, seems to be tightly regulated and forms the basis of complex response properties of several cell classes in the DCN that vary non-monotonically in the frequency and amplitude domains (**Figure 1.5**). These complex response maps and the underlying connectivity patterns that define them give rise to response properties to complex inputs (that is, inputs consisting of more than a

single tone) of these same cells , such as selective tuning to notch-filtered broadband noise (Young and Davis, 2002), that likely underlie a functional role for the DCN in monoaural sound source localization (Oertel and Young, 2004).

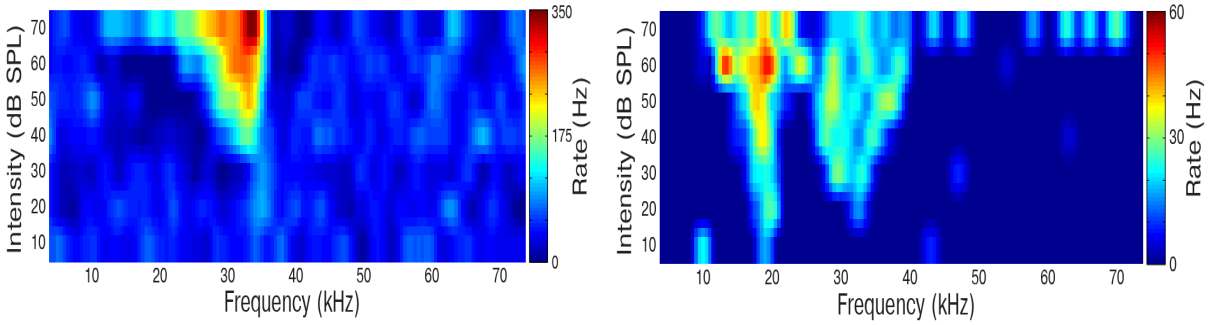

Figure 1.5 Example response properties of DCN neurons.
Neurons of the dorsal cochlear nucleus have complex response properties, varying nonlinearly with frequency and intensity. (A) Response map of a putative fusiform cell to pure tones of varying frequency and amplitude. Note prominent areas of inhibition to the immediate left and right of the main excitatory region. (B) Response map of a cartwheel cell. Though CWCs do not receive direct peripheral auditory input, they demonstrate complex response patterns to acoustic stimuli, presumably receiving feedback from higher order auditory regions via parallel fibers.

As in other cerebellum-like structures, the DCN contains a prominent molecular layer, the PFs of which are the axons of glutamatergic granule cells and GABAergic Golgi cells, whose cell bodies reside in several distinct regions around the VCN called granule cell domains, as well as in the fusiform cell layer (FCL) discussed below (Mugnaini et al., 1980). The granule cell domains receive input from MFs which convey information from a wide range of sources such as corollary discharge, information from higher order auditory areas (e.g., inferior colliculus), inputs from other sensory modalities such as vestibular information related to head and external ear (pinna) movement and position, and proprioceptive inputs that encode jaw and tongue movements, among others (Oertel and Young, 2004). In sum, these inputs are likely to be those that are predictive of self-generated changes in auditory input such as endogenous modulations

of exogenous sounds, e.g. acoustic filtering of sound by the head and pinna for use in monaural sound location, and purely reafferent input such as sounds generated by body movements, e.g. chewing or licking. Of additional note is the presence of unipolar brush cells in the granule cell domains (Diño and Mugnaini, 2008; Floris et al., 1994; Mugnaini et al., 2011), which themselves receive MF input that is relayed to granule cells and may be involved in the DCN, as they are in the mormyrid ELL, in time-delaying granule cell output (Kennedy et al., 2014).

Parallel fibers synapse onto of the major class of efferent cells of the DCN, the fusiform cells, whose soma reside in the fusiform cell layer and whose apical spine-covered dendrites extend into the molecular layer. Fusiform cells, along with giant cells, form the output of the DCN and project to the IC via the dorsal acoustic stria, and in the IC these signals are brought together with the output of the VCN.

An additional class of cells in the DCN is the cartwheel cell , a cell type whose spine-covered dendrites arborize extensively in the molecular layer, where its cell body also resides. These cells make inhibitory synapses onto fusiform cells as well as onto each other, and are considered to be Purkinje-like because they are GABAergic (as well as glycinergic), display a Purkinje-like dendritic morphology, and share a similar pattern of gene expression with Purkinje cells (Bell et al., 2008).

The DCN seems to have at least two roles, though the two may be related. In its longer-recognized role, previous work has shown the DCN to be involved in monaural sound location, whereby cues to sound source elevation are derived from spectral notches imposed by acoustic filtering through interaction with the head and pinna in a location-dependent manner. That is, initially identical sounds arriving from different positions relative to the ear interact with the head and pinna, and via acoustic absorption, reflection, and refraction, arrive at the tympanic

membrane recognizably different from one another. This filter, termed the head-related-transfer-function (HRTF) allows for an (almost) one-to-one mapping between sound source elevations and filters, so knowing the filter implies the elevation (Musicant et al., 1990; Rice et al., 1992; Young et al., 1996).

These calculations are thought to be mediated at least partially by cells in the DCN that selectively respond to exactly the spectral properties that change with elevation (i.e., notches), at least for some species. Work in cat has shown that severing the dorsal acoustic stria, the efferent ouput of the DCN, while leaving VCN output intact effectively removes the ability to monoaurally identify sound source elevation, while maintaining localization acuity in other axes. (May, 2000). However, that role may not extend to mice, which like many common prey species (Heffner and Heffner, 1988), are relatively bad at sound localization, in particular vertical localization (Lauer et al., 2011). The role may perhaps not even extend to other mammals. The mountain beaver *Aplodontia rufa*, and the pocket gopher, *Geomys bursarius* have exceptionally large DCNs, the mountain beaver's being 4-7 times larger than that of any know rodent, but both display profoundly diminished hearing in both frequency and threshold, and nearly no acuity in sound localization (Godfrey et al., 2016; Heffner and Heffner, 1990; Merzenich et al., 1973). The DCN of the mountain beaver has become specialized for the detection of slow (~1Hz) changes in air pressure changes (Merzenich et al., 1973). Presumably this is related to its habitat: long subterrestrial tunnels. The pocket gopher lives in similar subterranean environments, though its hearing at the infrasonic frequencies noted for the mountain beaver has not been tested. Incidentally, the mountain beaver is commonly considered the most primitive extant rodent (Godin, 1964; Nowak and Paradiso, 1999).

Several lines of evidence have pointed to a role for the DCN in filtering out self-generated sound. First, there exist proprioceptive inputs to the DCN other than those related to head and neck position (Oertel and Young, 2004). Additionally, some patients who experience a type of tinnitus thought to be mediated by pathologies of plasticity in the DCN (coupled with peripheral hair cell loss or cochlear neuropathy) (Shore et al., 2016) report shifts in the pitch of the tinnitus hallucination in response to jaw movements (termed somatic tinnitus, this typically permanent form of tinnitus accounts for approximately 20% of tinnitus cases, and, incidentally, began to afflict the author in the weeks leading to the completion of this manuscript). This other role is discussed further in **Chapter 3**, where I present evidence that the DCN serves to decouple exafferent and reafferent auditory signals related to licking, extracting a channel of information that represents only sound generated by the outside world.

Electrosensory Lobe

Outside the elasmobranchs, electroreception is present in four groups of teleost fish – the siluriforms, or catfish, the monotypic subfamily *Xenomystinae*, represented solely by the African brown knifefish (*Xenomystus nigi*) (Bullock and Northcutt, 1982), as well as the weakly electric fish of Central and South America – Gymnotidae, and the weakly electric fish of Africa - Mormyroidea. Each of these groups possesses a cerebellum-like electrosensory lobe (ELL). The latter two have active electrosensory systems, that is, they have an electric organ in the tail that can generate and discharge a pulsatile or wave-like signal in addition to a passive system of electroreceptors. The ELLs of Gymnotids and Mormyrids display a remarkable number of structural similarities despite having evolved separately (Bell, 2002; Bullock et al., 1983). Though a comparison of features between the ELL structures of these groups is a fruitful

exercise, for the purposes of the remaining text, I will refer strictly to the ELL of the mormyrid *Gnathonemus petersii*, Peter's elephant-nose fish.

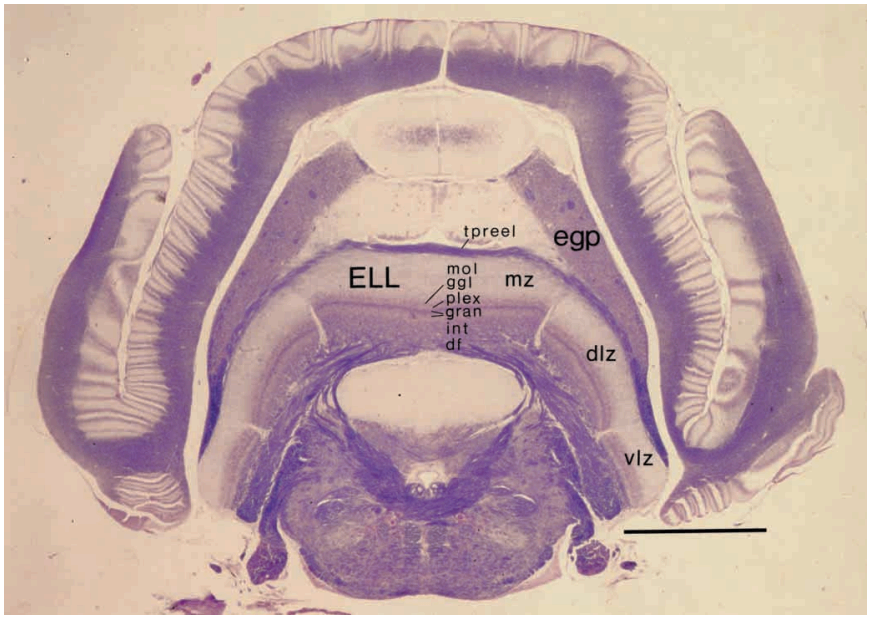

Figure 1.6 Histological section showing the mormyrid electrosensory lobe
Each major receptor class of the mormyrid is represented somatotopically in the ELL. Ampullary afferents terminate in the ventrolateral zone (VLZ). Two class of mormyromast afferents terminate in the medial zone (MZ) and dorsolateral zone (DLZ). Knollenorgen afferents project to the nucleus of ELL (Not labelled). Parallel fiber inputs originate from granule cells in the eminentia granularis posterior (EGp) (reproduced from)(Bell, 1989)

The ELL is an electrosensory processing organ but in fact is responsible for three separate types of input that correspond to the three morphological types of electroreceptors found in mormyrids, each serving different functions (Szabo, 1965; Bodznick and Montgomery, 2005; Kawasaki, 2005) (**Figure 1.6**). The one of primary concern to the work in this paper is the ampullary receptor, which is present in each of the four groups of fish mentioned above, with some morphological variation between groups (Szamier and Bennett, 1974). The ampullary receptor is the smallest of the three classes and is tuned to low frequency and DC bioelectrical signals typically produced by the locomotion and muscular contractions of prey such as insect larvae and worms (Kalmijn, 1974; Engelmann et al., 2010; Bodznick and Montgomery, 2005)

(**Figure 1.7A**). These receptors tile the ventral and dorsal surfaces of the trunk, the face, and the mormyrid's protuberant chin, the Schnauzenorgen, which is tiled particularly densely and is the location of approximately half the ampullary receptors. Concordantly, this chin takes up about half of the somatotopic homunculus representing ampullary inputs to the ELL. The Schnauzenorgen and a small area above the mouth are electrosensory foveas, the former for detection of objects directly below the animal, under the river bottom, and the latter pointing forward like an electrosensory headlight (Bacelo et al., 2008). In addition to responding to low-amplitude, low-frequency exogenous signals, the ampullary receptors are also strongly driven by the animal's own EOD (**Figure 1.7B,C**), which can be some five orders of magnitude larger than the lowest prey-generated signals the receptors can detect. Passive filtering by the ampullary receptor brings that difference to 10 to 100 fold (Chen et al., 2005). Ampullary receptor afferents project to the ventrolateral zone (VLZ) of the ELL, and that will be the area of our immediate focus.

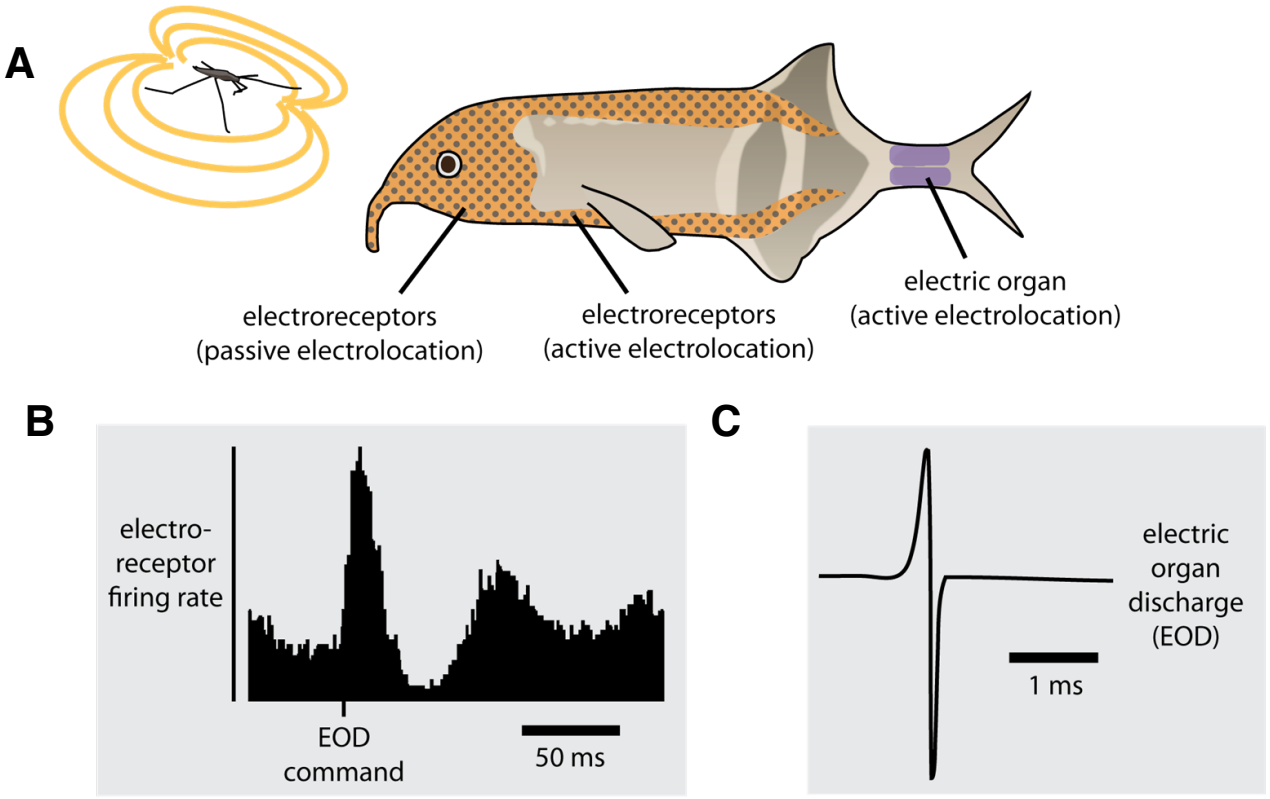

Figure 1.7 Schematic of electrosensory input in mormyrids
(**A**) Mormyrids use a passive system of ampullary receptors (orange) to detect low frequency biogenic electric fields generated by prey. An electric organ (purple) present at their tail generates pulsatile electric discharges called the Electric Organ Discharge (EOD) that are utilized by the active system of tuberous receptors (purple on body), but interfere with passive system encoding of prey signals. (**B**) The EOD is detected by ampullary receptors as prolonged, ringing response that lasts for 100+ms (**C**) The EOD is itself a pulsatile signal lasting about a millisecond.

The remaining two receptors types, the mormyromasts and the Knollenorgen, are used to process the animal's own EOD, and the EOD of conspecifics, respectively. The former is used as for active electrolocation and has been the subject of the majority of study in mormyrids. The Knollenorgen receptors represent a communication channel. Though the exact nature of these communicative signals is not well understood, mormyrids larger than *G. petersii* have been reported to engage in coordinated pack hunting (Arnegard and Carlson, 2005). Mormyromast

afferents project to the medial and dorsolateral zones of the ELL, and Knollenorgen afferents to the nucleus of ELL.

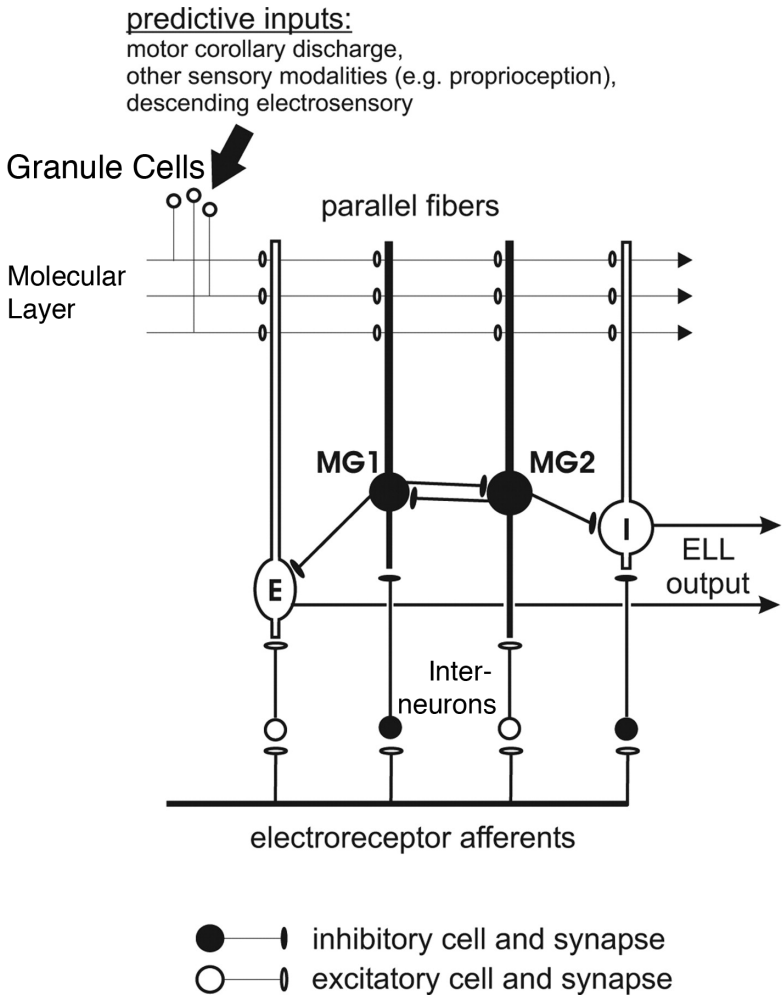

Figure 1.8 Simplified circuitry of the mormyrid ELL.
Principal glutamatergic output cells of the ELL, E and I cells, as well as GABAergic Purkinje-like MG cells receive electrosensory input via interneurons onto basilar dendrites. These interneurons induce a sign change for I-type output and MG cells. MG cells inhibit each other and the output cells. Each of these cell classes extends apical dendrites into the molecular layer, where they receive input from parallel fibers. Parallel fibers are the axons of granule cells, which receive a wide range of predictive inputs, including corollary discharge signals related to the electric organ discharge. (modified from (Sawtell and Williams, 2008))

Ampullary afferents terminate in the deep layers of the ELL (**Figure 1.8**) in a somatotopic arrangement, targeting the principal cells of the ELL either directly through

synapses onto their basilar dendrites, or via interneurons, some of which are inihitory and function to flip the sign of the afferent signal. As a result, principal cells of the ELL exist in two flavors, E-cells and I-cells, the former excited by an increase in electrical stimulation at the center of its receptive field, and the latter inhibited. These are the cells recorded from in the work described in **Chapter 2** A Purkinje-like interneurons called the medium-sized ganglion (MG) cells also exists in the ELL. MG cells are Purkinje-like cells, being GABAergic interneurons that receive peripheral input and arborize extensively in the molecular layer. They inhibit each other and surrounding efferent E and I cells. MG cells also exist as I-type or E-type. In conclsion: The MG cells are more numerous than the efferent cells and make more synapses onto parallel fibers (Meek and Grant, 1994), yet a clear explanation of their role in either negative image formation specifically, or peripheral/parallel fiber integration in general, has so far been lacking.

The output cells and the MG extend spiny apical dendrites into the molecular layer where they receive input from PFs. These PFs are the axons of granule cells that project from the eminentia granularis posterior (EGp). The MF inputs into EGp in mormyrids are well studied and represent a diverse source of inputs. These include a corollary discharge input corresponding to the motor signal that initiates the EOD, proprioceptive input related to bending of the body or fins, which is critical because the body position dictates the distance between the electric organ and electroreceptors thereby dictating the size of the EOD-associated reafference, and descending input from higher order electrosensory areas (Bell et al., 1992a). Together, these are sources of predictive information about ongoing sensory input into the electroreceptors. The EGp, like the granule cell layer of the cerebellum and the granule cell domains of the DCN, also contains GABAergic Golgi cells and unipolar brush cells (Bell, 2002).

Sensory Processing

Though the organ that was eventually recognized as the ampullary receptor was first described in the 17th century by Stefano Lorenzini, it's function as an electroreceptor wasn't identified until 1960 (Murray, 1960), presumably due to a kind of intellectual sensory anthropocentrism. Ampullary receptors exist in nearly all non-teleost fish, some teleosts as described, including the weakly electric, and a few amphibians. Monotremes such as the platypus (Scheich et al., 1986) and at least some dolphins (Czech-Damal et al., 2011) display passive electroreception but use a different receptor type innervated by the trigeminal nerve and will not be considered further herein. Behavioral thresholds for some elasmobranchs are as low as 5nV/cm (Kalmijn, 1982), corresponding to about a car battery between two antipodal points on Earth, circumferentially (Enikolopov, 2018). Individual receptors cells are less sensitive, about 2uV/cm in skates, for reasons discussed below. In *Gnathonemus petersii*, ampullary afferents have a threshold of approximately 40uV/cm at the low frequencies, 1-10Hz, that they are most responsive to (Engelmann et al., 2010, and confirmed in **Figure 2.2**).

Ampullary receptors in mormyrids and elasmobranchs are anatomically and functionally similar and both derive from mechanosensory lateral line receptors, but evolved separately, having been lost in the teleost ancestor and newly evolved at least twice (Bell, 2002; Bullock et al., 1983). Notably, ampullary organs are "more closely similar within habitat than they are taxonomically" (Keller, 2004) and so the below discussion references ampullae of Lorenzini as well as the teleost ampullary receptor.

Ampullary receptors detect small biogenic electric fields generated near their body by predator and prey and it is useful to consider the ethological context in which they are utilized. While many fish use vision for prey detection (Bell, 2002; Bullock et al., 1993) mormyrids are weakly electric fish are nocturnal (Moller et al., 1979; Westby, 1988), including *G. petersii*, which inhabits the bottoms of freshwater streams and rivers of Central Africa (Bleckmann and von der Emde, 1998; Okedi, 1965). Stomach analysis in wild-caught mormyrids show that they often feed on insect larvae, small crustaceans, and worms (I will spare the reader the impressively exhaustive entomological species-lists such research generates) (Corbet Philip S., 1961; Okedi, 1965). G. petersii thrives quite well on a diet consisting of the blackworm Lumbriculus variegatus in a laboratory setting. While they do use active electroreception as well as vision and chemoreception (Bleckmann and von der Emde, 1998), mormyrids are adept at prey detection even in the absence of these when relying solely on the passive system (Bleckmann and von der Emde, 1998; von der Emde, 1994).

Aquatic electrical signals that can be detected by passive electroreception are both biotic and abiotic in origin. Abiotic signals are caused by reduction/oxidation processes in sediment, seismic activity, lightning, and magnetic storms. These are mostly DC or low frequency signals (Emde, 2013; Keller, 2004) (See **Chapter 2** and **Conclusion** for speculation about how these may be dealt with). It is likely that biotic signals are of greater importance to electroreceptive animals, and these are mostly the result of muscle contractions and biochemical processes that induce ion flow across thin epithelia such as the gills (Emde, 2013; Peters and Bretschneider, 1972, wherein electric fields generated by some 60 species are measured). It's likely that all prey of the mormyrid produce such fields, and notably, wounded specimens produce fields

typically one to several orders of magnitude larger than intact ones (Kalmijn, 1988; Keller, 2004).

Sensory filtering begins the ampullary receptor. The ampullary receptor organ is comprised of several electroreceptor cells arranged with accessory cells in an approximately spherical subdermal invaginated chamber called the ampulla. This ampulla sits at the end of a narrow canal 100-200um long and filled with conductive gel. The electroreceptor cells are innervated by a single myelinated afferent fiber per organ which carries information to the ELL (Derbin, 1974).

The canal acts as a low-impedance shunt, but canal length serves as a low-pass filter. Tight junctions of accessory cells within the ampulla electrically isolate the receptor cell membrane into a basal portion electrically close to the internal milieu of the animal, and an apical portion facing the lumen of the ampulla, isopotential to the external world (Keller, 2004). It is this potential difference, between the canal pore and the inside of the animal that the receptor cell experiences.

Pooling across the multiple electroreceptor cells within a single organ been shown to be responsible for a noise reduction of approximately an order of magnitude in elasmobranchs, though teleost ampullary organs have many fewer electroreceptor cells per organ (Bodznick et al., 1993). Further convergence at central targets is likely responsible for more noise reduction, and has been theoretically shown to do so in the mormyrid (Engelmann et al., 2010).

Mormyrid ampullary receptors are linear encoders, responding to a combination of amplitude and slope, so-called fractional order filters (Engelmann et al., 2010). Neurons in many systems, however, are known to be non-linear (Koch and Segev, 2000), and this includes neurons of the ELL (Gabbiani et al., 1996).

Non-linear burst firing (Krahe and Gabbiani, 2004) is a salient feature of gymnotid and mormyrid (Sugawara et al., 1999) ELL neurons. Work in the gymnotid has shown them to extract, from the tonic firing of peripheral afferent, specific features about prey-like stimuli. This burst firing can be modulated by central feedback, allowing context-dependent modulation (Bastian and Nguyenkim, 2001). Theoretical work suggests that non-linear encoding is particularly important for encoding spatially diffuse stimuli (Chacron, 2006), and such spatial characteristics have been shown to determine response properties of gymnotid ELL neurons, including bursting, through feedback (Doiron et al., 2003).

While some principal cells in the mormyrid ELL have simple receptive fields (RFs), their response strongest to stimuli at the center of the RF and decaying to baseline with distance from the center, the majority display complex, antagonistic center-surround RFs. Others still have more complex RFs that consist of multiple center-surround RFs (Metzen et al., 2008), and display differential responses to field-strength-matched stimuli presented globally and locally (personal observation, data not presented).

Elasmobranch ampullary receptors are driven strongly across much of their dynamic range by reafferent input related to their own ventilation, the process in which water is driven through the mouth and across the gills for respiration. Work in the thornback ray *Platyrhinoidis triseriata* (Montgomery, 1984a), the carpet shark *Cephaloscyllium isabella* (Bodznick and Montgomery, 1992), and the little skate *Raja erinacea* (New and Bodznick, 1990) has demonstrated an approximately five-fold reduction in noise at the first stage of electrosensory processing, the DON (Bodznick and Montgomery, 1992). This reafference is detected by many cells across the body of the animal, and Montgomery and Bodznick demonstrated this fact can be used to perform 'common mode rejection'. Features broadly common to multiple receptors are

subtracted from each other, with interneurons that receive afferent sensory input inhibiting excitatory efferent cells that receive the same the ventilatory reafference (Montgomery and Bodznick, 1993a). Relatedly, integration of input from contralaterally positioned receptors in mormyrid has been theoretically shown to enhance coding of prey-like stimuli and increase bandwidth (Engelmann et al., 2010).

A more powerful noise-cancellation technique was first described by Bell in the mormyrid (Bell, 1982; Bell et al., 1997b) but has since been demonstrated in gymnotid ELL (Bastian, 1995) and elasmobranch DON (Bodznick et al., 1999). These cerebellum-like circuits perform as adaptive filters, learning to cancel signals correlated to body motion. The circuit and synaptic mechanisms for this are discussed below.

Formation of negative images for cancellation

The active electrosensory system of the mormyrid poses a significant challenge to passive electroreception. Active electroreception involves the emission of a brief, high frequency pulse from an electric organ on the tail of the fish, the EOD, at a rate of approximately 5Hz. The active regions of the ELL are exquisitely tuned to object-induced distortions in the electric field generated by this discharge. Though the ampullary receptors of the passive system are tuned to respond to low frequency bioelectric fields of aquatic animals, the power of the EOD so dwarfs those signals that the EOD produces a sustained ringing response in ampullary receptors that lasts for approximately 100ms (**Figure 1.7B**). Since the typical inter-EOD interval is about 200ms, but often as low as 30ms, reafference stands to incapacitate passive electroception (Bell and Russell, 1978). Zipser and Bennett (1976) showed that the active regions of the ELL receive a corollary discharge of the motor command that evokes the EOD. Positing that the passive

system VLZ may also receive such a signal to predict the incoming EOD, Curt Bell showed (Bell, 1981) that in fact it does, and that it is used to form a negative image of the ampullary receptor response to the EOD.

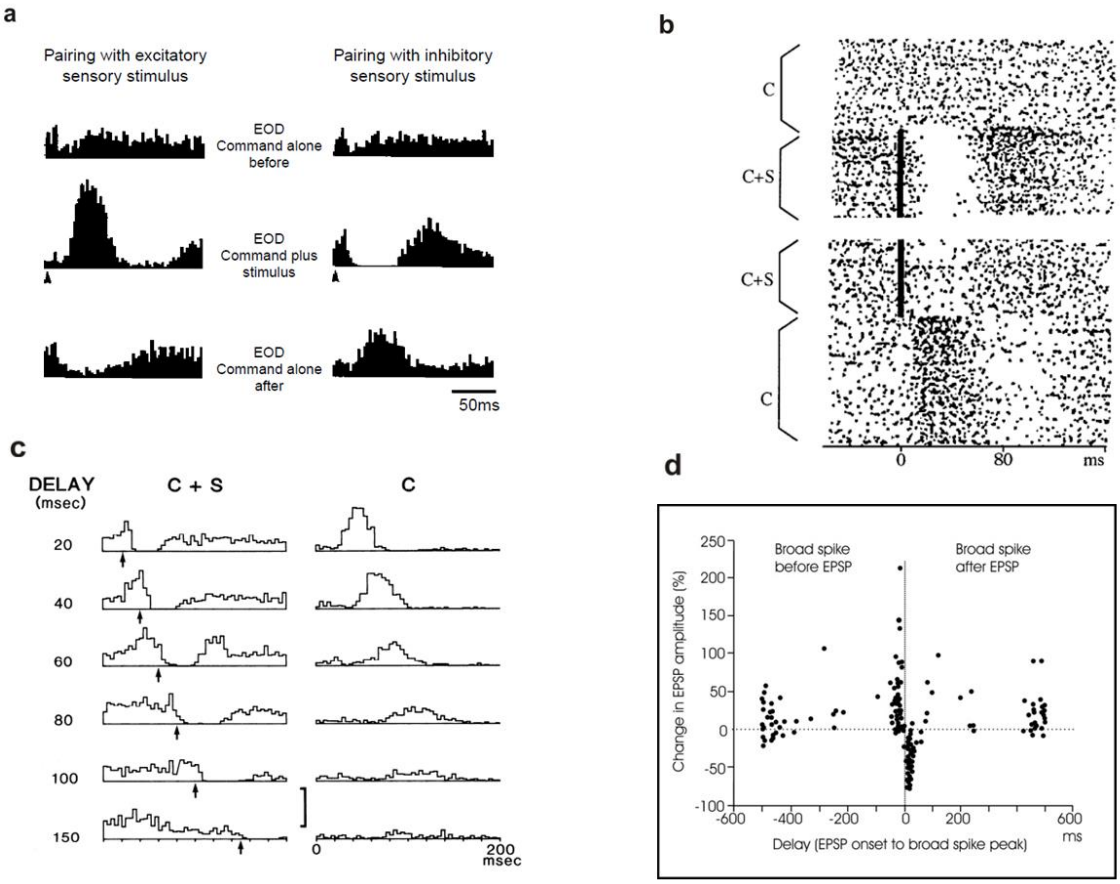

Figure 1.9 Plastic responses to sensory consequences of the EOD.
(**a**) Extracellular recording of corollary discharge response in ELL MG cell. (*top left*) Response to the EOD command before any pairing. (*middle left*) Pairing the EOD command with a 1ms-long excitatory stimulus (arrowhead) produces an immediate and vigorous response. (*bottom left*) following a brief pairing, the EOD command alone evokes a response opposite in effect to that during the pairing. (*right column*) Same as *left column* but using an inhibitory stimulus. (**b**) Raster of an MG cell showing timecourse of an experiment like that in (**a**). C=command, S=stimulus, t=0 on top of raster. Note the gradual decay of response during the C+S period, and the expression of a negative image following C+S pairing. (**c**) equivalent experiment to (**a** *middle left, bottom left*), but with inhibitory stimulus paired at increase delays (*left column*) from the EOD command. (**d**) Anti-Hebbian learning rule. *In vivo* experiment where PF-evoked ESPSs are paired at different delays with current-injection-evoked dendritic spikes. Points represent change in EPSP amplitude as function of this delay. Synaptic depression occurred only when EPSP preceded dendritic spike by <50ms. All other delays resulted in potentiation. (**a**) reproduced from Bell, 2001; (**b**) reproduced from (Bell 1981); (**c**) reproduced from (Bell, 1982); (**d**) modified from (Bell et al., 1997b)

Since the electric organ is a modified muscle, the EOD can be blocked by administering the nicotinic acetylcholine receptor antagonist curare, blocking transmission at the neuromuscular junctions of the electric organ. While this silences the EOD itself, it does not block the command that evokes it. The electromotor neuron volley (EMN) that would produce the EOD can easily be detected with surface electrodes near the electric organ, and the ELL continues to receive an electric organ corollary discharge (EOCD) via MFs. This allowed the presentation of an artificial mimic EOD, the amplitude and timing of which could be modified, or it could be omitted entirely. In vivo recording demonstrated that on presentation of a mimic EOD stimulus synchronized to the EOCD, principal cells of the VLZ first show a robust response (**Figure 1.9A**), but within minutes that response to the mimic diminishes without a loss of other responsiveness. Moreover, by omitting the mimic, the response of VLZ principal cells to the EOCD itself can be examined, and they respond with a negative image of the initial sensory response to the mimic (**Figure 1.9A** *bottom*, **Figure 1.9B**). Further work (Bell, 1982) showed that the system is capable of cancelling signals of varied shape, amplitude, and polarity, and at varying delays from the EOD command (**Figure 1.9C**). This then was the first evidence of the kind of system postulated by Sperry, von Holst and Mittelstaedt – a plastic corollary discharge, and one that was able to cancel out the effects of a self-generated signal.

In the ensuing three and half decades, a great deal of effort has gone into explaining how these negative images are formed, with the working assumption that cancellation of reafference is critical to providing a clean sensory stream for processing relevant information about the outside world. Further in vivo and in vitro work determined that plasticity in the ELL was implicated in forming these negative images: intracellular current injected into principal cells at fixed delays from the EMN led to the formation of in vitro negative images at current amplitudes

sufficient to elicit dendritic spikes. This implied that the change must occur at synapses onto principal cells, likely PF-principal cells synapse (Bell et al., 1993). One of the first demonstrations of spike-timing dependent plasticity (STDP) showed that in contrast to hippocampus and neocortex, plasticity at the PF-ELL principal cell synapse followed an anti-Hebbian learning rule. (Bell et al., 1993, 1997b) (**Figure 1.9D**). That is, in contrast to classic Hebbian learning (Hebb, 1949), correlation between presynaptic signals and postsynaptic depolarization leads to weakening of synaptic strength.

Principal cells of the ELL are able to create negative images at varied delays to the EOMC (**Figure 1.9C**) (Bell et al., 1992a). Critical for this is a mechanism that provides predictive signals at varied delays to granule cells. This is a necessary condition of the system that allows correlations of the EOMC to temporally delayed sensory consequences of the EOD to be detected and cancelled, and is fundamental to what differentiates the system from the gating and suppression mechanisms discussed earlier. Recently, groundbreaking work by Kennedy and coauthors (Kennedy et al., 2014) has elucidated this underlying mechanism. It was shown that granule cells, in concert with unipolar brush cells that produce a response delayed from the EOMC, provide the necessary temporal basis (**Figure 1.10**). That basis is shown to match the

temporal structure of the reafferent response to the EOD. That basis seems to be recapitulated in findings described in Chapter 2 (**Figure 2.10**).

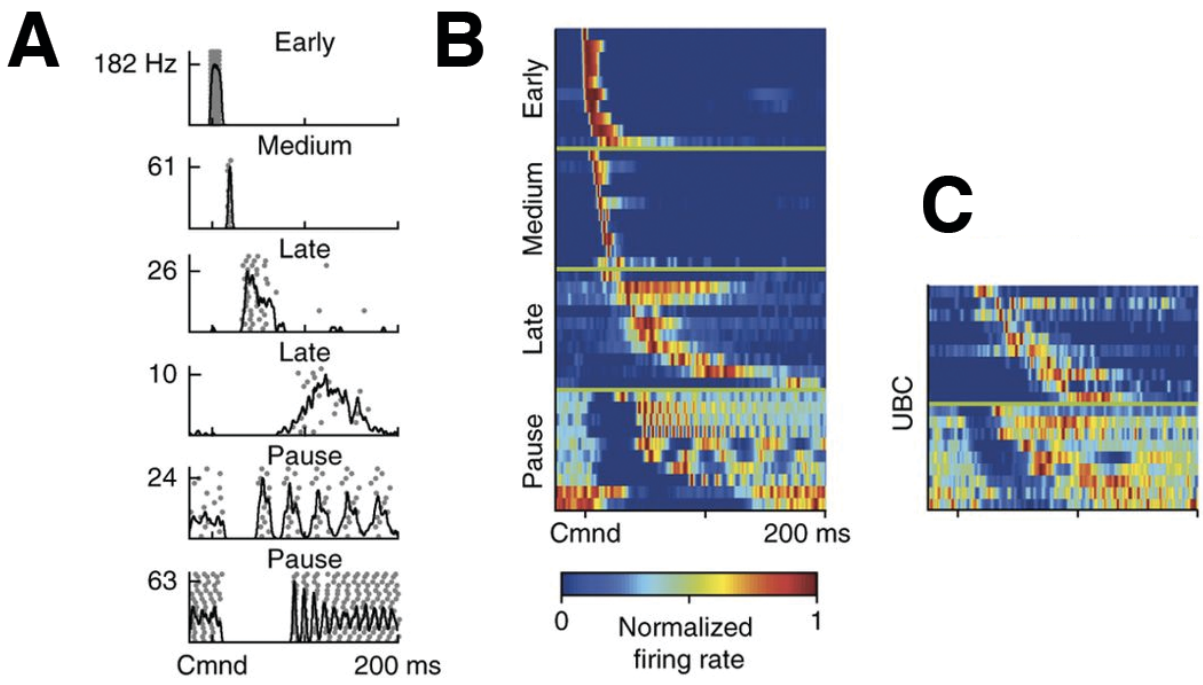

Figure 1.10 Mossy fiber and UBC responses to EOCD.
Example spike rasters (gray dots) and smoothed firing rates (black) of putative mossy fibers in response to corollary discharge, recorded extracellularly in EGp. Four temporal classes can be identified. (**B**) As in (A), but every line represents smoothed rate of a single cell, color corresponds to normalizing firing rate. (**C**) As in (B), but intracellularly recorded unipolar brush cells (UBC). Note similarity of identified UBC responses to 'Late' and 'Pause' responses recorded from mossy fibers. (duplicated from (Kennedy et al., 2014))

These characteristics, a cell that receives both peripheral sensory input and a corollary discharge input at a synapse that displays anti-Hebbian STDP, where that CD is available at multiple delays from the act itself, together constitute a mechanism by which negative images of self-generated sensory input can be formed. PF inputs that predict a postsynaptic (sensory) spike

are depressed, and all others are potentiated. While depression in the system is associative and N-Methyl-D-aspartate (NMDA) receptor dependent, potentiation is non-associative (Han et al., 2000a). Modelling work has shown that an anti-Hebbian learning rule is better at producing negative images and cancellation of self-generated sensory input than other types of learning rules (Roberts and Bell, 2000a). Early modeling work suggested that the system may work by way of a delay line, though (Kennedy et al., 2014) has shown otherwise. Work in gymnotids (Bastian, 1995) and elasmobranchs (Bodznick et al., 1999), and more recently mormyrids (Requarth and Sawtell, 2014) that the predictive signal need not be a CD but can be proprioceptive.

Despite the fact that decades of work have enlightened us as to the synaptic, cellular, and circuit mechanisms that produce negative images, until now it has remained unclear whether they serve any functional role for the animals that can form them, neither at the neural coding level nor at the level of behavior. On the one hand, a number of factors may prevent negative images from being useful – receptor saturation, nonlinearity of central neurons, error resulting from the subtraction of large negative images from large reafference. On the other hand, the role that negative-image-based cancellation has been assumed to hold may be performed by alternative mechanisms demonstrated to function in other systems, and theoretically in this one – common mode rejection, center-surround receptive fields, spatial filtering. In the following chapter, I will discuss these possibilities in further detail and demonstrate that negative images as formed in the mormyrid ELL do in fact have a functional role in improving neuronal coding of prey-like stimuli by predicting and removing the consequences of self-generated reafference, and the effect is seen at the behavioral level.

Chapter 2

Internally-generated predictions enhance neural and behavioral detection of sensory stimuli in an electric fish

Introduction

The notion that internally-generated predictions of the sensory consequences of behavior play vital roles in sensory processing and motor control has a long history (Grüsser, 1986). Seminal behavioral experiments performed in fish and flies in the 1950's suggested that corollary discharge signals cancel inappropriate reflexes that would otherwise be triggered by sensory reafference from voluntary movements (Sperry, 1950; von Holst and Mittelstaedt, 1950). Although fixed gating or generalized suppression of sensory responses by corollary discharge has been demonstrated in a variety of systems (Krasne and Bryan, 1973; Poulet and Hedwig, 2007; Richmond and Wurtz, 1980; Roberts and Russell, 1972; Zipser and Bennett, 1976), such mechanisms seem insufficient in cases where the effects of a motor command are complex, of long duration, or vary over time (e.g. due to growth, fatigue, or injury). Von Holst and others posited that the nervous system learns and stores negative images that are highly specific to the sensory consequences of particular motor acts (von Holst, 1954). Studies of cerebellum-like structures in three separate groups of fish have provided compelling neural correlates of such negative images and have elucidated their synaptic, cellular, and circuit mechanisms at a level of detail that has thus far not been possible in other systems (but see (Brooks et al., 2015; Kim et al., 2015; Leinweber et al., 2017). Rather than cancelling specific reflexes, negative images in electrosensory systems are hypothesized to play a more general function, namely, to cancel self-generated sensory input so that unpredictable, behaviorally relevant stimuli can be processed more effectively (Bell et al., 1997a; Bell, 2001; Bodznick et al., 1999). The present study takes advantage of unique features of the passive electrosensory system of weakly electric mormyrid fish to directly test this hypothesis.

Mormyrid fish, as well as a number of non-electrogenic fish, use a passive electrosensory system to detect small low-frequency electric fields generated by invertebrate prey (Bodznick and Montgomery, 2005). Detecting these signals is more complex for mormyrids, however, because, at the same time, they employ an electromotor system for both navigation and communication that involves the repeated generation of large pulsed electric fields known as electric organ discharges (EODs). Each EOD pulse sets the highly sensitive electroreceptors of the passive system into a ringing pattern of activation lasting 100-200 ms (Bell and Russell, 1978), as long as the typical interval between successive EOD pulses. Thus, downstream circuits of the passive electrosensory system face the challenge of pulling out small prey-related signals from ongoing, large-amplitude EOD-induced firing rate modulations in electroreceptor afferents (see **Figure 1** for an illustration of this problem). Moreover, since the frequency content of prey-evoked responses overlaps with that of EOD-evoked responses (Bell and Russell, 1978; Wilkens and Hofmann, 2005; Engelmann et al., 2010), temporal filtering is likely insufficient to solve this problem. Nevertheless, studies of foraging behavior in mormyrid fish have demonstrated that the passive electrosensory system plays a role prey detection even when other sensory modalities, including the active electrosensory system, are also used (Bleckmann and von der Emde, 1998).

Although it is easy to imagine how cancelling the effects of the EOD through the generation of negative images could enhance sensory processing (**Figure 2.1**), there are numerous reasons why such a scheme might fail to explain prey detection. For example, if the EOD saturates the electroreceptors, subtracting a negative image would not be sufficient to recover signals related to external stimuli. Other nonlinear properties of neurons in ELL might prevent the simple subtraction process schematized in **Figure 2.1** from being effective, or noise associated with such a subtraction might swamp tiny signals related to prey. Alternatively, non-

plastic mechanisms, rather than negative images, might play dominant roles in minimizing the effects of the EOD. Such mechanisms could include spatial filtering (BODZNICK and MONTGOMERY, 1992; Montgomery, 1984b; Montgomery and Bodznick, 1993b) or reductions in neuronal gain (Bastian, 1986; Rotem et al., 2007; Schneider et al., 2014).

Here we report on a series of experiments that addresses these issues and provides, to our knowledge, the first direct evidence that negative images enhance the neural coding and behavioral detection of external electrosensory stimuli. We also use pharmacological manipulations of synaptic plasticity in the ELL to provide support for a mechanistic model linking granule cell temporal representations, spike timing-dependent plasticity, and negative image formation (Bell et al., 1997b; Kennedy et al., 2014; Roberts and Bell, 2000b).

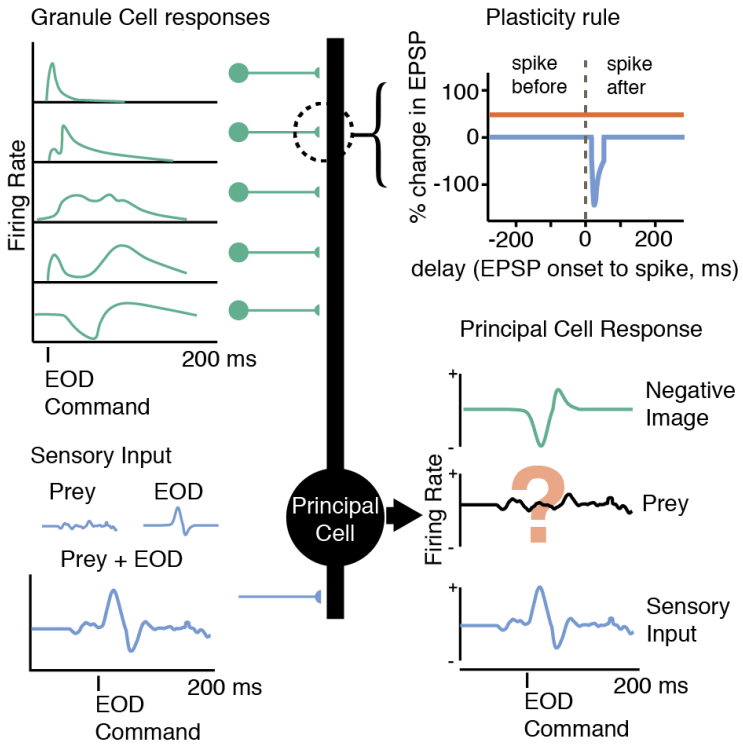

Figure 2.1 Schematic illustrating hypothesized role of negative images in enhancing neural coding of external stimuli.
ELL principal cells (center, black) receive sensory input via electroreceptors (lower left, blue) along with centrally-originating motor corollary discharge input via granule cells (upper left, green). The sensory input contains behaviorally relevant signals related to external objects, such as prey, contaminated by the response to the fish's own EOD. Previous results have provided evidence for negative images (lower right, green) formed by anti-Hebbian plasticity consisting of associative synaptic depression (upper right, blue) and non-associative synaptic potentiation (upper right, red) acting on a temporally diverse set of granule cell corollary discharge inputs (upper left, green). A major remaining question is whether such mechanisms are actually sufficient to allow principal cells to detect tiny prey-like signals despite interference due to the fish's EOD (lower right).

Results

ELL Neurons Respond to Prey-Like Stimuli despite Self-Generated Interference

Past studies of mormyrid fish have focused on characterizing negative images and their mechanisms but have never directly tested whether ELL principal neurons can detect external electrosensory stimuli in the presence of self-generated electrosensory input caused by the EOD. We recorded extracellular action potentials from electroreceptor afferent fibers terminating within the first central stage of passive electrosensory processing, known as the ventrolateral zone (VLZ) of the ELL. At the same time, we delivered small, low-frequency electrical stimuli via a dipole electrode positioned in the water near the electroreceptor innervated by the recorded fiber (**Figure 2.2A**). Such localized electrical stimuli mimic the electrical fields generated by the fish's invertebrate prey (Chacron et al., 2003; Doiron et al., 2003). In our preparation, neuromuscular paralysis blocks the EOD (the electric organ is a modified muscle) but the fish is unanesthetized and continues to spontaneously emit the motor command that would discharge the electric organ at rates of 3-5 Hz. After each spontaneously emitted EOD motor command (**Figure 2.2B**, green lines) we delivered a short electrical pulse that mimics the fish's EOD (see STAR Methods). In other experiments (**Figure 2.6, Figure 2.7, Figure 2.10**) we took advantage of this same setup to probe responses to corollary discharge in isolation from electrosensory input by turning the EOD mimic off or to probe the response to electrosensory input in isolation from corollary discharge by deliver the EOD mimic independently of the command.

Consistent with previous reports, electroreceptor afferents exhibit highly regular action potential firing at rates around 50 Hz in the absence of stimulation (Bell, 1982; Engelmann et al., 2010). As can be seen in the traces in **Figure 2.2B**, the EOD mimic evoked large firing rate modulations that masked responses to the prey-like stimulus. An off-line digital subtraction of the average response to the EOD revealed a reliable underlying encoding of the prey-like

stimulus (**Figure 2.2B**, dashed line). This observation is important because it rules out the possibility (mentioned in the Introduction) that the EOD prevents afferents from encoding prey-like signals entirely, for example by saturating their responses.

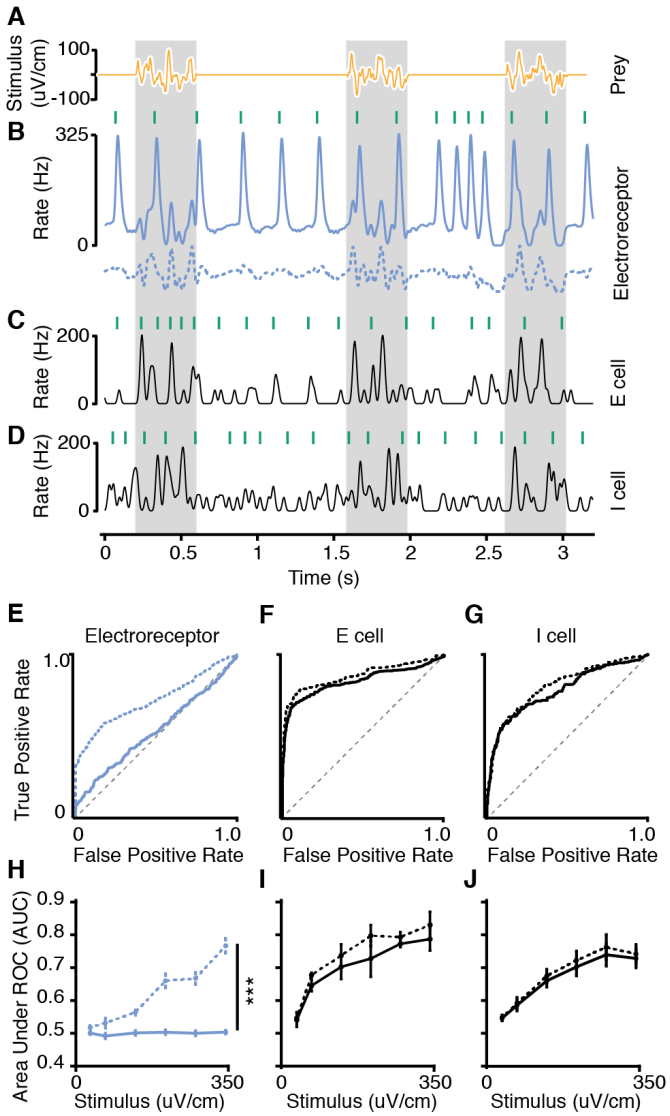

Figure 2.2 Accurate detection of prey-like stimuli in ELL despite self-generated interference
(A) Three repetitions of a prey-like stimulus consisting of 400 ms presentations of 5-20 Hz bandpassed noise. (B) Smoothed firing rate of an example electroreceptor afferent before (solid line) and after (dashed line) off-line subtraction of the average response of the afferent to the EOD. Green lines indicate the times of EOD commands emitted spontaneously by the fish. An EOD mimic pulse (0.2 ms duration) was delivered 4.5 ms after each EOD command. (C,D) Smoothed firing rates of example E and I cells in

response to a prey-like stimulus (stimulus amplitude and waveform same as used for B). (E) Quantification of prey-like stimulus detection for the example electroreceptor afferent in B. ROC curve was calculated based on the peak firing rate in 100 ms periods following the EOD. Gray dashed line indicates chance detection. Solid line indicates prey detection performance in the presence of the EOD. Area under ROC curve (AUC) (unsubtracted) = 0.53. Dotted line indicates detection performance after subtracting the average response to the EOD (dashed line in B). AUC (subtracted) = 0.72. (F) Quantification of prey-like stimulus detection for the example E cell in C. AUC (unsubtracted) = 0.84. AUC (subtracted) = 0.87. (G) Quantification of prey-like stimulus detection for the example I cell in D. AUC (unsubtracted) = 0.78. AUC (subtracted) = 0.81. (H) Summary of detection performance for electroreceptor afferents (n = 21) across a range of stimulus amplitudes before (solid line) and after (dashed line) off-line subtraction of the effects of the EOD. Mean AUC across stimulus intensities for electroreceptor afferents (n = 21) was greater after subtracting the effect of the EOD, $P < 0.0001$, one-tailed Wilcoxon signed rank test. Statistically significant differences are indicated by asterisks. (I) Summary of detection performance for E cells (n = 8). Mean AUC (unsubtracted) across stimulus intensities was greater for E cells than for afferents, $P < 0.0001$, one-tailed Wilcoxon rank sum test. (J) Summary of detection performance for I cells (n = 22). Mean AUC (unsubtracted) across stimulus intensities was greater for I cells than for afferents, $P < 0.0001$, one-tailed Wilcoxon rank sum test.

Identical experiments were performed while recording from principal cells in the VLZ. There are two main classes of ELL principal cells, termed E and I cells. Both are glutamatergic neurons that convey the output of ELL to higher stages of electrosensory processing in the midbrain (Bell, 1982) (see Methods). E cells, like electroreceptor afferents, increase their firing rates when the voltage outside the electroreceptor is positive, while I cells increase their firing rates when the voltage outside the electroreceptor is negative (**Figure 2.3**). In contrast to electroreceptor afferents, firing rate modulations in E and I cells due to prey-like stimuli are larger than the effects of the EOD mimic as can be seen in the example traces (**Figure 2.2C,D**).

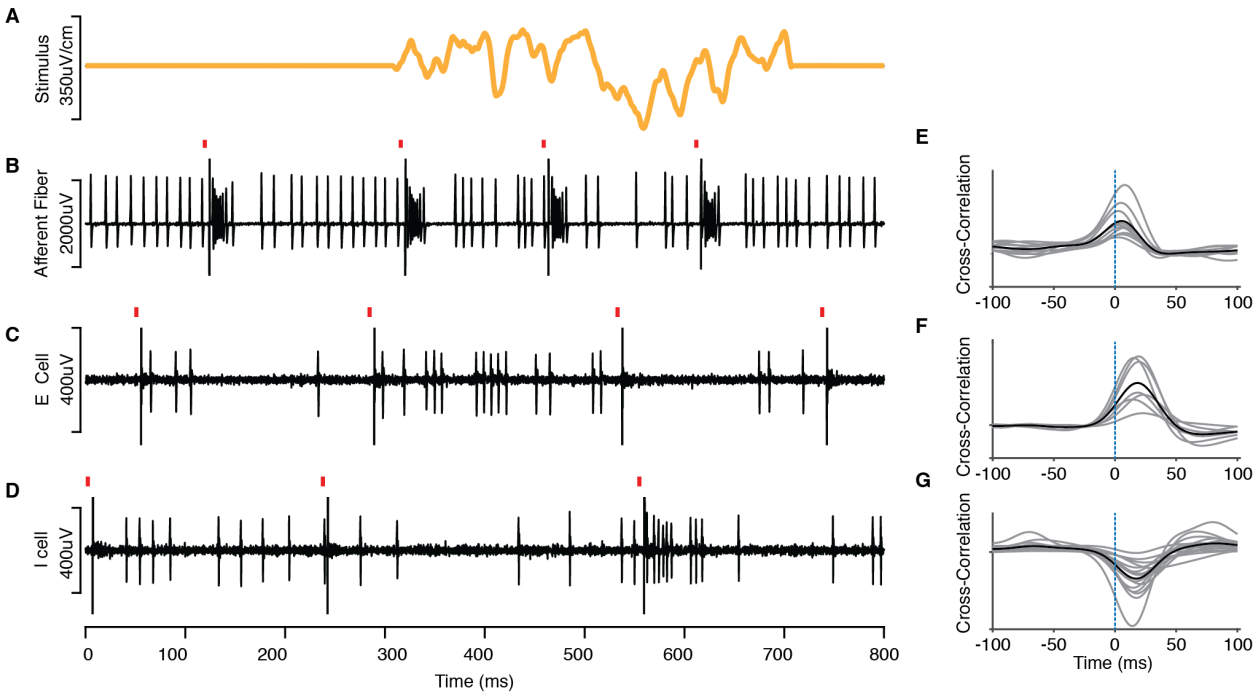

Figure 2.3 Basic properties of electroreceptor afferents, E cells, and I cells
(A) Prey-like stimulus waveform. (B) Sample voltage trace from an electroreceptor afferent recording. Red tics indicate the time of the EOD command and are followed by a stimulus artifact resulting from the delivery of the EOD mimic. Note the prominent bi-phasic response to the EOD mimic, a burst followed by a pause. Upstrokes and downstrokes in the prey-like stimulus evoke firing rate increases and decreases, respectively. (C) Sample voltage trace from an E cell recording. Note the minimal response to the EOD mimic, consistent with cancellation. Polarity of response to the prey-like stimulus is the same as for the electroreceptor afferent. (D) Sample voltage trace from an I cell recording. Note the minimal response to the EOD mimic, consistent with cancellation. Polarity of response to the prey-like stimulus is opposite that of the electroreceptor afferent and the E cell. (E-G) Gray lines, cross-correlations between the prey-like stimulus waveform and the firing rate for all the afferents (E), E cells (F), and I cells (G) included in the analysis for Figure 2.2. Black lines, average cross-correlation for each group.

Standard receiver operating characteristic (ROC) analysis was used to quantify these results (Dayan and Abbott, 2001). Such analysis confirmed that, in the presence of the EOD, detection of a prey-like stimulus based on afferent firing rate is poor over a wide range of stimulus amplitudes (**Figure 2.2E,H,** *solid lines*). An off-line subtraction of the average response to the EOD dramatically improved detection performance in afferents (**Figure 2.2E,H**, *dashed lines*). Detection performance in E and I cells is far better than that observed in electroreceptor afferents over a wide range of stimulus amplitudes, presumably due to cancellation of the effects of the EOD (**Figure 2.2F,G,I,J,** solid lines). This result was not sensitive to details of the ROC

analysis, such as the size of the analysis windows (**Figure 2.4**). Furthermore, off-line subtraction of EOD effects in E and I cells yields only small improvement in their detection performance (**Figure 2.2F,G,I,J,** *dashed lines*), consistent with the hypothesis that EOD effects are already subtracted by negative images. Together, these results show (1) that the EOD is a substantial source of self-generated interference for the passive electrosensory system of mormyrids and (2) that this interference is almost completely removed at the first central stage of processing in ELL.

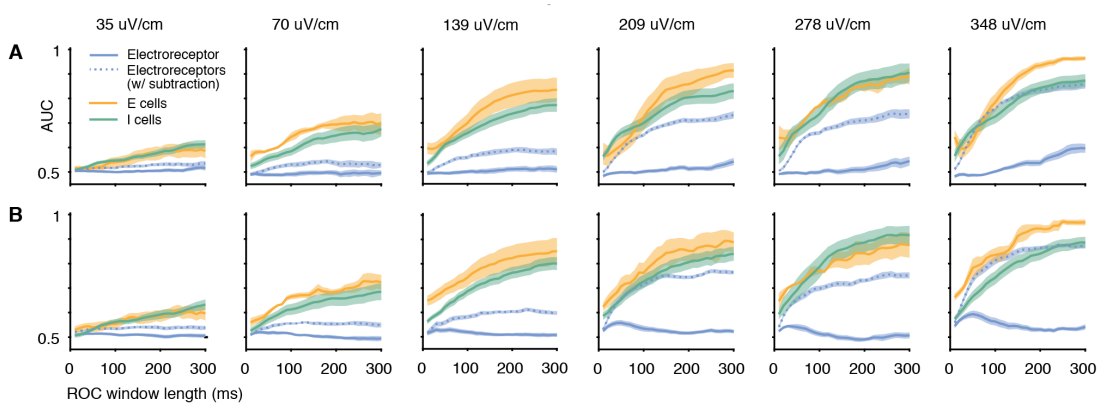

Figure 2.4 Superior detection in ELL principal cells versus electroreceptor afferents does not depend on ROC analysis window size
(**A**) AUC values as a function of the length of the analysis window (10- 300 ms), with the start of the window aligned to the time of the EOD. Rows show the same analysis for different prey-like stimulus amplitudes. Lines are averages and ribbons are SEM. Data are the same as for Figure 2.2. A value of 100 ms was used for the analysis in Figure 2. (**B**) Same as A, but for sliding analysis windows taken independent of the times of the EOD.

An important consideration for evaluating the function of negative images is the relative strength of electroreceptor responses evoked by prey versus those evoked by the EOD. We sought to confirm that our experiments were representative of natural conditions in this regard. We compared the strength of electroreceptor afferent responses evoked by artificial prey-like

stimuli to those evoked by actual prey (a live blackworm) (**Figure 2.5**). In the presence of a worm we observed increased variation in the normally highly-regular afferent firing rates. Large firing rate modulations were sometimes observed, presumably due to spontaneous movements of the worm which brought it very near to the pore of the electroreceptor innervated by the recorded afferent. Given the steep fall-off of electrical dipole fields with distance (Bodznick and Montgomery, 2005), a strong dependence of neural response magnitude on the exact location of the prey relative to the electroreceptor is expected. A comparison of the magnitude of firing rate variations in the presence of worms to those induced by artificial prey-like stimuli indicate that actual prey are capable of inducing firing rate modulations as large or larger than those used in the present study.

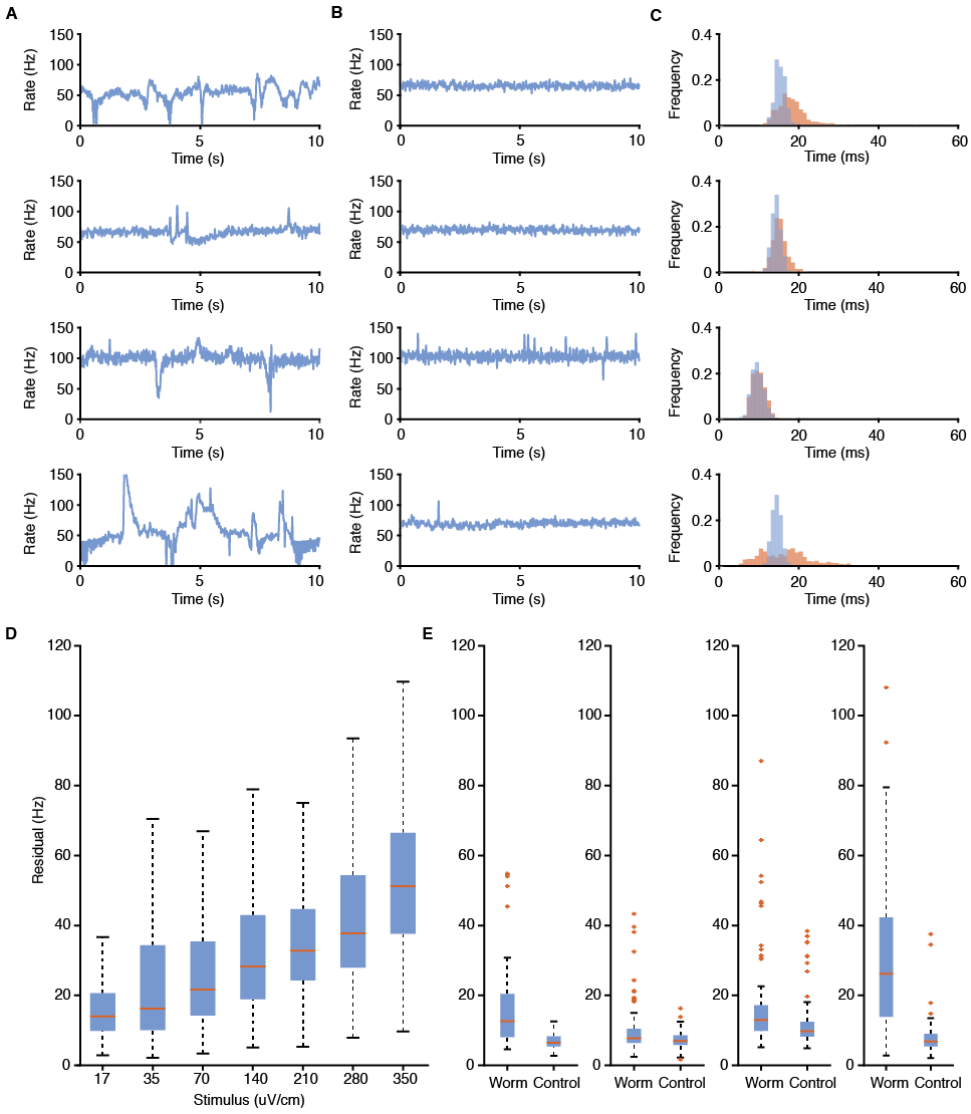

Figure 2.5 Electroreceptor responses to actual prey versus artificial prey-like stimuli
(**A**) Firing rate modulations due to blackworms in 4 electroreceptor afferents recorded in the VLZ. For the top 3 examples a live worm was attached to a glass pipette and positioned near the electroreceptor pore of the recorded afferent. The exact location of the worm relative to the fish depended on the movements and configuration of the wriggling worms, which were 1-1.5 cm in length. The bottom example shows the response to moving the cut tip of a worm glued to a pipette near the skin with a manipulator (distance < 5 mm). (**B**) Firing rates of the same afferents as in A but in the absence of worms. In the bottom example a glass pipette was moved near the pore but without a worm attached. (**C**) Inter-spike interval histograms in the presence (orange) and the absence (blue) of worms for the electroreceptor afferent recordings in A. (**D**) Firing rate residuals calculated as maximum deviations from the mean firing rate over sliding 100 ms windows for all electroreceptor afferents used in **Figure 2.2**. Box represents 25th-75th percentile, whiskers extend to 1.5*interquartile range. Outliers not plotted. (**E**) Firing rate residuals for responses of electroreceptor afferents to worms, as in **D**. Black dots represent data points > 2 S.D. from the mean. These data points likely come from periods when spontaneous movements of the worm brought it near the electroreceptor pore innervated by the recorded afferent. These results suggest that natural prey are capable of driving firing rate modulations as large or larger than the artificial prey-like stimuli used in this study.

Improvements in Neural Detection of Prey-Like Stimuli due to Negative Images

Although the results in **Figure 2.2** show a dramatic improvement in prey detection performance in E and I cells compared to electroreceptor afferents, they do not directly establish whether or to what extent this improvement is the result of negative images. Two approaches were devised to test this. The first takes advantage of our ability to decouple the EOD from the motor command that would normally evoke it, such that effects of the EOD on the neural detection of prey-like

stimuli can be tested in the same cell with and without negative images. Responses to prey-like stimuli in E and I cells were measured while delivering EOD mimic pulses paired with the fish's spontaneously emitted EOD motor commands, similar to the experiments shown in **Figure 2.2**, but with the addition of interleaved EOD mimics delivered independent of the fish's commands (**Figure 2.6A**). EOD commands were paired with the mimic for at least 2 hours prior to recording, to allow negative images to form. As expected based on past studies (Bell, 1981, 1982), E and I cell responses to EOD mimics paired with the command were reduced or, in some cases, completely cancelled (**Figure 2.6B**). In contrast, EOD mimics delivered independent of the command evoked strong responses (**Figure 2.6C**). Probing the response to the command alone revealed temporally-specific negative images of the effect of the EOD mimic (**Figure 2.6D**). Such negative images can account for the reduction of the response to EOD mimics paired with the command relative to those delivered independent of the command.

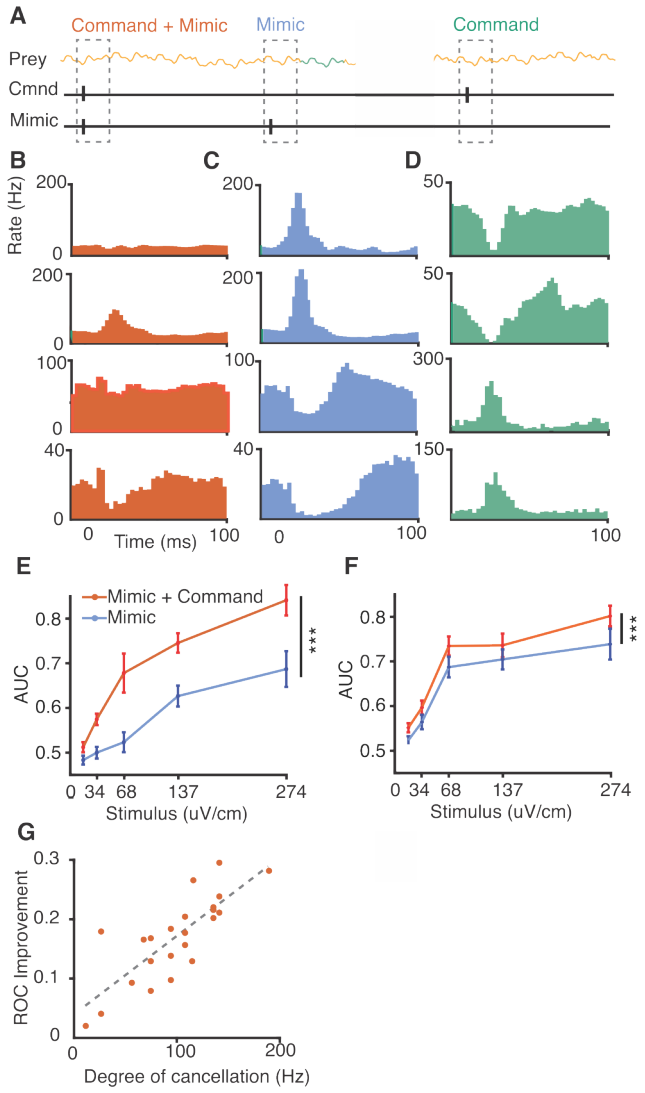

Figure 2.6 Improvements in neural detection of prey-like stimuli due to negative images
(**A**) Schematic of the experimental design. Neural detection of prey-like stimuli was quantified using ROC curves calculated for 100 ms periods following the EOD mimics paired with commands (red) as well as for interleaved mimics delivered independent of the command (cyan). (**B**) Firing rate histograms triggered on the EOD command for two example E cells (top two rows) and two example I cells (bottom two rows). (**C**) Histograms triggered on an identical EOD mimic delivered independent of the command in the same cells. (**D**) Histograms triggered on the EOD command without an EOD mimic reveal negative images of the effects of the mimic in the same cells. (**E,F**) Summary comparing detection performance for E cells (n = 17) and I cells (n = 31) in time windows following EOD mimics paired with the command (red) versus mimics delivered independent of the command (cyan). Mean AUC across stimulus intensities was greater when the mimic was paired with the command for both E and I cells, $P < 0.0001$ and $P < 0.0001$, respectively, one-tailed Wilcoxon signed rank test. (**G**) For E cells, improvements in AUC value for the paired versus independent condition is correlated on a cell by cell basis with the degree of cancellation of the EOD mimic in the paired condition, $R^2 = 0.57$.

Prey-like stimulus detection performance was better in time-windows following EOD mimics paired with commands compared to time-windows following EOD mimics delivered independent of the command (**Figure 2.6E,F**). Since the only difference between the two conditions in this experiment is the timing of the EOD mimic relative to centrally-originating electric organ corollary discharge signals, improvements in neural coding can be directly attributed to negative images. For E cells the difference in detection performance in the two conditions (EOD mimics paired versus independent of the command) was correlated on a cell-by-cell basis with the extent to which responses to the EOD mimic were cancelled by the negative image (**Figure 2.6G**). No such correlation was observed for I cells, possibly due to the fact that EOD mimic sometimes drove the spike rate to zero. Since the magnitude of the response to the mimic cannot be determined in such cases, our estimate of the magnitude of cancellation is expected to be less accurate for I cells than for E cells.

A second approach takes advantage of our ability to rapidly induce negative image formation, such that the neural detection of prey-like stimuli can be tested in the same cell over before, during, and after negative images have formed (**Figure 4A**). For these experiments EOD mimics were delivered in the same spatial configuration as prey-like stimuli, i.e. locally within the receptive field of the recorded unit in contrast to the more spatially uniform EOD mimics used in **Figure 2.2** and **Figure 2.6** (see **Methods**). Such conditions mimic situations in which the spatial pattern of EOD-induced current flow through the skin changes, e.g. due to the location of the fish relative to large objects or non-conducting boundaries. In addition, characterizing detection performance in a situation where the spatial characteristics of the EOD mimic and the prey-like stimulus match rules out a role for spatial filtering mechanisms in enhancing detection.

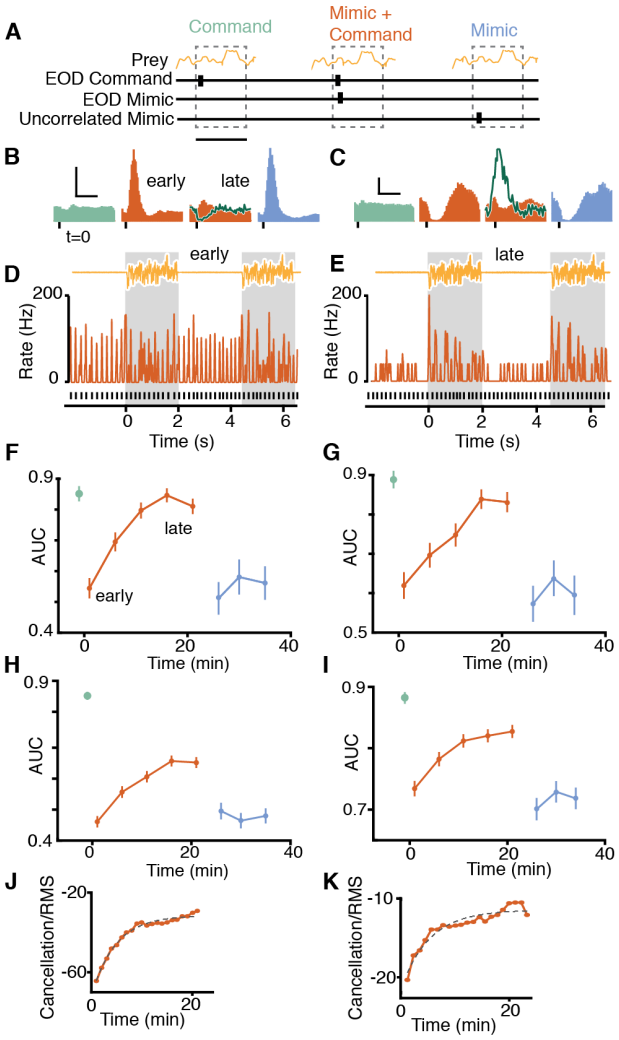

Figure 2.7 Time course of improvement in neural detection of prey-like stimuli due to negative images

(**A**) Schematic of the experimental design. Neural detection of prey-like stimuli was quantified using ROC curves calculated for baseline periods in which the fish issued EOD commands but no EOD mimics were delivered (green), pairing periods in which an EOD mimic was delivered following each command (red), and periods in which EOD mimics were delivered independent of the command (cyan). AUC was calculated over 100 ms windows following command or mimic onset. Scale bar: 100 ms. (**B,C**) Firing rate histograms triggered on EOD command or mimic for example E and I cells. Note the reduction in the response to the EOD mimic during pairing (early versus late) due to the formation of a negative image (green line, late). Scale bars: 50 Hz, 50 ms in B and 30 Hz, 50 ms in C. (**D,E**) Smoothed firing rate early versus late in the pairing period for the E cell shown in B. Black lines indicate time of EOD command and yellow trace shows two prey-like stimulus presentations. Firing rate modulations evoked by the prey-like stimulus are masked by the effects of the EOD early during pairing but become evident late in pairing

due to cancellation. (**F,G**) Time course of neural detection performance quantified using ROC analysis for the same example E and I cells. Error bars are S.E.M. calculated for repeated prey-like stimulus presentations. (**H**) Averaged data for E cells (n = 5), error bars are the S.E.M. across cells. Detection performance drops at the onset of pairing the command with an EOD mimic, $P < 0.0001$ and subsequently improves during pairing, $P < 0.0001$, multiple linear regression. For EOD mimics presented independent of the command, performance drops, $P < 0.0001$ but does not improve, $P = 0.83$, multiple linear regression. (**I**) Averaged data for I cells (n = 6) as in (G). Detection performance drops at the onset of pairing, $P < 0.0001$, and subsequently improves, $P = 0.034$, multiple linear regression. For mimics presented independent of the command, performance drops, $P < 0.0001$ and does not improve, $P = 0.73$, multiple linear regression. (**J**) Time course of cancellation of the effects of the EOD mimic during pairing for E cells as measured by the root mean square amplitude of the firing rate. Same data as in H. Dashed line indicates exponential fit. Adjusted R^2 =0.98. (**K**) Same display as J for I cells (n = 6). Adjusted R^2 =0.91.

E and I cells exhibit stable responses with little or no response to the EOD command alone prior to pairing with an EOD mimic (**Figure 2.7B,C,** light green). Pairing an EOD mimic with the command resulted in strong initial firing rate modulations that diminished over 10-20 minutes or ~2,500-5,000 commands (**Figure 2.7B,C**, red, compare *early* and *late*). Turning the mimic off revealed a temporally-specific negative image of the response to the mimic during pairing (**Figure 2.7B,C,** dark green), consistent with previous studies. The larger negative images observed at the level of firing rates in I versus E cells is likely due to rectification, as such differences are not observed in intracellular recordings of the subthreshold membrane potential (Bell et al., 1997a; Mohr et al., 2003). Finally, delivering the same EOD mimic independent of the command evoked a strong response similar to that observed at the start of pairing (**Figure 2.7B,C,** cyan*)*, consistent with the diminished response late in pairing being due to negative images rather than fatigue or peripheral adaptation. This pattern of results is consistent with previous studies (Bell, 1981, 1982).

The novelty of these experiments was to simultaneously deliver prey-like stimuli uncorrelated with the fish's EOD commands (**Figure 2.7D,E**), such that neural detection performance could be quantified before, during, and after negative image formation. Example E and I cells are shown in **Figure 2.7F,G** and averages across cells of each type are shown in

Figure 2.7H,I. Prey detection performance was initially high in the absence of an EOD mimic (**Figure 2.7F-I,** green) and dropped sharply when an EOD mimic was paired with the command (**Figure 2.7F-I,** red). We observed a gradual increase in detection performance during pairing, consistent with a role for negative images in improving neural coding (**Figure 2.7F-I,** early versus late). Finally, when we delivered the same EOD mimic but now independent of the EOD command detection performance dropped once again (**Figure 2.7F-I**, cyan). No gradual improvements in detection performance were observed in this condition, consistent with the observation that negative images only form when stimuli are time-locked to the fish's EOD command. The time course of improved prey detection performance during pairing matched the time course over which the effects of the EOD were cancelled in the same units (**Figure 2.7J,K**), again consistent with negative images improving neural coding of prey-like stimuli.

Though it is hypothesized that negative images perform a pure subtraction of the effects of the EOD, allowing ELL neurons to selectively encode behaviorally relevant stimuli, this has never been directly tested. Alternatively, corollary discharge inputs could reduce neural sensitivity to sensory inputs during behavior (Bastian, 1986; Rotem et al., 2007; Schneider et al., 2014). We looked for evidence of a change in the sensitivity of principal cell responses to prey-like stimuli that could contribute to changes in detection performance. Inspection of the responses of the E and I cells used in **Figure 2.7** revealed that firing rate modulations tracked the waveform of the prey-like stimulus with no changes in the root mean squared amplitude of responses early versus late during pairing with an EOD mimic (**Figure 2.8A-D**). Instead, we observed a clear reduction in the standard deviation of the response to prey-like stimuli late in pairing (**Figure 2.8E-G**). Because the timing of the EOD mimics are controlled by the fish and are uncorrelated with the prey-like stimulus, strong responses evoked by the EOD mimic early in

the pairing period contribute to the variance of the response to the prey-like stimulus. Hence the reduction in the standard deviation of the response to prey-like stimuli late in the pairing period is consistent with the improvements in neural detection performance being due mainly or entirely to the subtraction of a negative image without any overall changes in sensitivity to the prey-like stimulus.

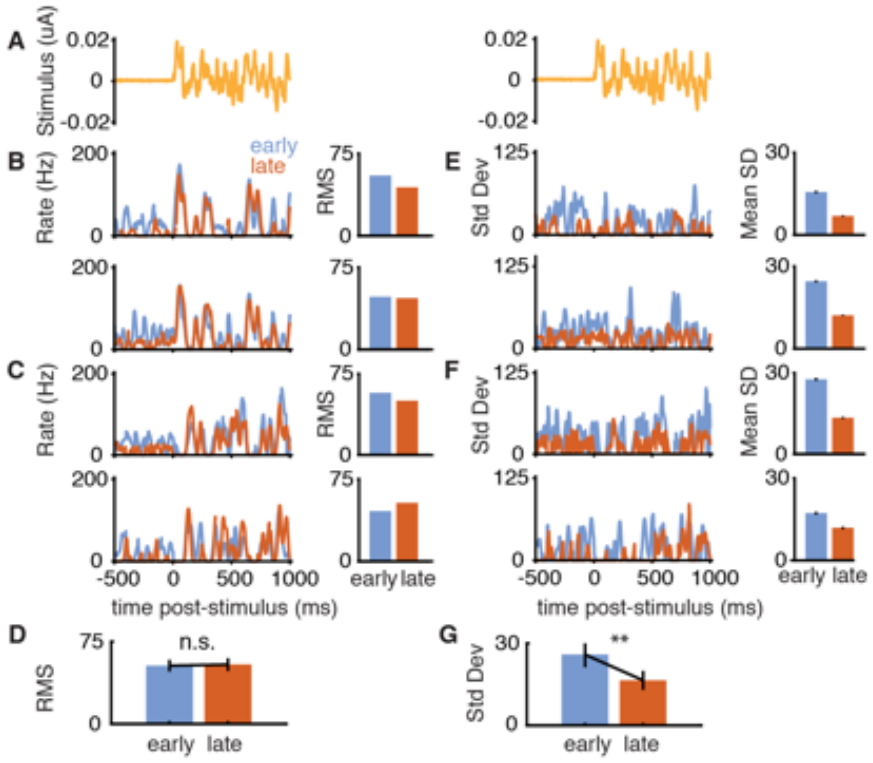

Figure 2.8 Cancellation reduces the variance of responses to prey-like stimuli.
(**A**) Prey-like stimulus waveform consisting of 2 seconds of frozen noise. (**B**) Left, firing rate of two example E cells averaged over multiple presentations of a prey-like stimulus early (first 2 minutes) versus late (last two minutes) in the pairing period. Only period 100 ms following the command are included in the averages. Right, root mean square (RMS) amplitude of the firing rate during the prey-like stimulus period for the same cells. (**C**) Same displays for two example I cells. (**D**) RMS amplitude of prey-like stimulus responses is not different early versus late during pairing for all E and I cells shown in Figure 4 (n = 11, $P = 0.831$, two-tailed Wilcoxon signed rank test). (**E**) Left, standard deviation of the firing rate of

two example E cells over multiple presentations of a prey-like stimulus early versus late in the pairing period (same cells as in **B**). Right, standard deviation of the firing rate during the prey-like stimulus period for the same cells. (**F**) Same displays for two example I cells (same cells as in **C**). (**G**) Standard deviation of prey-like stimulus responses is reduced late versus early during pairing (n = 11, $P = 0.00195$, two-tailed Wilcoxon signed rank test).

Enhanced Behavioral Responses to Prey-Like Stimuli associated with Negative Image Formation

Are the improvements in neural detection performance we observed accompanied by improvements at the behavioral level? To address this question, we took advantage of an electromotor behavior that can be readily measured in paralyzed fish under the same experimental conditions as the neural recordings described above. The electromotor novelty response (NR) is a transient increase in the rate of the EOD command elicited by a sensory stimulus (**Figure 2.9A**). This behavior has been studied extensively in weakly electric fish and shares characteristics with orienting responses in other vertebrates (Hall et al., 1995; Post and von der Emde, 1999). As in past studies, we use it as a behavioral indication that the fish has detected an external stimulus (Hall et al., 1995).

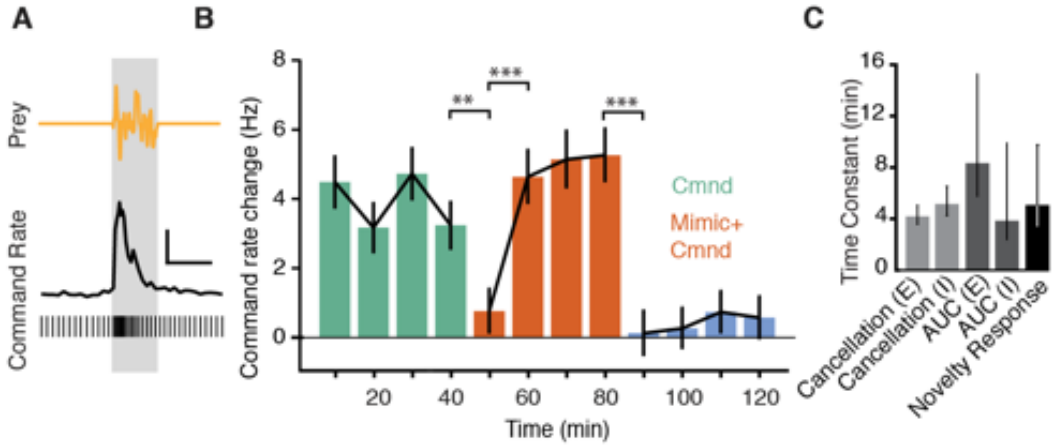

Figure 2.9 Improvements in behavioral responses to prey-like stimuli associated with negative image formation

(**A**) Sample EOD command times (bottom) and smoothed EOD command rate illustrating an abrupt increase in rate, the novelty response, evoked by the presentation of a prey-like stimulus (gray bar). Scale bar: 5 Hz, 2 seconds. (**B**) Command rate changes evoked by a prey-like stimulus during baseline periods in which the fish issued EOD commands but no EOD mimics were delivered (green), pairing periods in which an EOD mimic was delivered following each command (red), and periods in which EOD mimics were delivered independent of the command (cyan) (n = 12 repetitions of the experiment performed in 8 fish). Behavioral detection of prey-like stimuli, as measured by command rate changes, is stable during the first phase, $P = 0.31$, Friedman's non-parametric test; decreases on initial presentation of EOD mimic, $P = 0.0038$, Friedman's non-parametric test; and then improves during pairing, $P < 0.001$, Friedman's non-parametric test. Detection drops when the EOD mimic is delivered independent of command, $P < 0.001$ and does not improve, $P = 0.24$, Friedman's non-parametric test. (**C**) Time constants of cancellation of the effects of the EOD during pairing, improvements in neural detection or prey-like stimuli during pairing, and increases in behavioral responses to prey-like stimuli during pairing are similar.

We quantified the amplitude of NRs evoked by a prey-like stimulus. The experimental design, including both the prey-like stimulus and the EOD mimic amplitudes and spatial configurations were identical to those used for the neural recording experiments described in **Figure 2.7**. A baseline level of NRs was established by delivering prey-like stimuli in the absence of an EOD mimic (**Figure 2.9B,** green). Pairing a local EOD mimic with the command resulted in an initial drop in NR amplitude followed by a gradual return to baseline levels (**Figure 2.9B,** red), presumably due to the formation of negative images. When the EOD mimic was delivered independently of the EOD command NR amplitudes again dropped but without a gradual return to baseline (**Figure 2.9B,** cyan). The lack of improvement in responses to prey-like stimuli in this condition is presumably because negative images cannot form (Bell, 1982). Hence changes in behavioral detection of prey-like stimuli closely mirrored changes in neural detection performance measured under the same conditions. Moreover, cancellation of the effects of the EOD, improvements in neural detection performance quantified using ROC analysis, and improvements in behavioral detection performance measured using the NR all exhibited a similar timecourse (**Figure 2.9C)**. These results suggest that negative image formation not only improves the detection of prey-like stimuli at the level of neural coding in ELL but also enhances behavioral responses.

Manipulating Synaptic Plasticity in ELL disrupts Neural Coding and Behavioral Responses to Prey-Like Stimuli

To provide a causal test of the hypothesis that negative images improve prey coding and detection, we attempted to block the associative synaptic plasticity underlying negative image formation. *In vitro* studies have demonstrated that anti-Hebbian synaptic plasticity in ELL depends on N-Methyl-D-aspartate (NMDA) receptors (Bell et al., 1997b; Han et al., 2000b). Micropressure injections of the NMDA receptor antagonist 2-amino-5-phosphonopentanoic acid (AP5) into the VLZ molecular layer (**Figure 2.10A**) led to gradual changes in the responses of ELL principal cells to the EOD command. By 10-20 minutes after AP5 injections both E and I cells exhibited increased firing with a prominent peak at a short delay (~15-20 ms) after the command and subsequent pairing with an EOD mimic failed to induce negative images (**Figure 2.10B, Figure 2.10**). Such large, sharply peaked command responses are never observed in the VLZ of naïve fish and are opposite to what would be expected if AP5 acted mainly to block excitatory synaptic transmission. Moreover, E and I cell responses to the EOD mimic (delivered independently of the command) were unchanged in the presence of AP5 (**Figure 2.10**). In an additional set of experiments we compared the effects of AP5 application on command responses and negative image formation with several agents reported to block long-term depression (LTD) in other systems and brain regions (Bear and Malenka, 1994; Jörntell and Hansel, 2006). We obtained preliminary data for an effect of the broad spectrum kinase inhibitor H7 and no effect of phosphatase inhibitors (**Figure 2.12**), suggesting a similarity with LTD in Purkinje cells and the gymnotid ELL (Belmeguenai and Hansel, 2005; Harvey-Girard and Maler, 2013; Harvey-Girard et al., 2010). However, since the effects of H7 were not as large and consistent across cells as

those of AP5 and since there is no *in vitro* data confirming the effects of H7 in the mormyrid ELL, we chose to use AP5 for further experiments.

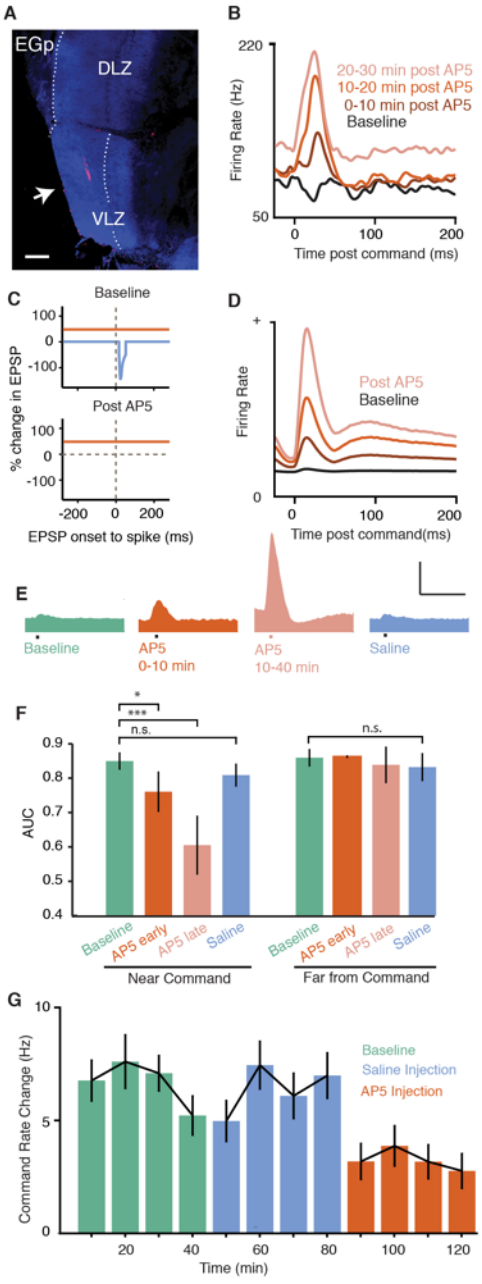

Figure 2.10 Manipulating synaptic plasticity in ELL disrupts neural and behavioral detection of prey-like stimuli
(A) Fluorescent dextran (arrow) marks micropressure injection site of the NMDA receptor antagonist AP5 into the ELL molecular layer. Dotted line marks the boundary between the molecular and ganglion

cell layers of VLZ. EGp = eminentia granularis posterior, VLZ = ventrolayeral zone, DLZ = dorsolateral zone. Scale bar = 100 um. (B) Smoothed firing rate triggered on the EOD command for an example E cell before and after an AP5 injection. (C) Schematic of plasticity rule in ELL principal cells under normal conditions (top) and with NMDA receptors blocked (bottom). (D) Changes in EOD command responses in a model ELL principal cell induced by setting the rate of associative synaptic depression to zero (compare with panel **B**). (E) Average command responses of ELL principal cells before AP5 injection (n = 40, green)) (left), 0-10 minutes after injection (n = 3, red), 10-40 minutes after injection (n = 11, light red), and following saline injections (n = 22, blue). Scale bar: 100 Hz, 50 ms. (F) Left, prey-like stimulus detection quantified in 100 ms windows triggered on the EOD command before (green), 0-10 minutes after (dark red) and 10-40 minutes after (light red) AP5 injection and following saline injection (blue). Same data as in E. AP5 injection resulted in a significant decrease in detection performance at 10-40 minutes, $P < 0.0001$, one-tailed Wilcoxon rank sum test. No significant changes in detection performance were observed after saline injections or when detection performance was quantified late in the command cycle when effects of AP5 on firing rate were minimal (right, 100 ms analysis window beginning 100 ms after the command). (G) Command rate changes evoked by a prey-like stimulus during a baseline condition (green) and following micropressure injections of saline (blue) or AP5 (red) into the ELL molecular layer. AP5 injections reduced command rate changes evoked by a prey-like stimulus, $P < 0.0001$, whereas saline injections had no effect (P = 0.97, Friedman's non-parametric test, n = 6 repetitions of the experiment in 6 fish).

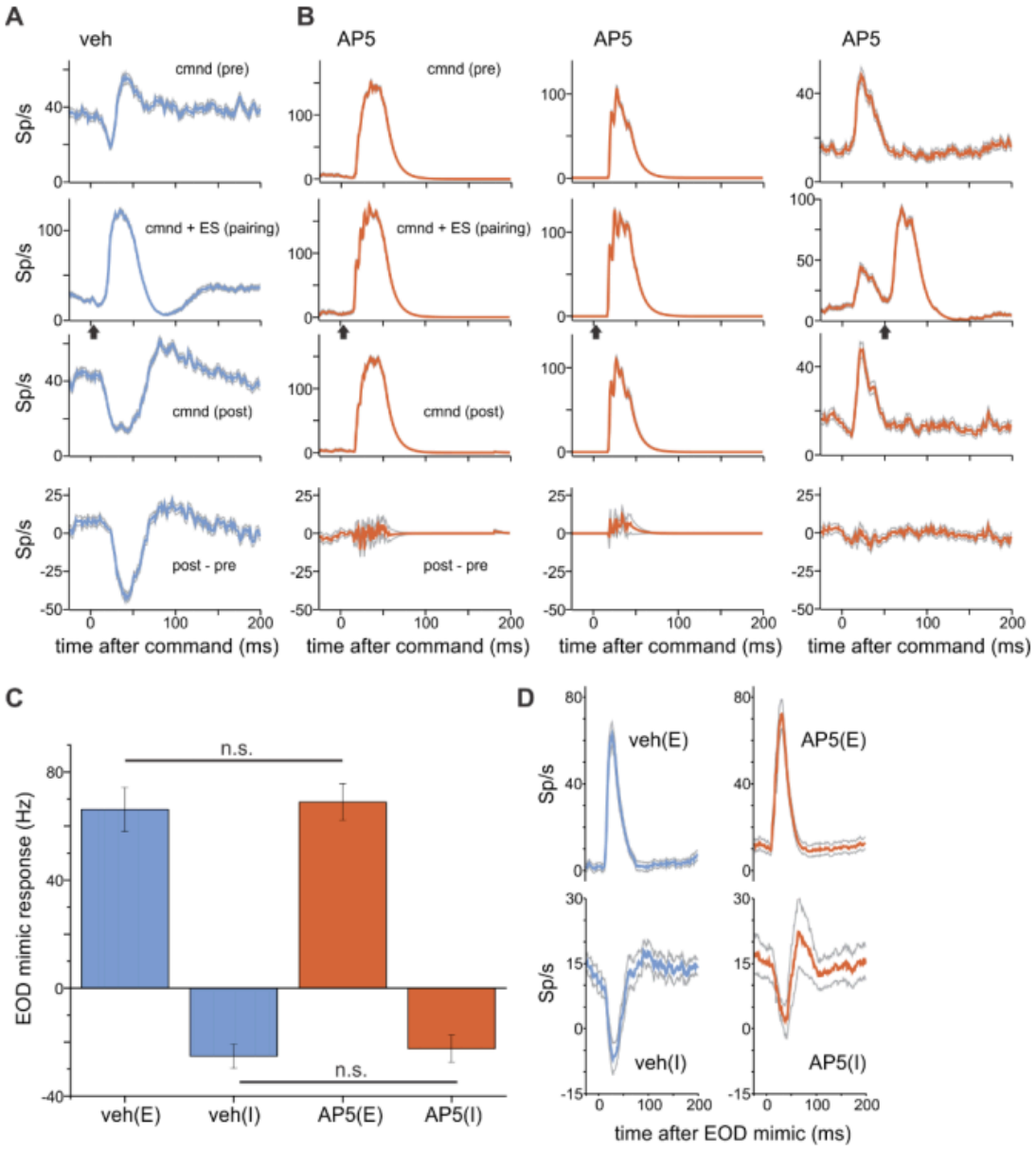

Figure 2.11 Effects of NMDA receptor blockade on negative image formation and responses to the EOD mimic in ELL neurons

(A) Example cell from the vehicle condition showing the formation of a negative image (bottom panels) after 4 minutes of pairing the command with an EOD mimic (-25 uA, arrow). The difference in the command response after pairing (post-pre, bottom row) is temporally matched and opposite in polarity to the response during pairing (2nd row). Gray outline are s.e.m. (B) Three cells from the AP5 condition showing the failure of pairing to induce negative images. Conditions for pairing are the same as for the veh condition. Note the prominent responses to the EOD command alone (see main text for explanation). (C) Average peak or trough firing rate responses evoked by global EOD mimics (±25 uA) in E and I cells in vehicle treated versus AP5 treated fish. Neurons were recorded >15 minutes after application of vehicle (fish Ringer's solution or 0.9% NaCl) or AP5 (300 uM-1 mM) directly onto the exposed surface of the VLZ molecular layer. Both excitatory (E) and inhibitory (I) effects on firing rate were evoked for both E

and I cells by switching the polarity of the EOD mimic and cells were pooled according to response polarity. AP5 treatment did not alter responses to the EOD mimic (E responses: P = 0.797, Student's t-test, n= 15 (veh), n = 16 (AP5); I responses: P = 0.688, Student's t-test, n= 15 (veh), n = 11 (AP5). (D) Average traces showing the timing and polarity of responses to the EOD mimics for all of the cells included in C.

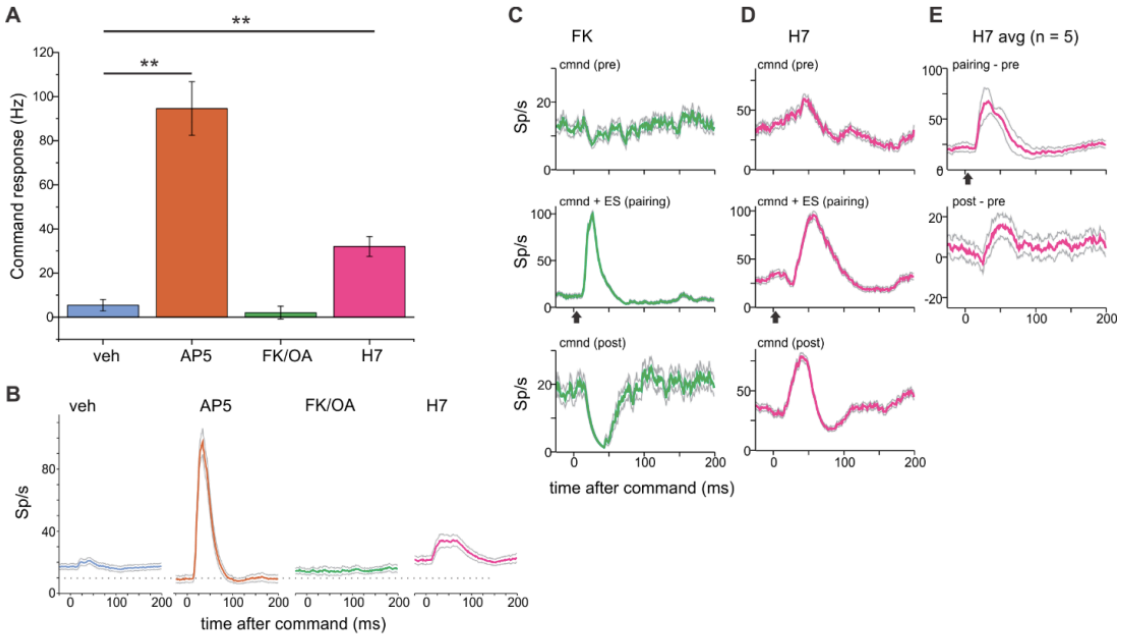

Figure 2.12 Effects of kinase and phosphatase inhibitors on command responses and negative image formation

(A) Average peak or trough firing rate responses to the EOD in E and I cells in vehicle treated versus drug treated fish. Neurons were recorded >15 minutes after application of either a vehicle solution (n = 27), AP5 (300 uM-1 mM) (n = 27), FK506 (1 mM) (n = 6), Okadaic acid (1 mM) (n = 3), or the kinase inhibitor H7 (0.5- 2 mM) (n = 32) directly onto the exposed surface of the VLZ molecular layer. Command responses were increased relative to the vehicle condition following AP5 or H7 treatment (P < 0.0001, Student's t-test), although the magnitude of the increase for AP5 was larger than for H7. (B) Average traces showing temporal profiles of command-evoked firing rates for all of the cells and conditions summarized in A. Gray outline are s.e.m. (C) Example cell from the FK506 (phosphatase inhibitor) condition showing the formation of a negative image (bottom panels) after 4 minutes of pairing the command with an EOD mimic (-25 uA, arrow). (D) Example cell from the H7 (kinase inhibitor) condition showing a failure of negative image under the same pairing conditions as used in C. (E) Average of 5 cells tested for negative images after H7 treatment. Note, the difference in the command response after pairing (post-pre) is not a negative image of the response to the stimulus (pairing-pre)

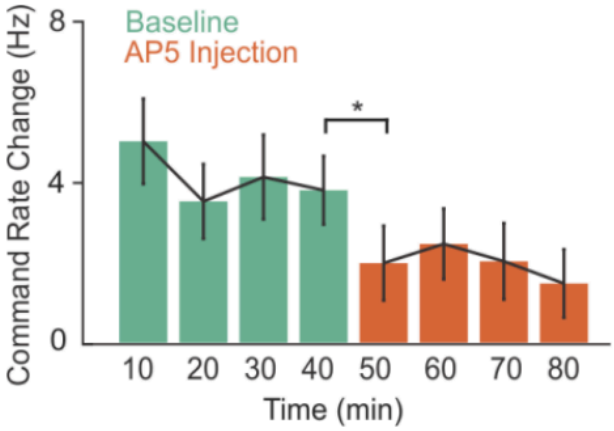

Figure 2.13 Effects of NMDA receptor blockade on behavioral NRs evoked by prey-like stimuli
Command rate changes evoked by a prey-like stimulus during a baseline condition (green) and following micropressure injections of AP5 (red) into the ELL molecular layer. AP5 injections reduced command rate changes evoked by a prey-like stimulus ($P < 0.001$, Friedman's non-parametric test, $n = 6$ repetitions of the experiment in 6 fish)

The striking effect of AP5 injection provides a confirmation of models of negative image formation based on anti-Hebbian spike timing dependent plasticity at parallel fiber synapses. *In vitro* studies have shown that, although NMDA receptor antagonists block associative synaptic depression of parallel fiber synapses, non-associative potentiation of parallel fiber synapses remains intact(Bell et al., 1997b; Han et al., 2000b). We used a computational model to understand the effects of blocking associative depression *in vivo*. The model is the same as that used in a previous study and consists of a single ELL principal cell that receives a large set of realistic granule cell corollary discharge responses generated based on past *in vivo* recordings (Kennedy et al., 2014). After each command the strength of granule cell inputs are adjusted according to the measured anti-Hebbian spike timing-dependent plasticity rule. To mimic the effects of AP5 injection we set the magnitude of the associative depression component of the

plasticity rule to zero while leaving the non-associative potentiation unchanged (**Figure 2.10C,** *left*). Without any additional tuning, the model principal cell exhibits a gradual increase in response at a short delay after the EOD command (**Figure 2.10C**, right), similar to the effects of AP5 injections on actual principal cells responses. With associative depression blocked, presynaptic action potentials driven by the EOD command lead to unchecked potentiation of granule cell synapses. The emergence of an early peak in the principal cell response can be explained by the observation from a past study that a large majority of granule cells fire at a short delay after the EOD motor command (Kennedy et al., 2014).

Next we tested the effects of AP5 injection on responses to prey-like stimuli in ELL neurons. Gradual increases in responses to the EOD command following AP5 injection (**Figure 2.10D**; histograms represent pooled responses of E and I cells) were paralleled by a decline in neural detection performance (**Figure 2.10E,** left). A direct effect of AP5 on granule cells in these experiments is unlikely because of their remote location in an external granule cell mass overlying the ELL molecular layer (**Figure 2.10A**). To rule out the possibility that NMDA receptor blockade interferes with electrosensory encoding in ELL independent of its effects on synaptic plasticity (Marcoux et al., 2015), we analyzed prey-like stimulus detection performance in time windows far from the EOD command. Detection performance was unaffected away from the command (**Figure 2.10E,** right), consistent with effects of AP5 being exerted mainly or entirely through the elevated firing induced by non-associative potentiation of corollary discharge inputs.

Finally, we measured behavioral NRs induced by prey-like stimuli before and after AP5 injections. NRs were evoked by prey-like stimuli delivered to a spatially restricted region of the skin, as in the experiments shown in **Figure 2.9**. Micropressure injections of AP5 were made

into the VLZ molecular layer, targeting a somatotopic location corresponding to the location of the prey-like stimulus delivered to electroreceptors on the skin. AP5 injections strongly reduced the amplitude of NRs evoked by prey-like stimuli relative to baseline conditions, whereas saline injections had no effect (**Figure 2.10F**). Additional experiments showed similar reductions in NRs when AP5 injections were performed immediately after the baseline period (**Figure 2.13**). Agents that block non-associative potentiation in ELL have yet to be identified (Han et al., 2000b). Hence we were not able to directly test the effects of blocking negative image formation on neural or behavioral detection performance. Nevertheless, the results described above indicate the potential for synaptic plasticity to powerfully shape the output of ELL and impact behavior.

Discussion

Extensive past studies of cerebellum-like structures at the first stage of electrosensory processing in fish (Bastian, 1996; Bell et al., 1997a, 2008; Bodznick et al., 1999; Harvey-Girard et al., 2010; Harvey-Girard and Maler, 2013; Bol et al., 2011; Marsat and Maler, 2011; Harvey-Girard and Maler, 2013) and a more recent study of a cerebellum-like structure at the first stage of auditory processing in mice (Singla et al., 2017), suggest that the subtraction of internally-generated predictions of the sensory consequences of behavior enhance the detection and processing of external sensory stimuli. The present study provides both neurophysiological and behavioral evidence supporting this hypothesis. We showed that the formation of negative image of the predictable electrosensory consequences of the fish's own EOD was accompanied by improvements in the neural coding of external, prey-like stimuli in ELL principal cells. Importantly, the improvements could not be accounted for by other processes, such as spatial

filtering or gain changes. Such improvements were also observed under several different experimental conditions (e.g. different relative strengths of external versus self-generated sensory inputs) intended to represent a range of behaviorally relevant conditions. An additional set of experiments demonstrated an enhancement of behavioral responses to prey-like stimuli that paralleled negative image formation. Finally, disrupting synaptic plasticity in ELL interfered with both neural coding and behavioral responses to prey-like stimuli. Together with past studies, these results provide an integrated account--spanning levels of synapses, circuits, sensory coding, and behavior--of how combining external sensory input with internally-generated prediction enhances sensory processing.

Although it is has long been hypothesized that cancelling self-generated inputs via the generation of negative images could enhance sensory processing (Sperry, 1950; von Holst and Mittelstaedt, 1950)(**Figure 2.1**), there are a number of reasons why implementing such a scheme in neural circuits could be problematic. First, while such models assume linear operations, actual neurons, including those in ELL, are non-linear in numerous respects (Gabbiani et al., 1996; Koch and Segev, 2000). Cancellation in principal cells is hypothesized to be due to the linear summation of electrosensory input onto basilar dendrites and corollary discharge input onto apical dendrites. Such linear summation is desirable because it would allow negative images to cancel the effects of the EOD without altering the manner in which they encode behaviorally relevant sensory inputs. However, studies of ELL in weakly electric gymnotid fish have shown that lesions or inactivation of the granule cells dramatically increase the gain of responses to electrosensory stimuli in principal cell (Bastian, 1986). Studies of gymnotid ELL have also demonstrated that non-linear, burst firing mechanisms are critical for encoding prey-like stimuli(Chacron et al., 2003; Gabbiani et al., 1996; Metzner et al., 1998; Oswald et al., 2004) and

that the dynamics of burst firing can be altered by dendritic inputs (Chacron et al., 2005; Mehaffey et al., 2007; Turner et al., 2002). Principal cells in the mormyrid ELL also exhibit burst firing (Sugawara et al., 1999), raising the possibility that the negative image—a large dendritic input—might interfere with burst dynamics and the coding of prey-like stimuli. Nevertheless, our results show that negative images improve neural detection performance (**Figure 2.6** and **Figure 2.7**) without grossly altering responses to prey-like stimuli (**Figure 2.8**). Hence our findings are consistent with the notion that negative images perform a pure subtraction of the effects of the effects of the EOD. How linear behavior arises out of interactions between nonlinear components is an important general question in neuroscience that may be illuminated by further studies of ELL.

Variability or noise is an additional key consideration for any scheme relying on the subtraction of two large signals. ELL neuron responses to prey-like stimuli are expected to be subject to noise (for example associated with synaptic transmission) proportional to the sum of the variance of the negative image and the variance of the response to the EOD. Noise due to the subtraction of these two large signals might be expected to overwhelm responses to prey. Results of the present study indicate that this is not the case, as demonstrated for example, by the observation that negative images enhance neural detection performance across a range of prey-like stimulus amplitudes (**Figure 2.6**). Whether ELL employs specific mechanisms for reducing noise is another topic for future studies. Revising existing models of ELL to incorporate realistic assumptions regarding nonlinearities in the system and estimates of noise constrained by the data will further strengthen our understanding of how synaptic plasticity operating within the well-defined circuitry of ELL shapes adaptive neural processing and behavior. Failure of more realistic models to match the data will motivate studies of additional aspects of ELL circuitry

that are not well understood. For example, current models largely ignore the role of inhibition and do not distinguish between two distinct classes of ELL neurons—the glutamatergic efferent cells studied here versus the GABAergic medium ganglion (MG) cells. Both classes integrate peripheral electrosensory input and plastic corollary discharge signals (Bell et al., 1997c). MG cells inhibit efferent cells and share numerous similarities with cerebellar Purkinje cells (Bell et al., 2008).

The dramatic effects of blocking NMDARs in ELL provide strong support for existing models of negative image formation based on anti-Hebbian spike timing-dependent plasticity (Kennedy et al., 2014; Roberts and Bell, 2000b). Such models predict that with NMDAR-dependent associative synaptic depression blocked, non-associative potentiation will proceed unchecked and the response of an ELL principal cell to the EOD command will reflect the sum of its granule cell inputs. The temporal profile of ELL principal cell responses after NMDAR blockade, indeed, closely resembled the summed granule cell corollary discharge response as determined by recordings from a large number of granule cells in a previous study (Kennedy et al., 2014). Regarding the cellular mechanisms for synaptic plasticity in the mormyrid ELL, several comparisons to other systems can be drawn based on previous studies and our present results. The NMDA receptor dependence of associative depression in the mormyrid ELL is shared by some forms of long-term depression (LTD) in the neocortex, hippocampus, dorsal cochlear nucleus, gymnotid ELL, and cerebellum (Bear and Malenka, 1994; Harvey-Girard and Maler, 2013; Harvey-Girard et al., 2010; Jörntell and Hansel, 2006; Tzounopoulos et al., 2007). However, unlike at mature parallel fiber-Purkinje cell synapses, transmission at parallel fiber synapse-principal cell synapses in ELL exhibits a prominent NMDA receptor-mediated component (Berman and Maler, 1998; Grant et al., 1998b). Moreover, the NMDA receptor-

dependence of LTD in Purkinje cells is due to NMDA receptor-mediated calcium influx at climbing fiber synapses rather than at parallel fiber synapses (Piochon et al., 2010). Preliminary evidence from in vivo drug applications in the present study (**Figure 2.12**) suggests that kinase inhibitors may be necessary for associative depression in the momyrid ELL. This requires verification *in vitro.* However, if correct, it would indicate an additional similarity between plasticity in cerebellum-like structures (including the ELL of both mormyrid and gymnotid fish) and the cerebellum (Belmeguenai and Hansel, 2005; Harvey-Girard et al., 2010; Harvey-Girard and Maler, 2013). In contrast, NMDA receptor-dependent LTD depends on phosphatases in the neocortex and hippocampus (Bear and Malenka, 1994). More broadly, these observations are interesting in light of the evidence that dysregulation of synaptic plasticity may play a role in neurological disorders ranging from autism to tinnitus (Auerbach et al., 2011; Bear and Malenka, 1994; Shore et al., 2016). Our results provide a clear case in which dysregulation of synaptic plasticity leads to aberrant circuit output and disruptions of sensory processing and behavior.

Methods

EXPERIMENTAL MODEL AND SUBJECT DETAILS

Male and female Mormyrid fish (7-12 cm in length) of the species *Gnathonemus petersii* were used in these experiments. Fish were housed in 60 gallon tanks in groups of 5-20. Water conductivity was maintained between 40-65 microsiemens. both in the fish's home tanks and during experiments. All experiments performed in this study adhere to the American Physiological Society's *Guiding Principles in the Care and Use of Animals* and were approved by the Institutional Animal Care and Use Committee of Columbia University.

METHOD DETAILS

Surgery

Fish were anesthetized (MS:222, 1:25,000) and held against a foam pad. Skin on the dorsal surface of the head was removed and a long-lasting local anesthetic (0.75% Bupivacaine) was applied to the wound margins. A plastic rod was cemented to the anterior portion of the skull to hold the head rigid. The posterior portion of the skull overlying ELL was removed. In a subset of experiments the valvula cerebelli was reflected laterally allowing direct visualization of the molecular layer of the caudal lobe of the cerebellum and the eminentia granularis posterior (EGp). Gallamine triethiodide (Flaxedil) was given at the end of the surgery (~20 μg/cm of body length) and the anesthetic was removed. Aerated water was passed over the fish's gills for respiration. Paralysis blocks the effect of electromotoneurons on the electric organ, preventing the EOD, but the motor command signal that would normally elicit an EOD continues to be emitted by the electromotoneurons at a variable rate of 2 to 5 Hz. The timing of the EOD motor command can be measured precisely (see below) and the central effects of electric organ corollary discharge inputs can be observed in isolation from the electrosensory input that would normally result from the EOD.

Electrophysiology

Extracellular single-unit recordings were made using glass microelectrodes (2-10 Mohms) filled with 2M NaCl, as described previously (Bell, 1982; Requarth and Sawtell, 2014). Recording locations within the VLZ were first established using characteristic field potentials evoked by the EOD command (Bell et al., 1992b). The precise location of the recording pipette with respect to the VLZ somatotopic map was subsequently determined by finding the skin

region for which low-frequency electrosensory stimulation delivered via a dipole electrode evoked multi-unit responses. Ampullary electroreceptor afferents, E cells and I cells are located in different layers of ELL and have distinctive electrophysiological characteristics (Bell, 1982; Bell and Szabo, 1986). Ampullary afferents terminate in the deep layers of ELL, exhibit highly regular spontaneous firing at around 50 Hz, and increase firing rate in response to an electrosensory stimulus that makes the pore of the receptor positive with respect to the basal face within the body (Bell and Russell, 1978; Engelmann et al., 2010). E cells are located in the plexiform layer and I cell in the ganglion layer. E and I cells both fire much more irregularly and at lower rates than afferents (Bell, 1982). E cells are excited by the same stimulus polarity as afferents while I cells are excited by the opposite polarity. Cross-correlation analysis confirmed that units identified as E and I cells are non-overlapping groups with respect to their responses to low-frequency electrosensory stimuli (**Figure 2.3**). Previous studies using intracellular recording and biocytin labeling and antidromic stimulation from the midbrain have shown that E and I cells correspond to two morphologically distinct types of ELL efferent cells known as large fusiform and large ganglion cells (Bell et al., 1997c). In addition to efferent cells, the other major large cells of ELL are the medium ganglion cells (Bell et al., 1997c; Grant et al., 1998b; Han et al., 1999). Recordings were occasionally obtained from medium ganglion cells identified, as in previous studies, by the presence of two distinct spike types (Bell et al., 1997c; Grant et al., 1998b). Such recordings were not included in the present analysis.

EOD mimics

The EOD motor command signal was recorded with a Ag-AgCl electrode placed over the electric organ. The command signal is the synchronized volley of electromotoneurons that would

normally elicit an EOD in the absence of neuromuscular blockade. The command signal lasts about 3 ms and consists of a small negative wave followed by three larger biphasic waves. Onset of EOD command was recorded as the negative peak of the first large biphasic wave in the command signal. When locked to the electric organ motor command, the EOD mimic was presented 4.5ms following this time. For **Figure 2.2** and **Figure 2.6** the EOD mimic was a 200 us duration square pulse delivered between an electrode in the stomach and another positioned near the electric organ in the tail. The amplitude was 200 uA at the output of the stimulus isolation unit for **Figure 2.2** and 30-50 uA for **Figure 2.6**. For both experiments the electrode in the stomach was negative. A previous study has shown that the effects of such pulses on ampullary afferent firing are similar to those of the fish's natural EOD (Bell and Russell, 1978). Past studies of the natural EOD in non-paralyzed mormyrid fish show that its effects on passive electroreceptors vary in magnitude depending on water conductivity (Bell and Russell, 1978), which is subject to large variation in the natural habitat of mormyrids (e.g. due to rainfall and seasonal flooding). The spatial pattern of activation due to the EOD may also vary, for example depending on the location of the fish relative to large objects or non-conducting boundaries or due to physical damage to the skin. For these reasons, the amplitude and spatial patterns of EOD mimics were varied in our experiments (see STAR Methods). The amplitude of the EOD mimic used in **Figure 2.2** was chosen to evoke firing rate modulations in ampullary afferents at the top of the range reported previously for the natural EOD (Bell and Russell, 1978). Smaller EOD mimic amplitudes were chosen for **Figure 2.6** because their effects were cancelled relatively rapidly (within 1-2 hours), making it easier to study the significance of cancellation and negative images for prey detection. The effects of EOD mimics in these experiments are still within the range reported previously for the natural EOD. For **Figure 2.7 - Figure 2.10** EOD mimics were

delivered locally through a dipole stimulus. The mimic used in these experiments was a previously recorded natural EOD waveform digitized, stored on a waveform generator (Rigol DG1022U) and presented through an analog stimulus isolation unit (SIU) (A-M systems, Model 2200). The peak-to-peak amplitude of the mimic measured at the output of the SIU was 8 uA. Local delivery of the EOD mimic in these experiments minimized the possibility that spatial filtering could play a role in suppressing responses to the EOD mimic relative to prey-like stimuli. Local delivery of EOD mimics also made it possible to tightly connect electrophysiological measurements of prey-like stimulus detection performance with behavioral responses to prey-like stimuli. For local stimuli, behavioral novelty responses are presumably driven by a spatially restricted set of cells including those from which we recorded. This is not necessarily the case if the mimic is delivered globally since the entire ELL map is activated.

Prey-like stimuli

Prey-like stimuli consisted of white noise to which a 5-20 Hz band-pass Butterworth filter was applied. Previous studies have shown that ampullary afferents in mormyrid fish respond well to stimuli within this frequency range (Engelmann et al., 2010). Sampling frequency was 10 kHz, and duration was 400 ms (Figure 2.2) or 2000 ms (remaining experiments). Stimuli were stored and delivered via a Cambridge Electronic Designs (Cambridge, UK) Power 1401 mkII device which performed digital to analog conversion. This signal was passed to an analog stimulus isolation unit (A-M Systems, Model 2200) which in turn was connected to a stimulating dipole (two Ag-AgCl balls 3 mm apart). For experiments in **Figure 2.2** and **Figure 2.6** the dipole was positioned 1 cm from the skin using a spacer connected to the dipole. In the remaining experiments the dipole was positioned 1-2 mm from

the skin. The amplitude of prey-like stimuli used in **Figure 2.7 - Figure 2.10** was 0.04 uA peak-to-peak at the output of the stimulus isolation unit.

AP5 injections

Micropipettes for pressure injections were constructed immediately preceding use using three-barrel glass pipette (1.2mm OD per barrel, #3B120F-4, World Precision Instruments, Sarasota, FL) pulled to a long taper and tips broken to ~20 uM under visual guidance. One barrel was filled with 1 mM APV in 0.9% saline, and the remaining barrels filled with saline, and 1 mM glutamate. In most experiments alexa 594 dextran was included in the pipette to allow for histological verification of the injection site. Prior to use, suitable ejection duration to deliver 15 nL at 20 PSI was calculated for each pipette barrel using previously described techniques (Bastian, 1993; Malpeli and Schiller, 1979). Typical ejection times were ~600 ms. After finding a suitable site for recording VLZ principal neurons, the location was noted, the recording pipette retracted, and the injection pipette tip placed at the recording pipette tip's point of entry. Basic trigonometric calculation was used to target a point 125 uM lateral to the recording site to target the VLZ molecular layer. The recording pipette was reinserted, and neurons within ±100um of the initial recording targeting site were recorded. Injection sites in the VLZ molecular layer were verified histologically using standard methods as described below.

Novelty Response Experiments

Experiments were performed in an isolation chamber. An open-bottomed chamber (60 x 60 x 60cm) was constructed from ¼ inch plywood and lined with sound isolating open-cell foam. Following paralysis and resumption of spontaneous EOD commands, the chamber was lowered

over the preparation and fish were allowed to adapt for 60 min before initiation of the experiment. Experiments shown in **Figure 2.9** consisted of three 40 minute periods in succession with each period consisting of 20 prey-like stimulus presentations. Each presentation was 2 sec in duration with an approximately 120 s interstimulus interval. Custom software was used to make delivery of a prey-like stimulus conditional on a stable EOD rate in the preceding 10 seconds. This was done to avoid spontaneous EOD accelerations from contaminating the results. Both the prey-like stimulus and the EOD mimic were presented via a local dipole situated over the face, between the eye and nares. The amplitude of the prey-like stimulus and the EOD mimic were identical to those used in the electrophysiological experiments shown in **Figure 2.7**. Analysis included only those fish which the prey-like stimulus evoked an average command rate increase of >1.5 standard deviations above baseline during the initial command-alone period, as calculated by bootstrap analysis described below.

Modeling

We used a previously described model of negative image formation to simulate the effects of blocking associative synaptic depression on ELL neuron corollary discharge responses (Kennedy et al., 2014). Briefly, we modeled an ELL neuron as a passive, current-based leaky unit receiving excitatory input from 20,000 model granule cells $(r^i(t))$, with anti-Hebbian spike timing-dependent plasticity at granule cell-ELL neuron synapses (w^i), and EPSPs fit to granule cell-evoked EPSPs recorded intracellularly (Grant et al., 1998). Because effects of AP5 were observed on responses to the command alone without an electrosensory stimulus, sensory input

to the ELL neurons was not included in the model. The granule cell-ELL neuron learning rule has the form: $\dot{W}_i = \Delta^+ r^i(t) - \Delta^- \delta_{post}(t) \int_{-\infty}^{t} r^i(t')\zeta(t-t')\,dt'$.

$\delta_{post}(t) = 1$ if the ELL neuron spiked at time t, and 0 otherwise; $\zeta(t)$ determines the time dependence of associative depression. *In vivo* and *in vitro* recordings have demonstrated an anti-Hebbian synaptic plasticity rule in efferent cells of mormyrid and gymnotid fish (Harvey-Girard et al., 2010), although the exact timing dependence has not been characterized in mormyrids. We simulated the effects of pharmacological blockade of NMDA receptors by setting Δ^- to zero, i.e. turning associative depression off.

Histology

After recording, fish were deeply anesthetized with a concentrated solution of MS:222 (1:10,000) and brains removed and fixed in 4% paraformaldehyde for at least 24 hours. 60 uM sections of ELL were cut on a cryostat or vibratome and a fluorescent microscope was used to visualize AP5 injection sites marked by Alexa 594 dextran.

QUANTIFICATION AND STATISTICAL ANALYSIS

Analysis of spike train data

Electrophysiological data was digitized with a CED Power1401 MkII (Cambridge Electronic Design, Cambridge, UK) and analyzed in accompanying Spike2 software (v7.12c). Extracellular voltages were digitized at 20 kHz, and action potentials times extracted using the built-in peak-finding algorithm. Further analysis was performed in Matlab using custom scripts.

ROC analysis

Spike trains were smoothed with a 10 ms symmetrical Gaussian kernel to create a continuous firing rate. Maximum firing rate over the 100 ms period following either the EOD command in the case of command + mimic or command-alone periods, or the 100 ms period starting 4.5ms before an EOD mimic delivered independent of the command. Only time windows within which no other EOD commands or mimics appeared were analyzed. Additionally, time windows which include the start or end of a prey-like stimulus were ignored. Analysis was performed using custom Matlab scripts for calculating the ROC curve, and trapezoidal approximation was used to calculate the area under the ROC curve (AUC). **Figure 2.4** demonstrates that results are qualititatively similar across a range of such periods from 10-300ms. Additionally, performing the analysis over randomly chosen time points along the spike train, not locked to a command or mimic also shows qualitatively similar results.

Novelty response analysis

Novelty responses were quantified by taking the maximum EOD command rate during the 1 s following the onset of a prey-like stimulus presentation. A baseline rate was calculated by bootstrapping, as described below. Data is presented as deviation from this baseline. For bootstrapping we calculated the maximum command rate for all 1s long segments in the experiments (spaced 200 ms apart, so overlapping by 800 ms) and used the mean of that as baseline, deviations from which are plotted as the command rate change (**Figure 2.9B** and **Figure 2.10G**).

Chapter 3

A cerebellum-like circuit in the auditory system cancels responses to self-generated sounds

Introduction

The first central stage of mammalian auditory processing occurs within the dorsal and ventral divisions of the cochlear nucleus (Cant, 1992). Based on similarities in their evolution, development, gene expression patterns, and anatomical arrangement, the DCN is considered to belong to a class of so-called cerebellum-like sensory structures (Bell, 2002; Berrebi et al., 1990; Lorente de Nó, 1979; Mugnaini et al., 1980; Oertel and Young, 2004). Other cerebellum-like structures include the first central stages of electrosensory and mechanosensory lateral line processing in several groups of fish. Numerous cell and fiber types are shared by all of these cerebellum-like structures and the cerebellum itself including: mossy fibers, granule cells, parallel fibers, Golgi cells, molecular layer interneurons, and Purkinje or Purkinje-like cells. A hallmark of the circuitry of cerebellum-like sensory structures is the integration of direct input from peripheral sensory receptors (e.g. electroreceptors in the case of cerebellum-like structures in fish and auditory nerve fibers in the case of DCN) with a diverse array of sensory and motor signals conveyed by a granule cell-parallel fiber system.

A primary site of this integration within DCN is the fusiform cell. Fusiform cells are also the major output cell of DCN and project to higher stages of auditory processing such as the inferior colliculus. The basilar dendrites of fusiform cells are contacted by auditory nerve fibers, which form a tonotopic map within the deep layer of DCN (**Figure 3.1**) (Cant, 1992; Oertel and Young, 2004). Their apical dendrites extend into a superficial molecular layer where they are contacted by parallel fibers. Parallel fibers arise from granule cells located in so-called granule cell domains (GCDs) around the margins of the nucleus and cross through different tonotopic regions of DCN (Mugnaini et al., 1980). Granule cells receive a wide variety of signals, both auditory and non-auditory, from mossy fibers originating in a number of different brain

regions(Oertel and Young, 2004). Parallel fiber, but not auditory nerve fiber synapses, have been shown to exhibit forms of long-term associative synaptic plasticity *in vitro* (Fujino and Oertel, 2003; Tzounopoulos et al., 2004; Zhao and Tzounopoulos, 2011). Though previous *in vivo* studies of DCN have extensively characterized auditory response properties in anesthetized or decerebrate animals (Young and Davis, 2002), much less is known about the functional significance of its cerebellum-like circuitry (Kanold and Young, 2001; Shore and Zhou, 2006; Wigderson et al., 2016).

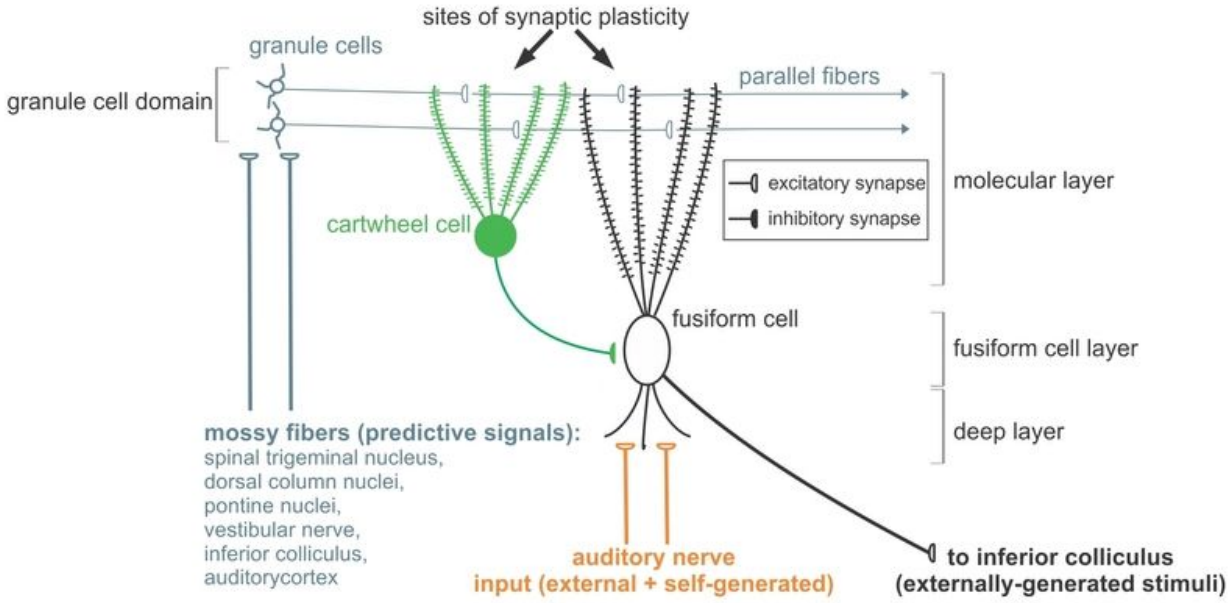

Figure 3.1 Cerebellum-like circuitry of DCN.
Fusiform cells integrate direct auditory nerve fiber input (orange) with a diverse array of auditory and non-auditory inputs conveyed by a mossy fiber-granule cell-parallel fiber system (blue) similar to that found in the cerebellum and cerebellum-like structures associated with electrosensory processing in fish. Cartwheel cells (green) also receive parallel fiber input but lack direct input from the auditory nerve. Cartwheel cells inhibit fusiform cells. Our hypothesis regarding DCN function is that mossy fibers convey information related to the animal's own movements and behavior, which serves to cancel out responses to self-generated acoustic stimuli. Such cancellation could be achieved by anti-Hebbian plasticity at parallel fiber synapses onto fusiform and/or cartwheel cells, as has been shown for cerebellum-like sensory structures in fish. For clarity, some DCN cell types and inputs have been omitted.

Some of the best clues come from studies of cerebellum-like structures associated with electrosensory processing in fish. Such studies have shown that anti-Hebbian synaptic plasticity

acting on proprioceptive, electrosensory, and motor corollary discharge signals conveyed by parallel fibers serve to cancel principal cell responses to self-generated electrosensory inputs, e.g. those arising from the fish's own movements or electromotor behavior (Bell et al., 1997a, 2008). Cancellation of self-generated electrosensory inputs allows externally-generated, behaviorally relevant stimuli to be processed more effectively. Guided by these results, we set out to test the hypothesis that the cerebellum-like circuitry of the DCN functions to cancel responses to self-generated sounds.

To this end we developed a preparation to study neural responses to self-generated sounds in the auditory brainstem of awake, behaving mice. We chose licking behavior because it is stereotyped and repetitive, can be elicited in head-fixed animals during electrophysiological recordings, and, as we demonstrate, generates sounds which are a potential source of interference for the mouse auditory system.

Results

DCN neurons respond preferentially to external versus self-generated sounds

We found that rhythmic licking generates sounds within the hearing range of the mouse and that such sounds exhibit stereotyped spectral and temporal profiles that were similar across mice (**Figure 3.2a**, **Figure 3.3**). The temporal profile of the licking sound is shown by the root mean squared (RMS) amplitude of the microphone recording aligned to tongue contact with the lick spout (**Figure 3.2a**, *white trace*). Though the exact physical origin of the licking sounds was not determined, tongue-to-spout contact appears not to be the main cause. As can be seen in both the spectrogram and RMS amplitude trace from the representative mouse shown in **Figure 3.2a**, licking sounds typically consist of an early component that begins before contact as well as a

larger late component that peaks ~50 ms after contact, during tongue retraction (**Figure 3.2a** and **Figure 3.3**)

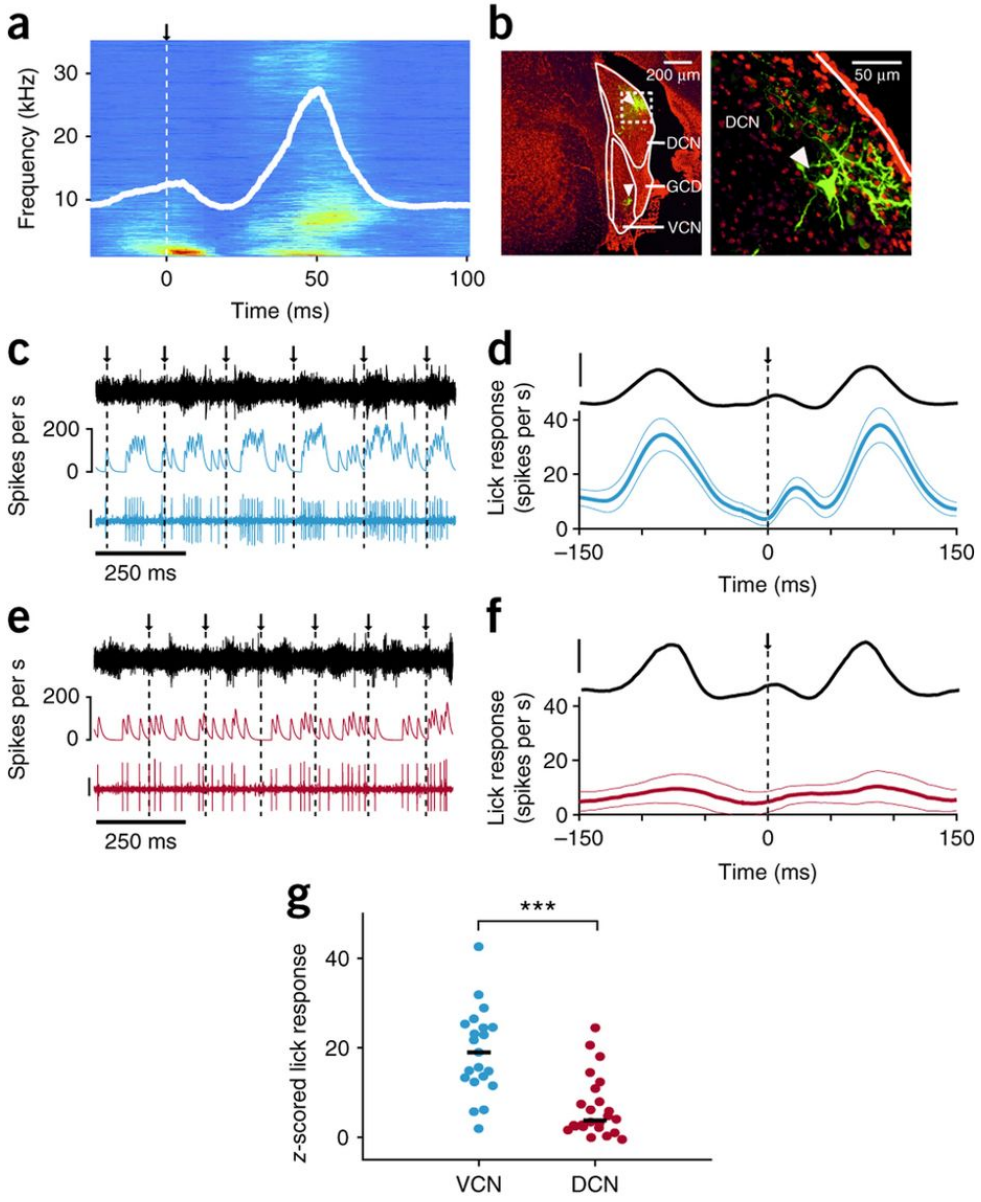

Figure 3.2 Self-generated sounds strongly affect VCN but not DCN neurons.
(**a**) Average spectrogram of self-generated sounds during licking for a representative mouse. Arrow and dotted line indicate time of tongue contact with the lick spout. Solid white line indicates the root mean squared (RMS) amplitude of the microphone recording. (**b**) *Left*, dextran-conjugated Alexa 594 labeling (*green*) at recording sites in DCN and VCN (*arrowheads*). DAPI, *red*. *Right,* higher magnification of dashed white box on left showing a labeled fusiform cell (*arrowhead*). (**c**) Example ventral cochlear nucleus (VCN) unit response during licking. *Arrows* and *dotted lines* indicate times of tongue contact with the lick spout. Traces represent the microphone recording (**top**), smoothed firing rate (**middle**), and the VCN unit recording (**bottom**; scale: 30 µV). (**d**) **Top**, average RMS amplitude of the licking sound

during VCN unit recordings (scale bar: 1 a.u.). **Bottom**, average VCN lick-triggered firing rate (n = 21). Thin lines are s.e.m. (**e)** Example DCN unit response during licking. Scale bar and display same as in **c**. (**f**) **Top**, average RMS amplitude of the licking sound during DCN unit recordings. **Bottom**, average lick-triggered responses of all DCN units (n = 25), excluding those exhibiting complex-spikes. Compared to VCN units, DCN units exhibited smaller temporal modulations related to licking (peak-to-trough firing rate for VCN: 43.8 ± 26.9 Hz, n = 21; for DCN: 19.7 ± 19.9 Hz, n = 25, mean and S.D., P = 0.0005, Wilcoxon Rank Sum Test). Scale bar and display same as in **d**. (**g**) Z-scored lick responses (see **Methods**) were significantly smaller in DCN compared to VCN units (P = 0.00002, Wilcoxon Rank Sum Test). Median responses are indicated by solid lines.

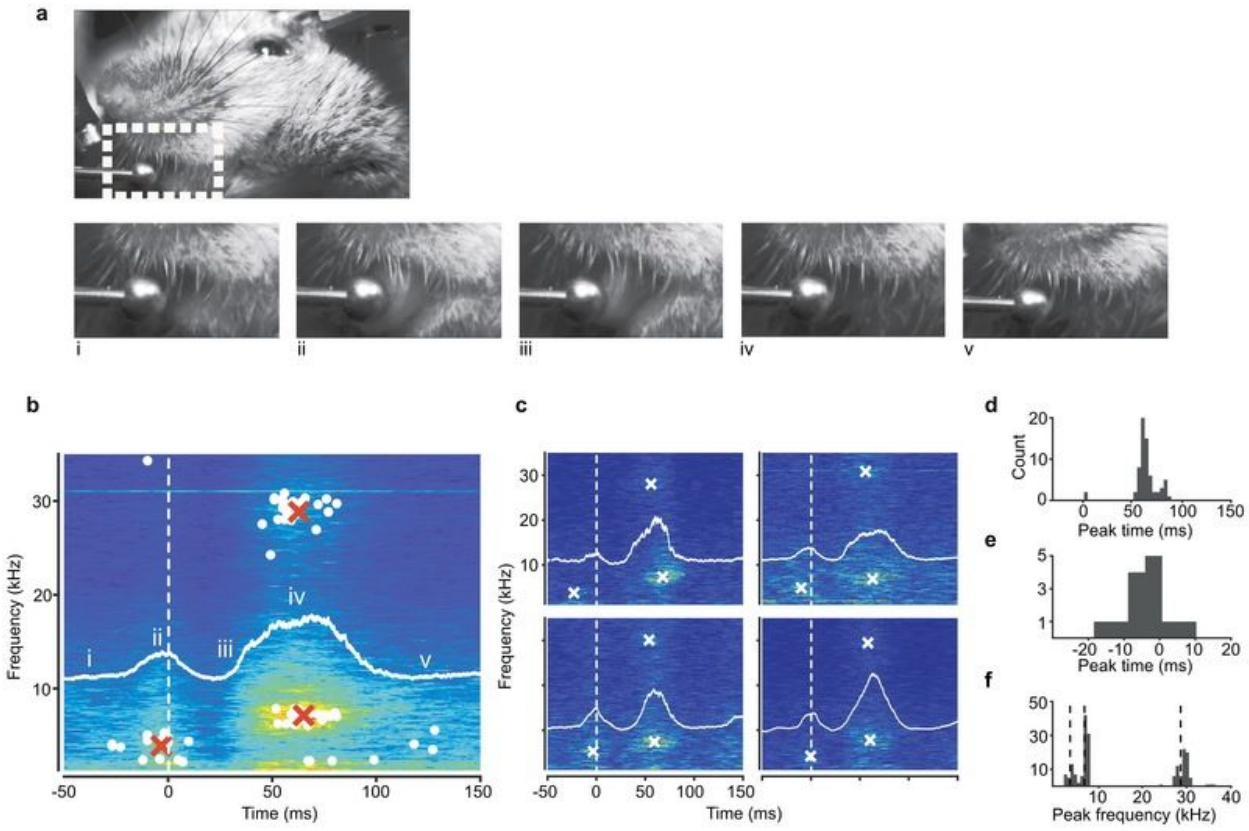

Figure 3.3 Characteristics of self-generated licking sounds in head-fixed mice.
(a) Video stills from a representative mouse. Top, still of the mouse at rest. Bottom, zoomed in stills of the dash white box at different points during the lick cycle: i. jaw opening, ii. tongue protrusion and lick spout contact, iii-iv. tongue retraction, v. jaw closure. (b) The average spectrogram of licking sounds across mice (n = 20) triggered on tongue contact with the lick spout. W*hite circles* show the time-frequency peaks of the spectrograms of each individual mouse. *Red crosses* show time-frequency peaks of the average spectrogram. Dotted white line indicates time of tongue contact with the spout. Solid white line indicates the average RMS across mice. Roman numerals indicate the timing of the video stills shown in a. (c) Four examples of lick-triggered spectrograms from individual mice. *White crosses* show time-frequency peaks. Dotted line shows time of tongue contact with spout. (d) Histogram of the timing of the largest RMS peak of the licking sound with respect to onset of tongue contact with the lick spout. (e) Histogram of the timing of the largest RMS peak of the licking sound with respect to offset of tongue

contact with the lick spout. (f) Histogram of the frequencies at which peaks in the lick-triggered spectrogram occur, showing that the lick-triggered sound consists of three distinct spectral peaks (dotted lines).

To determine whether licking sounds evoke neural responses that could interfere with auditory processing and, if so, whether such responses are cancelled out in the DCN, we compared neural activity during licking in well-isolated single-units in the ventral cochlear nucleus (VCN) and DCN. Since VCN receives direct auditory nerve input but lacks cerebellum-like circuitry, we hypothesized that VCN units would respond to acoustic stimuli regardless of whether they are self- or externally-generated. Recording locations were judged based on characteristic reversals of tonotopy at the DCN/VCN border (Luo et al., 2009; Muniak, 2013) and verified by iontophoresis of a dextran-conjugated fluorescent dye (**Figure 3.2b,** *white arrowheads* indicate recording sites, **Figure 3.4** and **Methods**). Though unambiguous criteria for linking physiological response properties with morphological cell classes have not yet been established for the awake mouse DCN (Ma and Brenowitz, 2012), several properties of the recorded units indicate that they likely correspond to fusiform cells, including their high spontaneous firing rates and purely excitatory responses to acoustic stimuli (**Figure 3.5** and **Methods**) (Davis et al., 1996; Hancock and Voigt, 2002; Rhode, 1999; Young, 1980; Young and Brownell, 1976). Units exhibiting complex spikes, putative cartwheel cell interneurons (Manis et al., 1994; Zhang and Oertel, 1993) (**Figure 3.1**), were also encountered and analyzed separately. Results for complex-spiking units are reported in **Figure 3.8**.

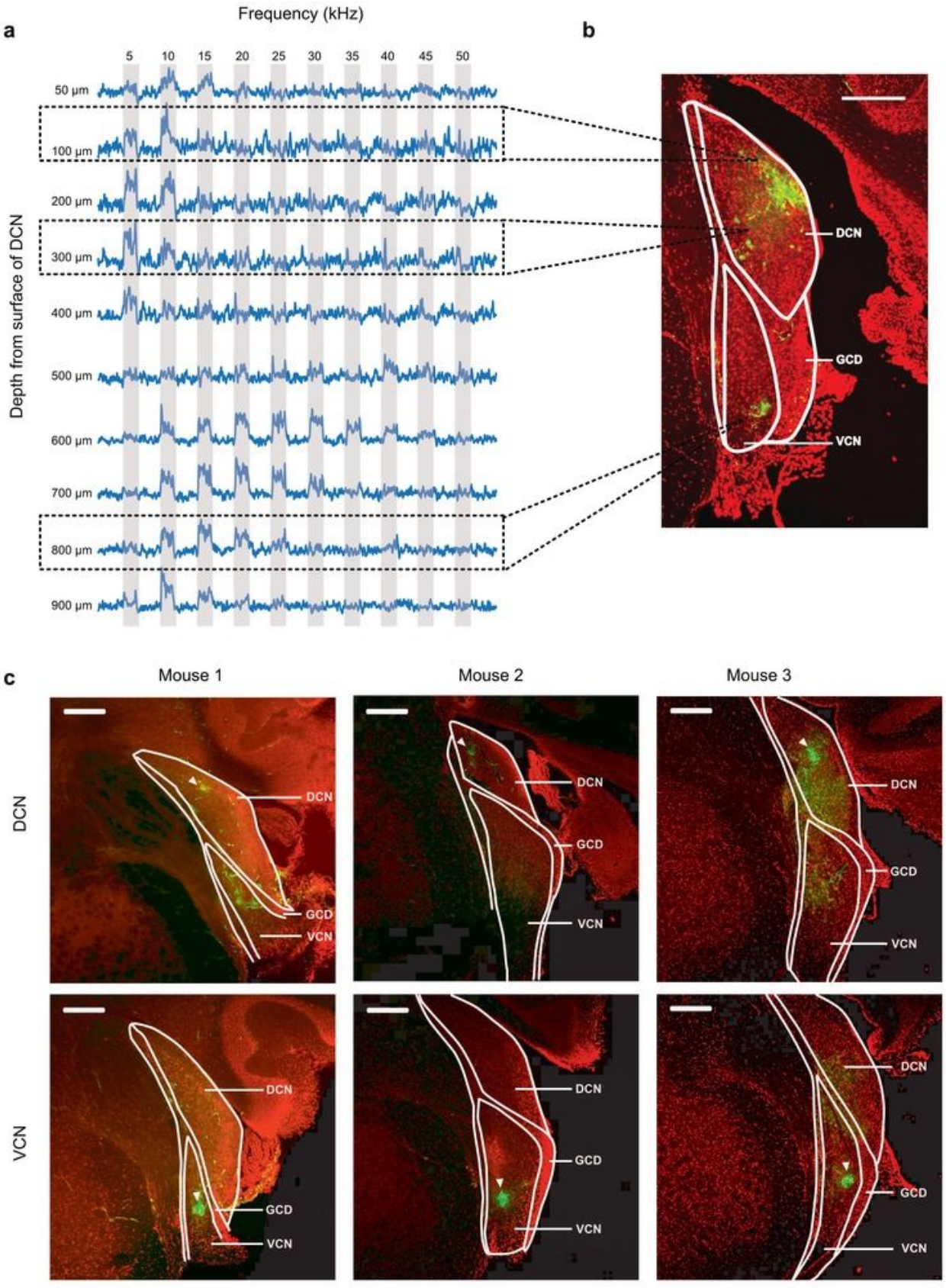
a
Frequency (kHz)
5
10
15
20
25
30
35
40
45
50
Depth from surface of DCN
50 µm
100 µm
200 µm
300 µm
400 µm
500 µm
600 µm
700 µm
800 µm
900 µm
b
DCN
GCD
VCN
c
Mouse 1
Mouse 2
Mouse 3
DCN
VCN
DCN
GCD
VCN

Figure 3.4 Identification and verification of recording sites in VCN and DCN.
(a) Rectified extracellular multiunit activity (each row is the average of 15 presentations) recorded on an electrode penetration through the auditory brainstem in response to 100 ms tones ranging in frequency from 5-50 kHz (gray rectangles). As the electrode passes through DCN the frequency evoking the largest multiunit response smoothly decreases. DCN units were isolated in DCN at depths between 100 μm and 300 μm. A sudden increase in frequency (occurring between depths of 400 μm and 600 μm) indicated entrance into VCN. VCN units were isolated at depths between 800 μm and 1000 μm. **(b)** Histological verification of recording sites in the same animal as the multiunit recordings shown in **a**. Dextran-conjugated Alexa 594 (*green*) was iontophoretically injected at depths of 100 μm and 800 μm. Scale bar = 200 μm. **(c)** Iontophoretic injections of dextran-conjugated Alexa 594 at recording sites (*arrows*) in DCN (*top*) and VCN (*bottom*) in 3 additional animals. Scale bars = 200 μm.

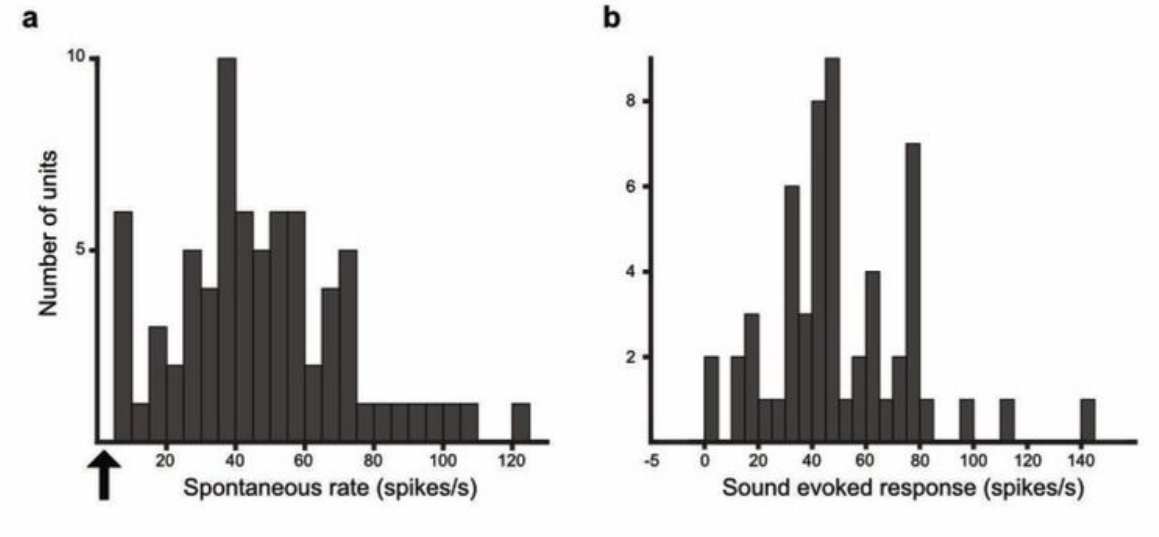

Figure 3.5 Baseline firing and sound-evoked responses in DCN units.
(a) Histogram of spontaneous firing rates of all units recorded in DCN (n = 73), excluding complex-spiking units. The average spontaneous rate was 48.3 ± 28.2 Hz (mean and s.d.). No DCN units met previously established criteria for type II or type I/III responses, i.e. a spontaneous rate less than 2.5 Hz (*arrow*). Type II and I/III responses are associated with a major class of DCN interneuron known as vertical cells. (b) Histogram of responses to sound stimuli in DCN units (n = 60), excluding units with complex spikes. Stimuli included the mimic of the licking sound (12 dB SPL), 5-15 kHz bandpassed noise (15 dB SPL), and broadband noise used in pairing experiments recorded with a silicon probe. Average maximum noise response was 50.6 ± 26.3 Hz (mean and s.d.). No units showed inhibitory sound responses, a criterion for type III-i response cell types.

Consistent with the possibility that licking behavior causes significant self-generated sounds, VCN units exhibited an overall firing rate elevation during licking as well as firing rate modulations (**Figure 3.2c,d**, *blue traces*) that tracked the RMS amplitude of the licking sound (*black traces*). In contrast, DCN units exhibited substantially weaker firing rate modulations during licking (**Figure 3.2e-g,** *red traces* and *circles*). Though these results are consistent with cancellation of self-generated sounds in DCN, an alternative explanation is that differences between VCN and DCN responses during licking are due to systematic differences in their auditory response properties.

We evaluated this possibility in a subset of VCN and DCN units by comparing activity during licking to activity during delivery of an externally-generated acoustic stimulus with temporal and spectral properties that roughly matched the licking sounds recorded across mice (**Figure 3.6a**, **Methods**). This stimulus is referred to henceforth as the lick mimic and was presented outside of licking bouts, when the mouse was still. Though the match between actual sounds generated by licking and the lick mimic is not expected to be perfect, for example due to issues such as bone conduction, this stimulus nevertheless provided a simple and principled means of comparing auditory responses in VCN and DCN. Strong responses to the lick mimic were observed in both VCN (**Figure 3.6b,c,** *blue traces*) and DCN units (**Figure 3.6d,e,** *red traces*). The strength of responses during licking was highly correlated with the strength of responses to the lick mimic in VCN units (**Figure 3.6f,** *blue circles*). This is exactly what is expected if VCN licking responses are indeed due to self-generated sounds. In contrast, there was no significant correlation between mimic and licking responses in DCN units (**Figure 3.6f,** *red circles*), such that even units with strong responses to the lick mimic failed to respond during licking. These

observations suggest that weaker responses to licking in DCN compared to VCN cannot be explained by differences in auditory sensitivity between the two regions. What then is the mechanism underlying the apparent reduction of responses to self-generated sounds during licking behavior in DCN?

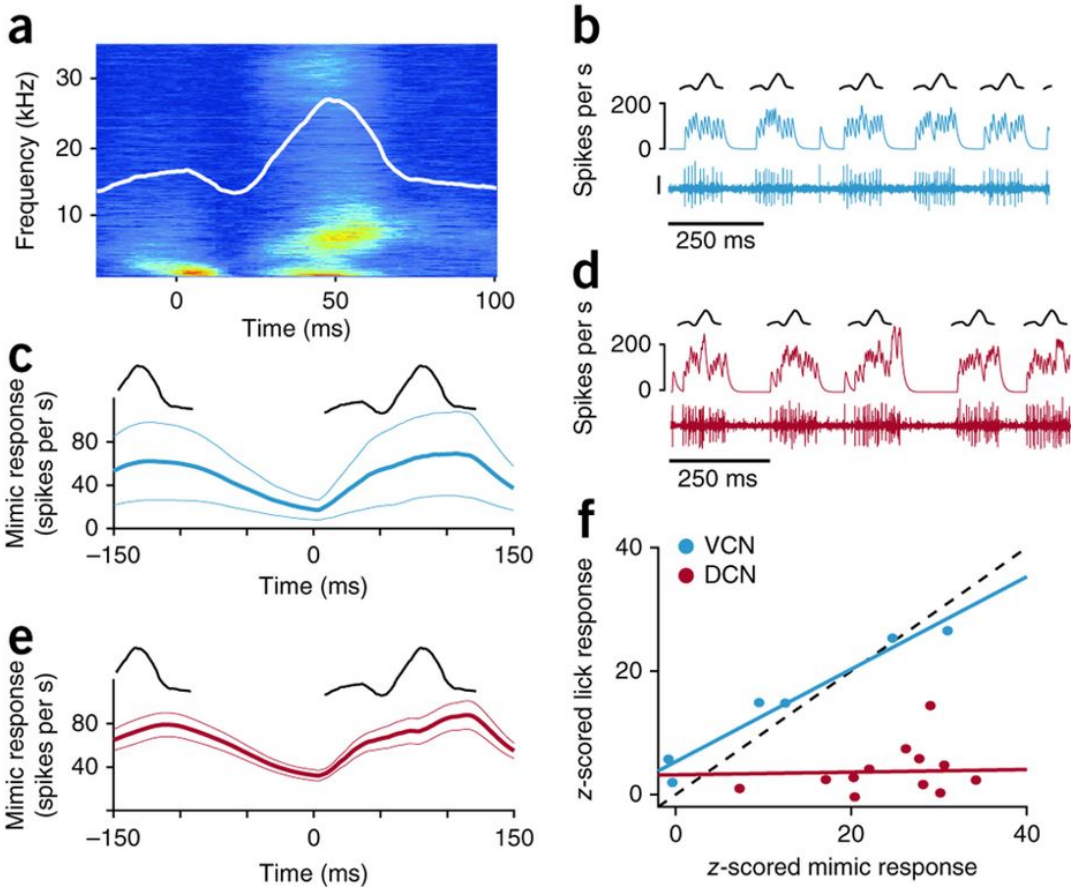

Figure 3.6 Responses to self-generated versus external sounds in VCN and DCN
(**a**) Spectrogram of the lick mimic generated from microphone recordings from 5 mice (**Methods**). Overlaid white line represents the RMS amplitude. (**b**) Example VCN unit response to the lick mimic. Same unit as in **Figure 3.2c**. Traces represent a schematic of the RMS of the mimic (**top**), smoothed firing rate (**middle**), and the VCN unit recording (**bottom**; scale bar: 30 μV). (**c**), **Top**, schematic of the RMS of the lick mimic. **Bottom**, average VCN unit response to the lick mimic ($n = 6$). Thin lines are s.e.m. The lick mimic was delivered at 12 dB SPL in all experiments. (**d, e**) Same scale bar and display as **b**, **c** but for DCN unit responses to the mimic ($n = 13$). Traces in **d** are from same unit shown in **Figure 3.2e**. VCN and DCN unit responses to the mimic were not significantly different ($P = 0.32$, Wilcoxon Rank Sum Test). (**f**) Responses to licking were highly correlated to those observed in the same units to the lick mimic for VCN ($n = 6$, $P < 0.001$, $r = 0.95$, linear regression t-test) but not DCN recordings ($n = 13$, $P = 0.79$, $r = 0.0007$, linear regression t-test).

One possibility is that the overall sensitivity of DCN units to sound is reduced during licking behavior. Indeed, an overall suppression of auditory responsiveness during behavior has been reported in a variety of systems (Eliades and Wang, 2003; Poulet and Hedwig, 2002), including the mouse auditory cortex(Rummell et al., 2016; Schneider et al., 2014). To test this, we compared DCN unit responses to an externally-generated acoustic stimulus (bandpassed noise 5-15 kHz, 15dB SPL) delivered either during licking (**Figure 3.7a**, *lick and noise*) or when the mouse was still (**Figure 3.7a**, *noise alone*). Responses to the acoustic stimulus were indistinguishable under the two conditions (**Figure 3.7a,b**). In addition, overall firing rates in DCN units were similar when mice were licking versus still (**Figure 3.7c**). Together, these results are inconsistent with an overall suppression of auditory sensitivity in DCN during licking and point instead to a mechanism for selectively canceling self-generated sounds.

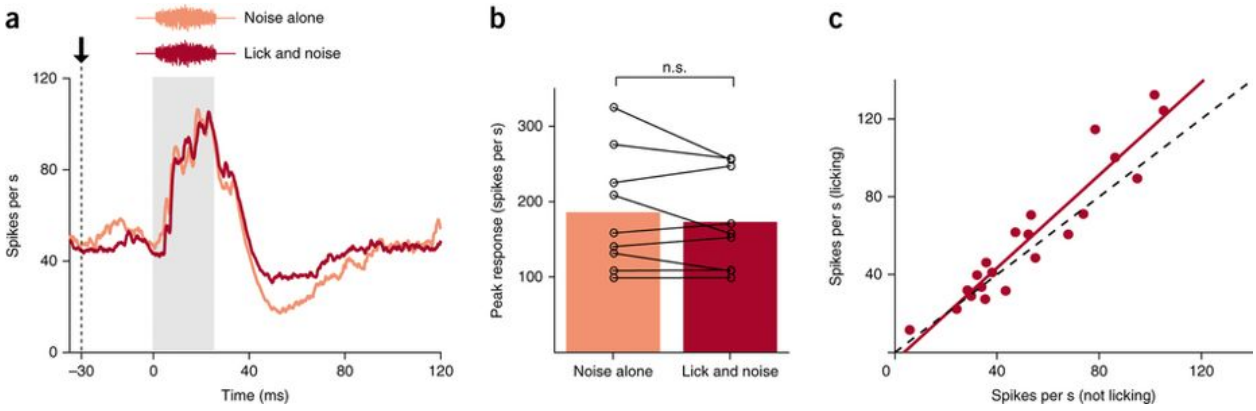

Figure 3.7 DCN responses to acoustic stimuli are not suppressed during licking.
(**a**) Example DCN unit response to an acoustic stimulus (bandpassed filtered 5-15 kHz, 15 dB SPL) played while the mouse was still versus during licking. Gray bar indicates stimulus duration. (**b**) No differences in responses were observed when the mouse was still versus licking ($n = 9$, $P = 0.49$, Wilcoxon Signed Rank Test). (**c**) Overall firing rates for DCN units were similar when the mouse was licking versus still.

Non-auditory signals related to licking revealed in DCN of deafened mice

In addition to auditory nerve input, DCN receives non-auditory, behavior-related signals conveyed by mossy fibers. Previous studies of cerebellum-like structures in fish have shown that behavior-related signals conveyed by mossy fibers serve to selectively cancel self-generated electrosensory input(Bell et al., 1997a, 2008). Though electrophysiological correlates of non-auditory mossy fiber inputs to DCN have been characterized in anesthetized or decerebrate preparations, e.g. using electrical stimulation of somatosensory brain regions projecting to DCN (Kanold and Young, 2001; Shore and Zhou, 2006; Wigderson et al., 2016), responses to non-auditory inputs have not yet been demonstrated in awake, behaving animals. To isolate non-auditory responses related to licking behavior we recorded from DCN in deafened mice (n = 3). Deafening (see **Methods**) was confirmed by a lack of observable behavioral responses to acoustic stimuli and by recording auditory-evoked field potentials in DCN before and after deafening (**Figure 3.8a**). For recordings in deafened mice we focused exclusively on units that exhibited both isolated action potentials, known as simple spikes, and brief, high-frequency bursts of action potentials, known as complex spikes (**Figure 3.8b,** *green boxes*). Such complex-spiking units correspond to a class of DCN interneuron known as cartwheel cells (CWCs) that share numerous similarities with Purkinje cells in the cerebellum (**Figure 3.1**) (Manis et al., 1994; Zhang and Oertel, 1993). CWCs lack auditory nerve input, receive massive input from parallel fibers, and inhibit fusiform cells. Our reasons for focusing on CWCs were twofold: (1) the complex spike is a distinctive electrophysiological signature of CWCs, which allowed us to be confident that we were recording in the DCN even in the absence of sound-evoked responses in the deafened mice and (2) CWCs provide a convenient readout of non-auditory inputs

conveyed by granule cells. Granule cells themselves are too small to be reliably isolated using conventional extracellular recording techniques.

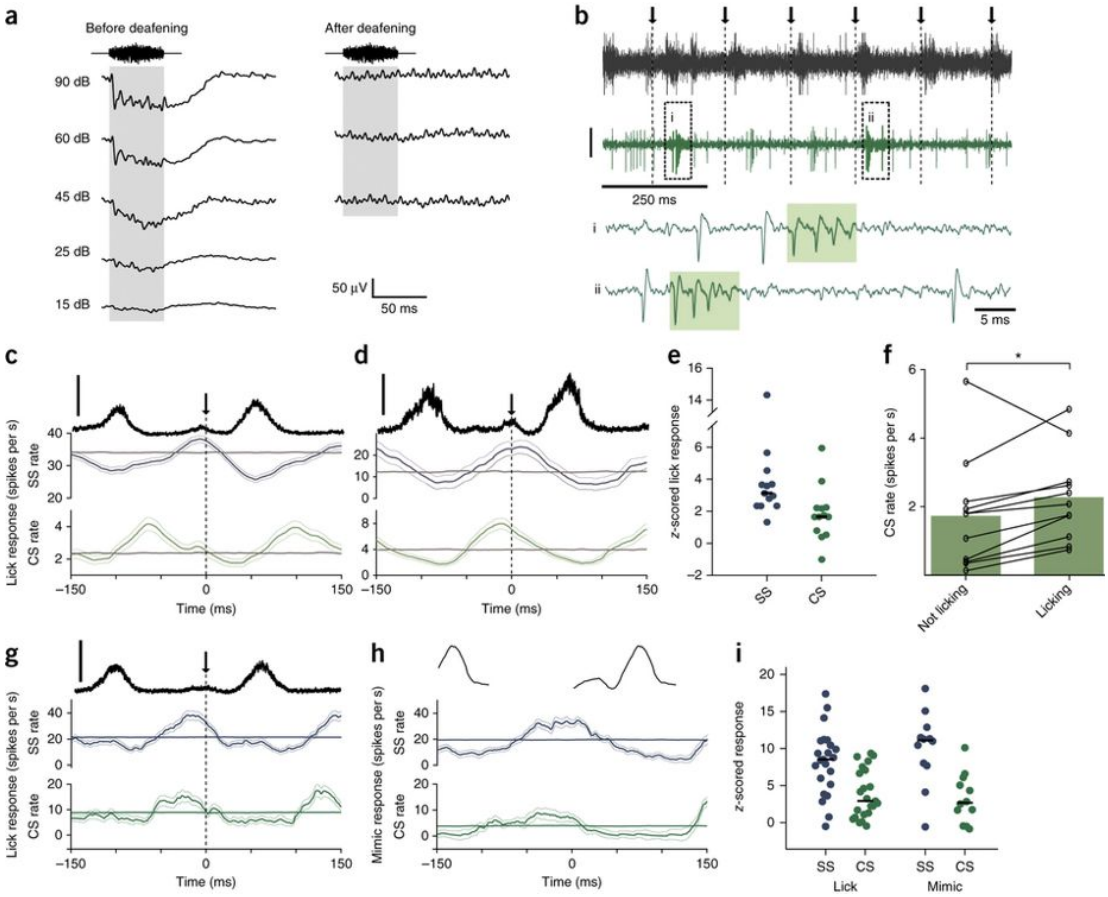

Figure 3.8 Non-auditory responses related to licking in DCN complex-spiking units.
(**a**) Sound-evoked field potentials (50 ms, broadband noise, averaged over 50 presentations) recorded in DCN of the same mouse before (*left*) and after (*right*) surgical deafening. Note complete absence of sound-evoked field potentials after deafening. (**b**) Example DCN complex-spiking unit recorded during licking in a surgically deafened mouse. Arrows and dotted lines indicate times of tongue contact with the lick spout. **Top trace**, microphone recording. **Below**, extracellular voltage from a DCN complex-spiking unit (scale: 30 µV). **i, ii,** Expanded traces from boxed regions showing complex spike (CS) (shaded rectangle) and simple spike (SS) waveforms. (**c,d**) Lick-triggered SS and CS firing rates for two complex-spiking units recorded in deafened mice. Thin lines are s.e.m. Gray traces show the average lick-triggered response of shuffled spike trains. Data in **c** are from same unit as example traces in **b**. **Top trace** (black) is the RMS amplitude of the licking sound (scale bar = 1 a.u.). (**e**) Summary of z-scored lick responses of 11 complex-spiking units recorded in 3 surgically deafened mice. 8 showed significant lick responses in their SS firing and 3 showed significant lick responses in their CS firing (α=0.01, see **Methods**). Median responses are indicated by solid lines. (**f**) Overall CS firing rates increased slightly during periods of

licking in deafened mice (n = 11, P =0.04, Wilcoxon Signed Rank Test). (**g**) Lick-triggered SS and CS firing rates for a complex-spiking unit recorded in a hearing mouse. Same display as in **c**. (**h**) Mimic-triggered SS and CS firing rates for a complex-spiking unit recorded in a hearing mouse. Same unit as shown in **g**. (**i**) Summary of licking and mimic responses in complex-spiking units recorded in hearing mice. Average Z-score responses to licking (n = 23) were 8.2 ± 4.4 for SSs and 3.8 ± 4.4 for CSs. Average Z-score responses to the mimic (n = 12) were 10.1 ± 4.9 for SSs and 3.2 ± 3.3 for CSs.

In deafened mice, 9 of 11 complex-spiking units exhibited significant simple and/or complex spike firing rate modulations related to licking (**Figure 3.8c-e,** *green traces*). The overall rate of complex spike firing also increased slightly during licking (**Figure 3.8f**). These results indicate that DCN receives non-auditory information related to licking behavior. Granule cells provide the main excitatory input to CWCs. Hence the non-auditory, licking-related responses we observed in CWCs are likely due to signals conveyed by parallel fibers.

We also recorded from complex-spiking units in hearing mice. Most complex-spiking units exhibited simple and complex spike firing rate modulations related both to licking (**Figure 3.8g**) and to presentation of the mimic when the mouse was still (**Figure 3.8h**). Prominent responses to both licking and to the mimic (**Figure 3.8i**) are consistent with the notion that CWCs receive both non-auditory and auditory signals conveyed by granule cells. This is consistent with anatomical evidence for prominent non-auditory as well as auditory input to GCDs (Oertel and Young, 2004) and previous electrophysiological evidence for prominent auditory responses in complex-spiking units in awake mice (Portfors and Roberts, 2007).

A role for the spinal trigeminal nucleus in cancelling self-generated sounds

Based on previous microstimulation and anatomical tracing studies, the spinal trigeminal nucleus (Sp5) is expected to be the major source of mossy fiber input to DCN conveying somatosensory information related to licking behavior (Haenggeli et al., 2005; Shore and Zhou, 2006; Zhou and Shore, 2004). As expected from past studies in other mammals, injection of an anterograde viral

tracer (AAV2-GFP) into mouse Sp5 resulted in labeled mossy fibers in the granule cell domains (GCDs) of DCN (n = 3; **Figure 3.9a,** *arrowheads*) as well as in the cerebellum (data not shown). If non-auditory, licking related inputs from Sp5 serve to cancel out responses to self-generated acoustic stimuli in DCN, transiently silencing such inputs should reveal prominent licking-related responses in DCN neurons. Indeed, micropressure injection of the action potential blocker lidocaine into Sp5 led to an increase in overall firing in putative DCN output cells during licking as well as an increased modulation of firing (**Figure 3.9b**,**d** *red*) that tracked the amplitude of the licking sound (**Figure 3.9b**, *black lines*). No such changes were observed after saline injection (**Figure 3.9c,d,** *purple*). Furthermore, increases in licking responses after lidocaine injection cannot be explained by differences in sensitivity to acoustic stimuli between lidocaine and saline groups (**Figure 3.9e**), changes in licking rate after lidocaine injection (**Figure 3.9f**), or changes in the amplitude of licking sounds after lidocaine injection (**Figure 3.9g**).

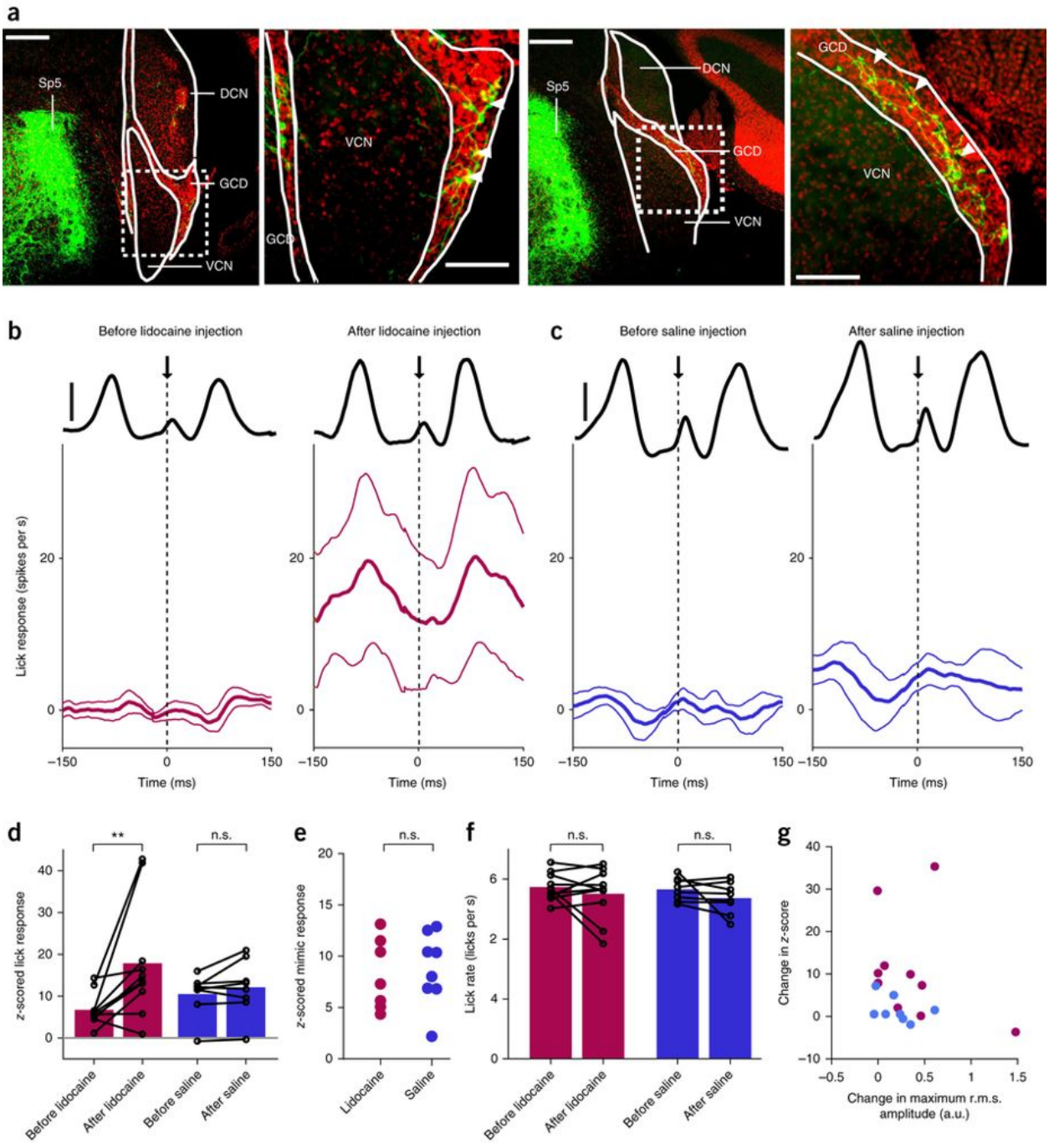

Figure 3.9 A role for the spinal trigeminal nucleus in cancelling self-generated sounds in DCN. (**a**) Labeled mossy fibers were observed in DCN granule cell domains (GCD) after injection of an anterograde viral tracer (AAV2-GFP) into the ipsilateral Sp5. Scale bars: 200 μm. *Right*, higher magnification views of areas indicated by dotted rectangle. Scale bars: 100 μm. White arrowheads indicate labeled mossy fibers in GCDs. (**b**,**c**) Lick-triggered response of DCN cells before (*left*) and after (*right*) injection of lidocaine (**b**, $n = 10$) or saline (**c,** $n = 8$) into Sp5. Thin lines are s.e.m. Solid black lines show the RMS amplitude of the licking sound (scale bars: 1 a.u.). (**d**) Lidocaine injection resulted in a significant increase in z-scored lick responses in DCN units ($P = 0.0098$, Wilcoxon Signed Rank Test, *red*) while no significant increases in z-scored lick responses occurred after saline injection ($P = 0.31$,

Wilcoxon Signed Rank Test, *purple*). (**e**) Auditory responses to the mimic were not significantly different in lidocaine and saline groups ($P = 0.87$, Wilcoxon Rank Sum Test). (**f**) Lick rate did not differ before and after injection of lidocaine ($P = 0.77$, Wilcoxon Signed Rank Test) or saline ($P = 0.25$, Wilcoxon Signed Rank Test). (**g**) Changes in z-score lick responses were not correlated with changes in the maximum RMS of the licking sound after lidocaine injection (*red*, $P = 0.36$, linear regression t-test). Changes in the maximum RMS of the licking sound did not differ between lidocaine and saline groups ($P = 0.51$, Wilcoxon Rank Sum Test).

Adaptive cancellation of sounds correlated with behavior in DCN neurons

Studies of cerebellum-like structures in fish have shown that cancellation of self-generated inputs is not fixed but reflects an adaptive filtering process in which anti-Hebbian synaptic plasticity reduces correlations between principal cell activity and behavior-related signals conveyed by granule cells (Bell et al., 1997a, 2008). Similar anti-Hebbian plasticity rules have been described at granule cell synapses in DCN (Fujino and Oertel, 2003; Tzounopoulos et al., 2004; Zhao and Tzounopoulos, 2011). Adaptive filtering in DCN would explain both how diverse sources of mossy fiber input are sculpted into patterns of synaptic input that selectively cancel responses to self-generated sounds and how such patterns are updated if the auditory consequences of a given behavior change. To test whether DCN is capable of adaptive filtering we delivered an external sound (broadband or bandpassed noise 5-15 kHz) temporally correlated with licking (30 ms after tongue contact). The conditions were the same as those for the experiments shown in **Figure 3.7**, except that many more sound presentations were used. Recordings were made using both glass microelectrodes and multi-site silicon probe electrodes (**Figure 3.11**). Use of the latter aided the maintenance of single-unit isolation through long bouts of licking. Responses of putative DCN output cells to the correlated sound declined over the course of several minutes of pairing (>1000 paired lick-sound presentations) (**Figure 3.10a-d,h,** *red lines*). Such declines were not due to overall changes in firing rate, but rather were specific to the period of the noise-evoked response (**Figure 3.10a-d,h,** *black lines***)**. Decreases in DCN responses to sounds correlated with licking are unlikely to reflect adaptation of peripheral auditory input as they were not observed in a

separate group of DCN units in which an identical external sound was presented at the same rate but at random times relative to lick contact (**Figure 3.10e,f,h,** *yellow lines*). Furthermore, no changes in sound-evoked responses were observed in VCN units when the external sound was temporally correlated with licking (**Figure 3.10g,h,** *blue lines*). The magnitude of the reductions in response to acoustic stimuli correlated with licking varied substantially across DCN units (**Figure 3.10i**). We found no relationships between the magnitude of such reductions and a number of behavioral and neural parameters, including licking rate, licking variability, baseline firing rate, and the initial magnitude of noise-evoked responses (**Figure 3.12**). More definitive criteria for identifying DCN cell types, such as juxtacellular labeling and antidromic stimulation, along with a thorough characterization of auditory response properties may, in future, provide insights into the source of this variation. Overall, these results are consistent with a plastic cancellation or adaptive filtering of self-generated stimuli in DCN similar to that described previously in cerebellum-like structures in fish.

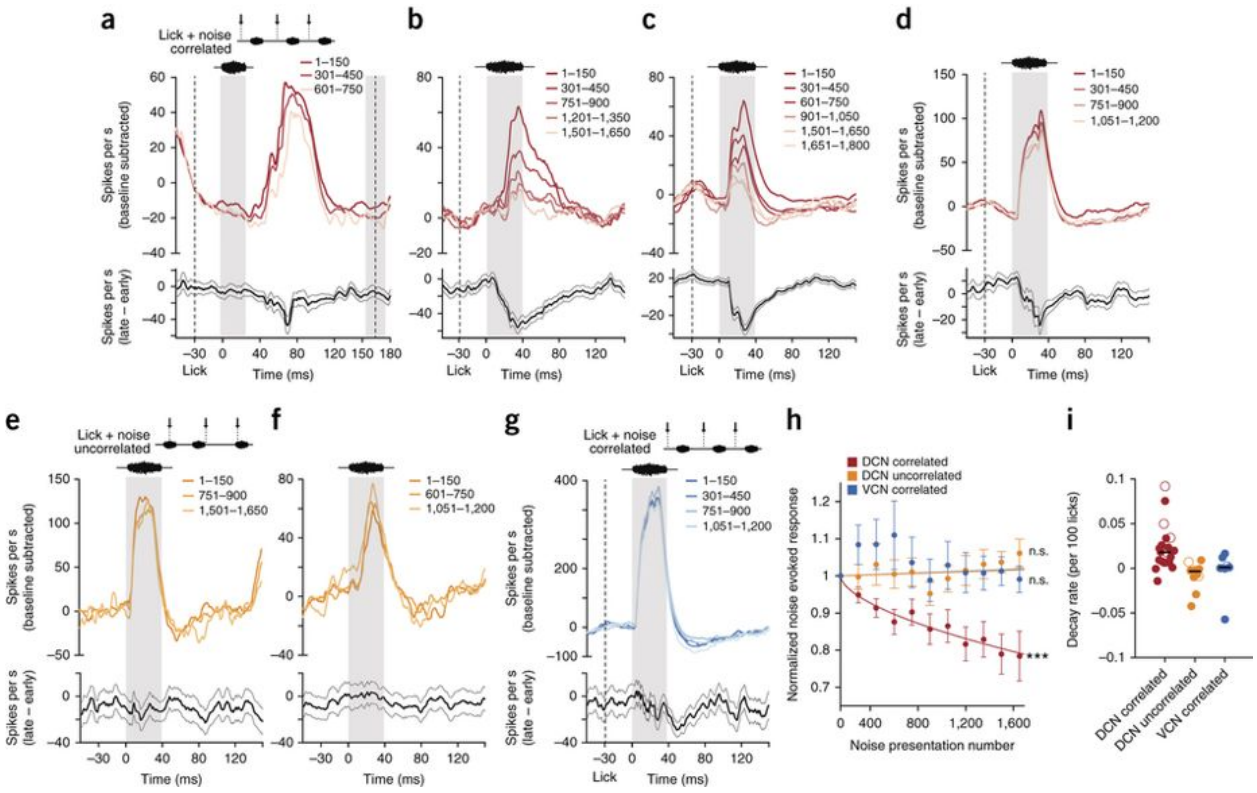

Figure 3.10 Adaptive cancellation of sounds correlated with behavior in DCN.
(a-d) *Top,* response of an example DCN unit to an acoustic stimulus (broadband or bandpassed filtered noise 5-15 kHz) presented correlated with lick onset. Lighter traces show responses to later licks, averaged in bins of 150 licks. *Bottom,* final response of this cell minus initial response to the sound plus lick. Thin lines are s.e.m. Left gray area shows the stimulus presentation period. Left dashed line shows the time of lick onset. Right dashed line and gray box show the mean and standard deviation, respectively, of the time of the next lick. (**e, f**) Same display for two DCN units for which the acoustic stimulus was played uncorrelated with the onset time of a lick. (**g**) Same display for an example VCN unit in which the acoustic stimulus was presented correlated with the onset time of a lick. (**h**) Group data showing average changes in noise-evoked responses over the course of repeated stimulus presentations. For DCN correlated units (*red*) the best fit decay rate was 0.0225 per 100 licks ($n = 20$, $P = 6 \times 10^{-15}$, linear regression t-test), for DCN uncorrelated units (*yellow*) the best fit decay rate was 0.001 but was not significantly different from 0 ($n = 11$, $P = 0.42$, linear regression t-test), and for VCN units (*blue*) the best fit decay rate was 0.001 but was not significantly different from 0 ($n = 7$, $P = 0.56$, linear regression t-test). Error bars are s.e.m. (**i**) Scatter plot of decay rates of best-fit exponentials fit separately for every unit. Horizontal black lines show the median value for each group. Open symbols correspond to the units used as examples in panels **a**-**g**.

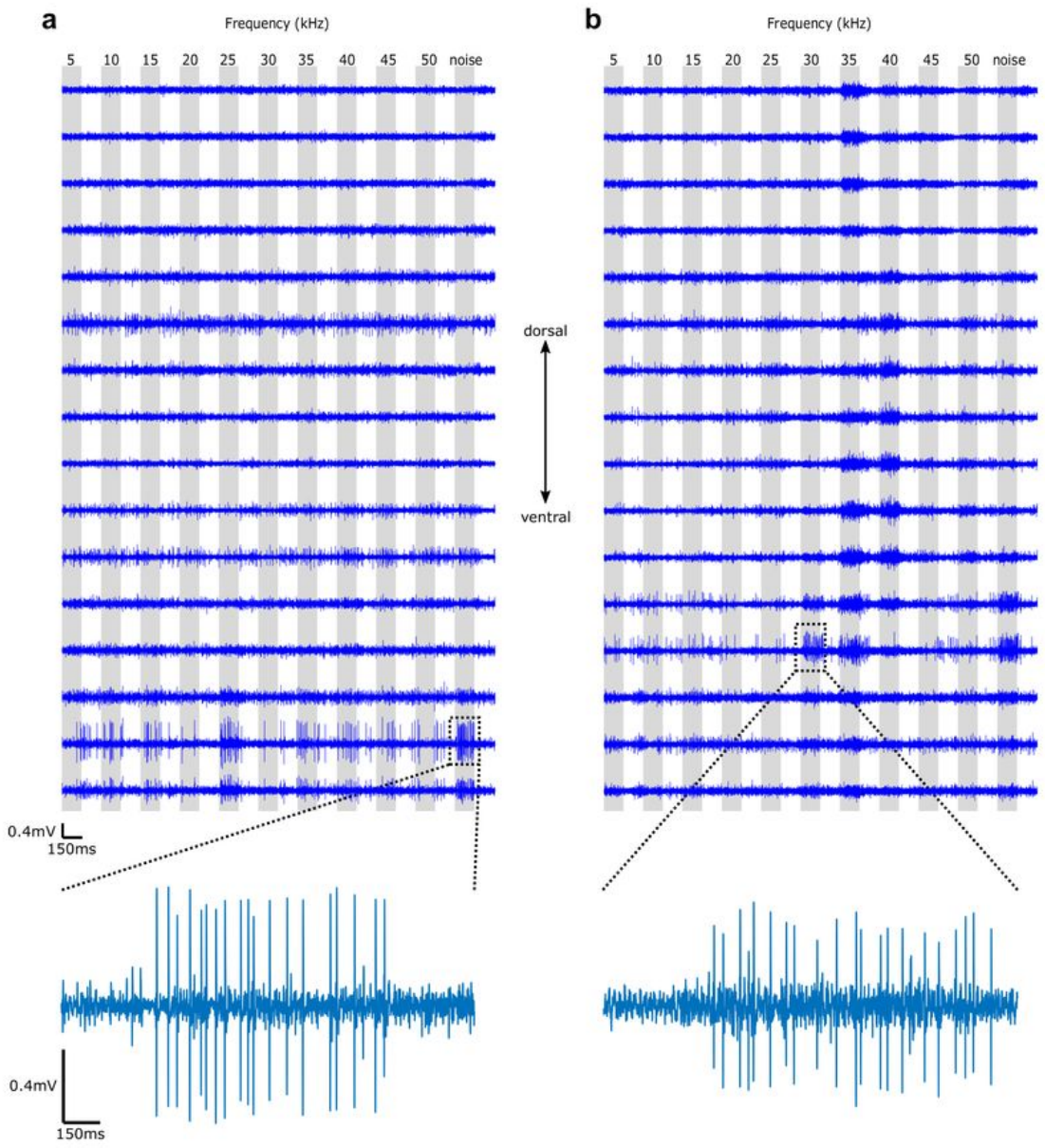

Figure 3.11 Silicon Probe Recordings in the DCN.
Representative 16-channel silicon probe recordings from the mouse dorsal cochlear nucleus. Electrode sites were arranged in a vertical linear array with individual sites separated by 25 µm. Tracks were made until a well-isolated unit emerged on a single electrode site. **(a)** A single unit with clear responses to 25 kHz and broadband noise (bottom trace). **(b)** A recording from the dorsal cochlear nucleus in another mouse showing multiunit responses to 35 kHz, 40 kHz, and broadband noise across multiple sites. A well-isolated single unit appears on the fourth most ventral site and has clear responses to 30 kHz (bottom

trace), 35 kHz, and broadband noise.

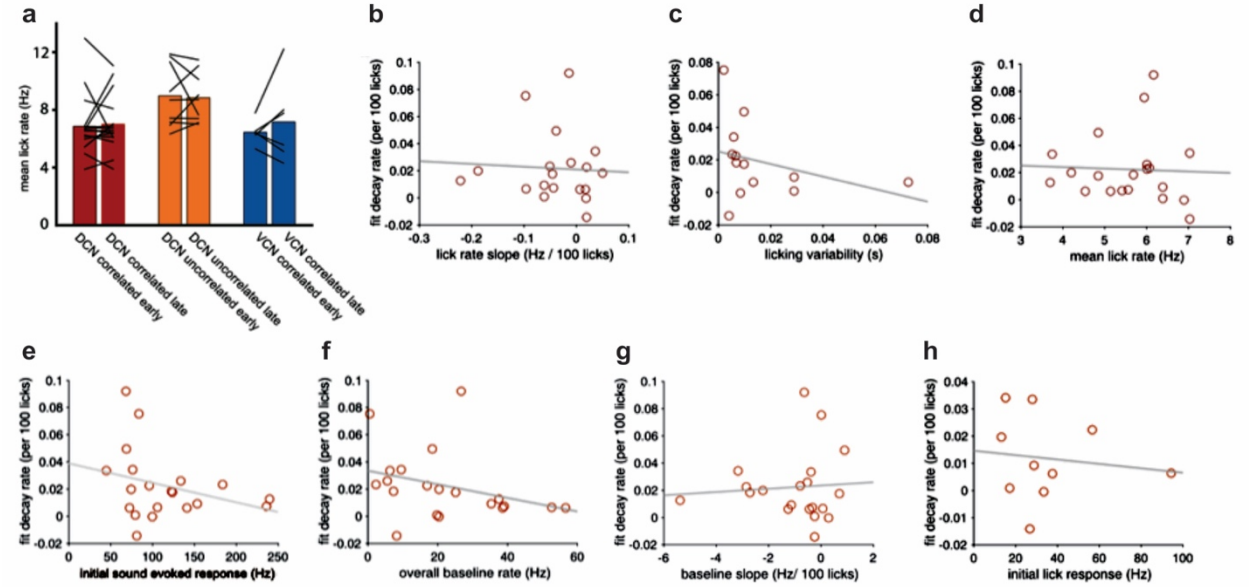

Figure 3.12 Pairing induced reductions in DCN responses to correlated sounds are not related to variability in behavior or neural responses.
(a) Changes in licking behavior cannot explain pairing induced reductions in DCN responses. Lick rates at the start (first 150 licks) and end (last 150 licks) of the pairing experiments shown in **Figure 3.10**. There was no difference in early versus late lick rates in DCN correlated (n = 20, P = 0.9, Wilcoxon Signed Rank Test), uncorrelated (n = 11, P = 0.9, Wilcoxon Signed Rank Test), or VCN correlated conditions (n = 7, P = 0.56, Wilcoxon Signed Rank Test). There also was no difference in lick rates between the three groups (P = 0.08, Kruskal Wallis test). (b-h) To examine possible sources of the variance in cancellation amongst DCN units in which acoustic stimuli were paired with licking, we also performed a multilinear regression with the variables shown in the figure as regressors. (b) The slope of the change during the pairing period (if any) in the lick rate did not correlate with decay rate during pairing (n = 20, P = 0.81). (c) The variability of licking, defined as the standard deviation of the interlick intervals between the twenty most recent licks, did not correlate with the decay rate during pairing (n = 20, P = 0.29). (d) The mean lick rate did not correlate with the decay rate during pairing (n = 20, P = 0.86). (e) Initial magnitude of DCN unit responses to the correlated sound did not correlate with the decay rate during pairing (n = 20, P = 0.19). (f) Mean baseline firing rate calculated for the entire recording did not correlate with decay rate during pairing (n = 20, P = 0.17). (g) The slope of the change (if any) in a unit's baseline firing rate, defined as the mean firing rate in periods at least 20 ms before the next lick and 150 ms after the previous lick, did not correlate with decay during pairing (n = 20, P = 0.98). (h) Magnitude of a unit's response to licking alone before pairing did not correlate with the decay rate during pairing (n = 10, P = 0.73).

Discussion

Distinguishing between external and self-generated sensory stimuli is fundamental for perception, and is thought to involve a comparison between external sensory input and internal

reference signals related to the animal's own behavior, for example motor corollary discharge or proprioception (Cullen, 2004). The present study provides evidence that such a comparison takes place at the first central stage of mammalian auditory processing in the DCN. More specifically, our results suggest a scheme similar to that already well-established in cerebellum-like structures in fish, in which behavior-related signals conveyed by a mossy fiber-granule cell-parallel fiber system cancel out responses to self-generated sensory stimuli in principal neurons (Bell et al., 1997a, 2008). Several independent lines of evidence from the present study support such a function for DCN. First, responses to sounds generated by licking are substantially weaker in DCN compared to VCN and such differences are not accounted for by weaker responses to external acoustic stimuli in DCN or by an overall suppression of DCN responses during licking. Second, non-auditory responses to licking behavior are observed in putative CWCs, presumably due to non-auditory signals conveyed by mossy fibers and granule cells. Third, inactivation of Sp5, a prominent source of somatosensory mossy fiber input to DCN, revealed responses to self-generated sounds in DCN units that resembled those observed in VCN units, suggesting that such input normally functions to cancel DCN responses to self-generated sounds. Finally, repeated pairing of acoustic stimuli with licking resulted in a gradual reduction of DCN responses to the paired stimulus. Importantly, such reductions were not observed when stimuli were presented at the same rate but uncorrelated with the time of lick contact.

Cancellation of self-generated sounds at an early processing stage could provide mammals with a dedicated channel through which salient or unexpected auditory signals can rapidly guide motor output, such as escape or orienting behavior. This interpretation is consistent with effects of DCN lesions, which disrupt orienting towards but not discriminating between

sound source locations (May, 2000; Sutherland et al., 1998) and the fact that, in addition to projecting to the inferior colliculus, DCN projects directly to auditory thalamus (Malmierca et al., 2002), auditory cortex (Anderson et al., 2009), and regions involved in the acoustic startle response (Lingenhöhl and Friauf, 1994). To our knowledge, responses to self-generated sounds have not been studied at the level of the inferior colliculus. Based on the present results, we would predict that a subset of inferior colliculus neurons selectively encodes external sounds and that this subset receives its dominant input from DCN rather than VCN. Though we focused on a single behavior and a single source of mossy fiber input, the fact that DCN receives mossy fiber inputs from numerous brains regions conveying a wide range of sensory and motor signals implies a much broader capacity for canceling predictable auditory input (Oertel and Young, 2004). We also note that our results by no means rule out the possibility that additional sources of mossy fiber inputs (besides those originating from Sp5) play a role in cancelling self-generated sounds caused by licking behavior. For example, mossy fiber input to DCN granule cell domains originating from the pontine nuclei could provide motor-related signals relevant for cancelling the auditory consequences of the animal's own movements, including licking (Ohlrogge et al., 2001).

Though our results suggest that the integration of non-auditory and auditory inputs to DCN serves to cancels responses to self-generated stimuli, they do not rule out other functions for multimodal integration in DCN. Numerous lines of evidence suggest that the DCN plays an important role in processing spectral cues for sound localization (May, 2000; Oertel and Young, 2004; Young and Davis, 2002). A recent study provided evidence that the integration of auditory and vestibular information in DCN could aid in distinguishing changes in auditory input due to

motion of an external sound source from those due to self-motion (Wigderson et al., 2016). Specifically, Wigderson et al. demonstrate that vestibular and auditory inputs are combined nonlinearly in putative DCN output cells. This is a different mode of integration from that suggested here and by studies of other cerebellum-like structures in fish in which behavior-related signals conveyed by mossy fibers are used to subtract out self-generated signals. Since vestibular inputs would not have been engaged during the head-fixed licking behavior we studied, no direct comparison between the two studies is possible. However, determining whether different sources of mossy fiber inputs to DCN, e,g. vestibular versus somatosensory, perform similar or different computations is an important question for future studies.

Key questions remain regarding the circuit mechanisms underlying the cancellation of self-generated sounds in DCN reported here. In cerebellum-like structures in fish cancellation is due to the generation and subtraction of negative images of the responses of principal cells to self-generated inputs. Such negative images are formed by anti-Hebbian synaptic plasticity acting on corollary discharge, proprioceptive, and electrosensory signals conveyed by parallel fibers (Bell et al., 1997a, 2008). Due both to limits on data collection imposed by satiation as well as the technical difficulty of maintaining stable single-unit recordings in brainstem through long bouts of licking we focused exclusively on providing evidence for cancellation. A crucial next step will be to determine whether cancellation of self-generated sounds in DCN is due to the generation of negative images. Furthermore, genetic tools available in mice should make it possible to perform a detailed dissection of the mechanisms underlying the cancellation of self-generated sounds in DCN. Key questions include the functional roles of specific cell types, such as the CWCs, and the roles of specific sites and mechanisms of plasticity, such as spike timing-

dependent plasticity at parallel fiber synapses onto fusiform cells and CWCs described in vitro (Fujino and Oertel, 2003; Tzounopoulos et al., 2004, 2007).

Finally, our results are intriguing from evolutionary and comparative perspectives. The brains of most vertebrates contain both a cerebellum and one or more sensory structures with circuitry closely resembling that of the cerebellum (Bell, 2002; Bell et al., 2008; Oertel and Young, 2004). Though similarities between different cerebellum-like structures and the cerebellum are well-established in terms of their evolution, development, gene expression patterns, circuitry and synaptic plasticity, the question of whether they perform similar functions has been more difficult to address. Cerebellum-like structures associated with electrosensory processing in three distinct groups of fish have been shown to act as adaptive filters (Bell et al., 1997a, 2008) and numerous lines of evidence also exist supporting such a role for the mammalian cerebellum (Dean et al., 2010; Fujita, 1982). In both cases granule cells convey a rich variety of signals (Chabrol et al., 2015; Huang, 2013; Ishikawa et al., 2015; Kennedy et al., 2014; Sawtell, 2010) and a separate, non-plastic input (peripheral sensory input in the case of cerebellum-like structures and climbing fiber input in the case of cerebellum) instructs plasticity at granule cell synapses such that output that is predictable (in the case of cerebellum-like sensory structures) or associated with errors in motor performance (in the case of the cerebellum) is gradually reduced. Interestingly, adaptive cancellation of self-generated vestibular inputs has been demonstrated in neurons of the fastigial nucleus and vestibular nucleus in primates (Brooks et al., 2015; Roy and Cullen, 2001). Hence evidence provided here for sensory cancellation and adaptive filtering in DCN suggests that a core function may be shared by cerebellum-like structures and the cerebellum across vertebrate phylogeny.

Methods

All experimental protocols were approved by the Columbia University Institutional Animal Care and Use Committee. Adult male wild-type mice (129S6/SvEvTac) were used for all experiments. Mice were purchased from Taconic Biosciences (Hudson, NY) and housed in an on-site animal facility on a 12 hour light-dark cycle. Most experiments were performed during the light cycle. Data collection and analysis were not performed blind to the conditions of the experiments.

Surgery

Mice were anesthetized with isoflurane (1.5-2%) and placed in a stereotax equipped with zygomatic ear bars (Kopf Instruments). The skull was exposed and a small craniotomy 200-500 μm in diameter was made over the right dorsal cochlear nucleus (5.5 mm posterior to bregma and 2.3 mm lateral to the midline). The craniotomy was covered with silicon elastomer (Kwik-Sil, WPI, Sarasota, FL). A custom headplate was attached to the skull using dental cement (C&B Meta-bond, Parkell, Edgewood, NY). Mice were allowed to recover for 3 days prior to the start of experiments.

Experimental apparatus and auditory stimulus presentation

All mouse behavior and neurophysiology experiments were performed in a double walled sound-attenuating chamber (Double Deluxe Model, Gretchken Industries). The ambient noise within the chamber was <30 dB SPL as measured by a sound pressure level meter (Bruel and Kjaer Type 2240). A custom head fixation device was used to secure the animal via two attachment points to a stainless steel headplate and allowed for consistent positioning across multiple

recording sessions. The animal's body was additionally secured between two pieces of styrofoam molded to its body. A stainless steel lick spout was positioned in front of the animal's mouth and licks were detected using standard methods. Acoustic stimuli were generated using Spike2 software (Cambridge Electronic Design) and delivered using an electrostatic speaker (ES-1 Tucker Davis Technologies) positioned approximately 10 cm in front of the mouse just to the right of the midline. Sound pressure levels of acoustic stimuli as measured in dB SPL were calibrated to the location of the animal's right ear. The frequency response of the sound system was measured to be flat (+/- 4dB) from 1 kHz to 50 kHz using a ¼'' condenser microphone (377C01, PCP piezotronics), attached to a preamplifier (426B03, PCP piezotronics) positioned at the location of the mouse's right ear. Sounds caused by licking were monitored by a small electret microphone (Knowles model 23329N) placed just above the lick spout. Microphone signals were sampled at 100 kHz and digitized using an analog to digital converter (Power 1401, Cambridge Electronic Design).

The lick mimic was constructed from segments of microphone recordings 50 ms before tongue contact to 150 ms after tongue contact, and bandpass filtered between 1 and 50 kHz (n = 5 mice). We transformed each segment to a spectrogram using a short-time Fourier transform (Hamming window with a width of 10.24 ms and a stride of 5.12 ms). We then constructed the mimic by performing principal component analysis on this set of lick-triggered spectrograms and making a weighted sum of the first five principal components. This resulted in a mimic spectrogram, which we used as a spectro-temporal filter to convolve with a random signal. This resulted in a stimulus (the lick mimic) which contained the most prominent spectro-temporal features of the licking sound (including distinct spectral peaks at 2, 8, and 30 kHz) with little power elsewhere.

Due to issues such as bone conduction we could not measure the exact loudness of natural licking sounds. The lick mimic was replayed at a loudness that evoked a response in VCN units that was, on average, similar to that evoked by licking. This same loudness (12 dB SPL) was used subsequently for all experiments involving the mimic.

Behavioral training

Mice were allowed to recover 3 days after surgery before to beginning water deprivation and habituation to head restraint in the experimental apparatus. Weight was monitored daily and additional water was given in the home cage if the animal's weight fell below 80% of its initial pre-surgical weight. Extracellular recordings from DCN and VCN units were then performed during daily sessions lasting 2-3 hours. Mice licked roughly 3,000 times per session.

Extracellular recording and identification of DCN and VCN neurons

Standard procedures were used for extracellular recording using glass microelectrodes (5-20 MΩ resistance). Pipettes with a long taper were used to avoid tissue damage. On the day of recording, mice were placed into the head restraint and the silicone elastomer was removed and 0.9% saline was placed over the exposed craniotomy. The microelectrode was lowered into the craniotomy vertically. As the electrode was advanced through the cerebellum a series of 200 ms long search tones from 5 kHz to 50 kHz (in 5 kHz steps) were delivered. Entrance into DCN was marked by a transient increase in electrode resistance along with the sudden appearance of tone-evoked multi-unit activity which occurred ~2700-3200 μm below the surface of the cerebellum. The microelectrode was then advanced in 1 μm steps until a unit was isolated. Complex-spiking units were the first units encountered on an electrode penetration through DCN

and could be unambiguously identified based on their distinctive complex spikes. Complex spikes are stereotyped, high-frequency action potential bursts superimposed on a slower depolarization and are not observed in any DCN cell types except CWCs (Manis et al., 1994; Zhang and Oertel, 1993). Similar to previous *in vivo* extracellular recording studies of DCN in a variety of species, including mouse (Ma and Brenowitz, 2012), we defined complex spikes as high-frequency bursts (ISIs < 3.5 ms) of 2-5 action potentials. Complex spikes were identified automatically in Spike2 using custom written scripts and then confirmed individually. Within such bursts, action potentials successively widened and decreased in amplitude (**Figure 3.8b**). Complex-spiking units were isolated 50-200 μm from the surface of the DCN. DCN units lacking complex spikes, referred to here as simple spiking units, were isolated 100-300 μm from the surface of the DCN. Complex-spiking units were never found ventral to simple spiking units on the same electrode penetration consistent with the known cytoarchitecture of the DCN. Passage from DCN into VCN was determined by monitoring the tone frequency that most strongly drove multi-unit activity for each 50 μm advance of the electrode. As the electrode advanced ventrally, the best frequency for driving multi-unit activity progressively decreased. A sudden increase in the best frequency (generally from ~5 kHz to ~20 kHz and usually occurring 500-600 μm below the surface of DCN) signified entrance into the VCN. Units which were isolated at least 100 μm ventral to the best frequency reversal (~800-1000 μm below the surface of the DCN) and which showed clear tone-evoked responses were classified as VCN units. Units isolated less than 100 μm from the best frequency reversal were not included in the analysis. Histological verification of DCN and VCN recording sites was performed by iontophoresis of dextran conjugated Alexa Flour 594 (D22913, Thermo Fisher Scientific) at recording sites between 100 and 300 μm below the surface of DCN (depths at which most DCN simple spiking

units were isolated) and at 900 μm (the depth at which most VCN units were isolated). Only units that remained well-isolated through at least 75 licks were included in the analysis. Sounds associated with licking contain most power between 2-15 kHz, which corresponds to the lower portion of the mouse hearing range. For this reason we focused our recordings on regions of the cochlear nucleus that represent these frequencies. A subset of the recordings in Figure 6 (DCN correlated, n = 10/20; DCN uncorrelated, n = 5/11; VCN correlated, n = 3/7) were performed using a 16 channel silicon probe (Neuronexus, A1x16-5mm-25-177-A16). Silicon probe recordings proved superior to glass microelectrode recordings in terms of their stability during licking behavior. Probes consisted of a vertical linear array of 15 micron diameter electrode sites spaced 25 microns apart. Impedances ranged from ~2-6 kOhms. Recording tracks were made in DCN or VCN until a well-isolated single unit emerged on at least one electrode site. Most sites exhibited only multi-unit activity and were not analyzed. The same electrophysiological signatures described above were used to identify the dorsal and ventral cochlear nuclei. Rank sum tests revealed no difference between probe and glass recordings in the median decay rate of cells in all three groups shown in Figure 6 (DCN correlated: P = 0.09, DCN uncorrelated: P = 0.79, VCN: P = 0.63).

Viral Injections

A nanoliter injector (504126, WPI instruments) was used to inject adeno-associated virus expressing green fluorescent protein. The pipette was positioned over the coordinates 7.2 mm posterior to bregma and 1.8 mm right of the midline and lowered until the tip touched the surface of the cerebellum. The pipette was then lowered 3.5 mm below the surface of the cerebellum to the base of the spinal trigeminal nucleus. 27 nL of the virus was injected in three 9 nL pulses.

Virus was also injected at depths of 3.2, 2.9, and 2.7 mm below the surface of the cerebellum. The pipette was then slowly raised out of the cerebellum and the incision was closed using cyanoacrylate glue (Vetbond, 3M, Maplewood Minnesota). Two weeks after surgery, mice were anesthetized with ketamine/xylazine and perfused with 4% formaldehyde. The brains were dissected from the skull and allowed to post-fix in 4% formaldehyde overnight. They were then cryoprotected in a 30% sucrose solution and sectioned on a cryostat. Sections were then mounted on glass slides (Superfrost, Fisher Scientific, Waltham, MA), counterstained with DAPI, and imaged on a confocal microscope (Carl Zeiss Microscopy, Peabody, MA).

Deafening

Mice were deafened bilaterally. Surgery for deafening mice was performed using 2-4% isoflurane. An incision was made just posterior to the tragus and extended ventrally. The tympanum, malleus, and incus were visualized through the auditory meatus. Using fine forceps the tympanum was ruptured and the malleus and incus were removed. The stapes was removed exposing the oval window with care taken not to damage the stapedial artery. Using a 30 gauge needle, approximately 10-20 μL of 1.0 mg/mL kanamycin was injected through the oval window and into the cochlea. The middle ear was packed with gel foam and the mouse was allowed to recover in its home cage. Deafening was verified by lack of observable behavioral responses to acoustic stimuli and by recording sound evoked field potentials to broadband noise (50 ms, 6-90 dB SPL) in DCN ~75 μm below the first observed complex-spiking unit. This was done both before and 2 days after surgical deafening in each mouse. DCN recordings were performed 2-4 days after surgery. Recording locations within DCN were confirmed histologically using iontophoresis of dextran-conjugated Alexa 594 as described above.

Lidocaine injections into Sp5

A small craniotomy (~300 μm diameter) was made prior to attachment of the headplate at coordinates 7.2 mm posterior to bregma and 1.8 mm lateral to the midline and covered with silicon elastomer. On the day of the experiment, a glass micropipette with a long taper was pulled using a pipette puller (PC-10, Narishige Group) and manually broken to 3.5 um diameter under a microscope. The pipette was then filled with 2% lidocaine in 0.9% saline with care taken to avoid air bubbles in the tip. The pipette was then coupled to a micropressure injector (Pikospritzer MK III, Parker Instrumentation) and successful ejection of lidocaine was confirmed visually to ensure tip was not clogged. The lidocaine pipette was advanced into Sp5 at an angle of 12.8 degrees. For Sp5 inactivation DCN unit responses were recorded for ~200 licks before ~100 nL of lidocaine was injected in a single pulse. Location of the lidocaine pipette within DCN was verified histologically using iontophoresis of dextran-conjugated Alexa 594 as described above.

Lick-sound pairing

After isolation of a unit, access to water was given and contact to the lick spout by the animal's tongue was paired with a 30 ms noise (15-71 dB SPL, broadband or bandpassed filtered 5-15 kHz). In the correlated condition the noise was presented 30 ms after contact with the lick spout. The pairing was conducted continuously until the animal stopped licking or unit isolation was lost. In the uncorrelated condition presentation of the noise during licking was unrelated to the tongue's contact with the spout and was instead presented at random intervals of 120-160 ms. Since these intervals are similar to inter-lick intervals the overall rate of sound presentations was

similar in the correlated and uncorrelated conditions. Correlated versus uncorrelated conditions were tested in the same mice on alternating sessions. The condition to be tested during a given session was pre-determined prior to isolating a unit.

Data analysis and statistics

All analyses were performed using custom written scripts for Matlab (Mathworks, Natick, MA) and Spike 2. No statistical methods were used to predetermine sample sizes. Comparisons between two groups were made by Mann–Whitney *U*-test or Wilcoxon signed rank test for paired groups. Tests of the significance of linear regression slopes used a linear regression t-test. For the linear regression t-test residuals were assumed to be normally distributed but this was not formally tested. Differences were considered statistically significant at $P < 0.01$. Data are presented as mean ± s.e.m. unless indicated otherwise.

Lick sound spectrograms: To compute the average spectrogram of the sound associated with licking we first bandpass filtered raw microphone traces removing frequencies below 1 kHz and above 50 kHz (the highest frequency that could be detected by our equipment). 300 ms segments of the filtered microphone recording centered on the onset of each lick were transformed with a short time Fourier transform (Hamming window with a width of 10.24 ms and a stride of 5.12 ms) to obtain a set of lick-centered spectrograms. These were averaged to obtain a lick-triggered average spectrogram. Time-frequency peaks were found by first applying a 2-D median filter (widths 290 Hz, 3 ms) to individual spectrograms and then convolving with a 2-D Gaussian kernel with widths 1.5 kHz and 20 ms. We then calculated local time-frequency maximums by finding local maximums of the filtered spectrograms.

RMS amplitude of microphone traces: To compute the RMS amplitude of the sound associated with licking microphone recordings were first bandpass filtered (1-50 kHz). We then computed the RMS amplitude of this filtered microphone trace by convolving the squared trace with a moving average kernel of width 1 ms and taking the square root of the result. These recordings were then aligned to the time of tongue contact with the lick spout and averaged across licks.

Average and Z-scored electrophysiological responses during licking and mimic presentation: To compute average responses to licking or during delivery of the mimic spike trains were convolved with a normalized sum-of-two-exponentials kernel, with a rise time of 5 ms and a decay time of 20 ms. Averages were aligned either on tongue contact with the lick spout or mimic delivery and average baseline firing was subtracted. Baseline firing rates was taken to be the average firing rates in periods at least 25 ms before the next lick or mimic onset and at least 150 ms after the previous lick or mimic onset. Peak-to-trough firing rates were computed by taking the average licking or mimic response in a 200 ms window centered on the tongue-to-spout contact or mimic onset and determining the difference in the maximum to minimum firing rates. To compute z-scores we first took the maximum of the average licking or mimic response in a 200 ms window centered on tongue-to-spout contract or mimic onset. We then created shuffled spike trains of approximately the same length as the original spike train by randomly sampling from the inter-spike-interval distribution of the real spike train. Each shuffled spike train was convolved with the same kernel as the real spike train, its lick- or mimic-triggered average computed, and the maximum firing rate of this triggered average taken in the same 200 ms window. This was repeated 500 times and the maximum of the triggered average of the real

spike train was expressed in units of the standard deviation from the mean of the shuffle distribution, i.e. z-scored based on the shuffle distribution. We determined the significance of neural responses by computing approximate p-values for the recorded maximum lick-triggered rate, which were estimated by the fraction of shuffled-spike trains showing maximum lick-triggered responses greater than that of the real spike train.

Correlated and uncorrelated sound-lick pairings: The noise-evoked response is defined in bins of 150 stimulus presentations. For each 150 presentations the response is defined as the maximum of the average noise-evoked response during that stimulus period minus the baseline rate during that period. For each unit the response is normalized to equal one in the first bin. We performed a linear regression between the stimulus bin and the log of the noise-evoked responses for each population, in order to extract a decay rate for each population.

Chapter 4

Conclusion

The work described in this dissertation aims to provide a more functional description of the role of sensory cancellation, higher order corollary discharge, and more specifically, cerebellum-like systems, in sensory processing, than exists. In Chapter 2, we demonstrate for the first time that negative images created through plastic corollary discharges have a functional role in both neural coding of sensory input and behavior. In Chapter 3, we demonstrate the long-predicted role of the mammalian dorsal dorsal cochlear nucleus in cancelling self-generated sound.

In cancelling the sound of licking, the DCN allows higher order auditory processing areas to have access to two streams of information – one, coming from the VCN, a complete representation of acoustic inputs to the cochlea, including self- and other-generated sounds. The other, from the DCN, a filtered stream of information which actively excludes predictable inputs generated by the self, retaining, potentially, an accurate representation of only externally-generated sounds – what the world would sound like in the absence of the agent of sensation. The extent to which this latter idea holds for the broad variety of self-generated sounds which corrupt the attempts by the auditory system to sense the world around it remains to be seen and is an area ripe for further study.

Concerning the dorsal cochlear nucleus

The auditory system is subject to a wide range of interfering self-generated signals that arrive through acoustic vibration of the air and impinge on the tympanic membrane (that is, signals that leave the body and re-enter it) and through bone conduction, directly acting on the sensory machinery of the middle and inner ear. Breathing, mastication, locomotion all actively produce sound, and rotations of the head, changes in body position, and motion of the external ear, the pinna, all modify the amplitude and spectral properties of external sounds, resulting in a

type of reafference. In unpublished work, colleagues and I have demonstrated that principal cells of the DCN are driven by breathing, motion of the jaw, and movement of the pinnae in the absence of external sound. The wide range of mossy fiber inputs to the granule cell domains, and the position of the DCN early in the auditory processing cascade lend themselves to a unique filtering role for the DCN. Locomotion has been shown to have suppressive effective on cortex, but it would be interesting to see whether some of the reafferent effects of locomotion are also dealt with at this earlier stage. Additionally, it's noteworthy that for small animals such as the mouse studied here, the reafference originates from processes that are often only a few centimeters, sometimes millimeters, from the ear. The concordant pressure levels at the ear for some behaviors may be considerably larger than breathing, the example dealt with in Chapter 3, and it would be instructive to know whether such cancellation works only for sounds near the threshold of auditory detection, or for higher pressure levels as well. For comparison, we used a breathing mimic of 15dB SPL, which is somewhere between "Grand Canyon at night" and "rustling leaves" (Berger et al., 2006). The related earlier (failed) efforts mentioned above looking at pinna-, jaw-, and breathing-related modulations in DCN focused on sounds at pressure levels some 50-150 times larger. While the experimental preparation was significantly different between the two attempts, continuing the current line of experiments for other behaviors known to have an effect on the DCN, and at a broader range of amplitudes, may well be fruitful.

As an aside, the above point that the auditory sensory organ is much closer to the sources of reafference in smaller animals isn't so clear – while the distance between the ear and the joints and muscles, jaws and feet generating such sound grows linearly as you scale the animal, and the sound pressure varies in inverse proportion to that distance, the dimensional volume, and mass, of these parts grows with the cube. A rat's jaw may be twice as far from its ear as that of a

mouse, and a given sound originating at the jaw of each would have half the pressure reaching the ear of the rat versus the mouse, but the rat's jaw is 8 times more massive. A theoretical and empirical accounting of the effect of body size would be useful in understanding the issues facing sensory systems in dealing with reafference.

The initial focus on the DCN for these experiments came directly from its resemblance to the mormyrid ELL and the well-studied system of reafferent cancellation and negative image formation therein (Oertel and Young, 2004). However, while cancellation has been demonstrated, negative images have not been, though the similarity between the ELL and DCN, including the existence of anti-Hebbian plasticity at PF-cartwheel cell and conditionally, PF-fusiform cell synapses (Tzounopoulos et al., 2004) strongly suggest negative images as an underlying mechanism for cancellation. Further work in that direction is necessary. In general, the circuit, cellular, and synaptic mechanisms for cancellation need to be explored, including the role of other cell types, in particular the Purkinje-like cartwheel cell, as well as unipolar brush cells and stellate cells. Preliminary work on cartwheel cell responses to self- versus externally-generated sounds was described by Singla (Singla, 2016). The general history of research in the ELL can serve as a blueprint for such work.

Finally, the current findings need to be integrated with the other putative role of the DCN, that of monoaural sound localization. The findings on this are less clear when applied to the mouse. While May (May, 2000) showed that lesions of DCN output disrupted vertical sound localization in cats, mice in fact perform poorly at localizing sound sources in the vertical axis as opposed to the horizontal even with an intact DCN. This may be due either to inter-species differences in DCN structure or to the demonstrated relative paucity of elevation-related spectral cues imposed by directional acoustic filtering of incoming sound by the mouse head and pinna

(Lauer et al., 2011). Fusiform and vertical cells in cats display non-linear, feature-detecting responses to spectral notches, which are the cues thought to be used in monaural sound localization (Reiss, 2005), but such results have not been reported in mice. Though these two roles, cancellation and localization, are at first blush functionally unrelated, spectral cues are themselves a form of reafference, but rather than *cancellation* of reafference as demonstrated in mouse, notch-detection in cat can be thought of as a kind of reafference *detection*. Extending the work in mouse to cat, or other species with demonstrated spectrally-based localization, would be informative.

Concerning the electrosensory lobe

In the mormyrid ELL we have demonstrated that negative images based on corollary discharge are utilized by the animal to improve neural coding and effect behavior, but many questions persist. Our work focuses on the glutamatergic output neurons of the ELL, the E-type Large Fusiform Cell and the I-type Large Ganglion Cell, but these cells are outnumbered by the other class of principal cell of the ELL, the Purkinje-like MG cells". The functional significance of these two classes of cells is an outstanding problem for the field, and no one has of yet been able to dissect their relative contributions to the function of the ELL, including in the formation of negative images. Both classes of cells, output and MG, produce negative images. The MG cells inhibit each other and the output cells. Output cells do not synapse directly onto MG cells, but may indirectly influence them by way of feedback from the preeminential nucleus (PE), which receives input from the output neurons. Excitatory inputs from PE terminate deep in the molecular layer with somatotopic organization. The effect of this feedback on negative images is unknown. An outstanding question is the spatial extent of negative images – what positive image are they being constructed to. It may be that the spatial extent of the electrosensory

receptive fields of ELL neurons is not the same as the spatial area for which they create a negative image. The previously described plastic mechanisms for generating negative images work on extracting predictable signals from the receptive field of that particular neuron, but network effect within the ELL may create a different net negative image. The negative image may represent, for example, negation of the reafferent response across some larger part of the body. Some evidence of this exists in 'over-cancellation' that we have observed. In a preparation where the EOD motor signal is paired with an EOD mimic, and presented globally – that is, affecting cells all over the body, not only at the receptive field of the recorded cell – the response of cells to the mimic and command presented together showed a kind of overcompensation for the excitatory or inhibitory response of E or I cells to the mimic alone. **Figure 4.1** demonstrates a case of over-cancellation. Under-cancellation, also observed, could result from the same effect. These observations imply that the negative image at a given cell may effectively be formed to some pooled response to reafference. Alternatively, the two cell classes may underlie multiple time scales of cancellation. The dynamics of PF-MG plasticity are known to be affected by feedback (Sawtell et al., 2007).

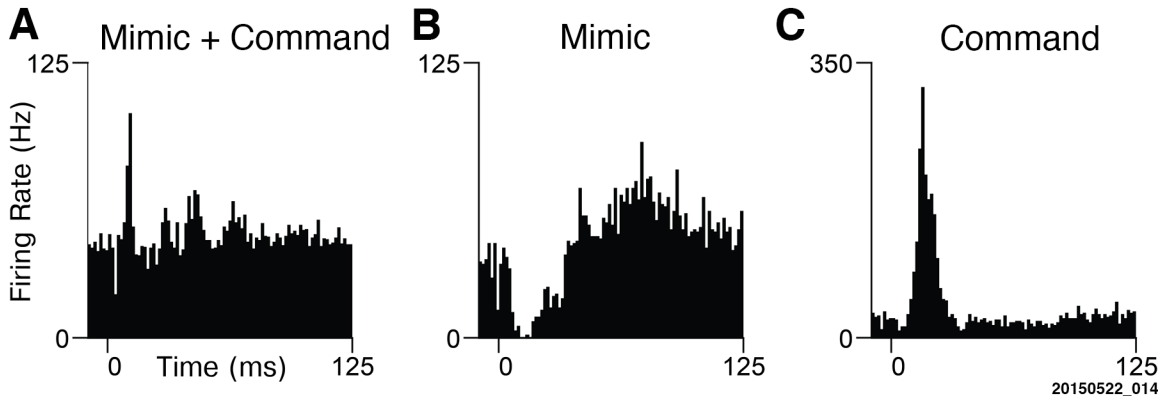

Figure 4.1 Over-cancellation in an ELL output cell.
(A) Peristimulus time histogram of extracellular recording of an I-type output cell in the VLZ of the ELL, response to EOD mimic presented globally and synchronized to an EOD motor command, after pairing for several hours. T=0 locked to onset of command. **(B)** Response of the same cell to EOD mimic

presented out of synchrony with the EOD motor command. **(C)** Response in same cell to the EOD motor command alone. This is the negative image.
Note that the prominent 'over-cancellation' **(A)** shortly after onset of command and mimic. The strong negative image demonstrated in **(C)** over-cancels the inhibited response of the cell to the EOD mimic shown to **(B)**, bringing the total response past baseline.

Our work has focused on the VLZ of the ELL as a circuit for removing correlations between external electrosensory and self-generated input, in this case the electromotor EOD. Another possible role for the ELL, by no means mutually exclusive with any of the above, is in removing *auto*correlation across time or space from the exafferent electrosensory input itself.

Electrosensory inflow may contain predictable information across either spatially, across the extent of the body because of local conditions, or across time, and removing it would increase information density in the signal. For example, wave-induced mixing of water oxygenated by photosynthetic activity can produce oxidation-reduction potentials of up to 500mV (Keller, 2004; Koch-Rose et al., 1994), 10-15 times the threshold of detection by ampullary afferents. Such a role is supported by the existence of indirect feedback from EGp onto granule cells, which provides a basis by which to perform such subtractions (Bastian, 1986; Bastian and Bratton, 1990; Bell et al., 1981; von der Emde and Bell, 1996; Sawtell, 2017). This is similar to proposed predictive coding schemes in visual cortex (Rao and Ballard, 1999) and auditory cortex (Crapse and Sommer, 2008b; Eliades and Wang, 2008), and in particular to a mechanism dependent on anti-Hebbian plasticity proposed to exist in the retina (Hosoya et al., 2005). Development of work in this direction is particularly interesting, and it would be informative to try to detect changes in signal detection of novel stimuli, by ROC or other methods, on a background of either spatially or temporally predictable electrosensory inputs.

In toto, I see this work as contributing to an understanding of the brain which is more directly concerned with function while insisting on ground-level mechanistic explanations of

phenomena, particularly in regard to how we sense the outside world and ourselves. In conclusion, thinking back to the Greeks in whose minds the first inklings of these questions developed, it's fitting to consider that the maxim famously inscribed on the entrance to the Temple of Apollo at Delphi, Γνώθι Σεαυτόν, "know thy self", may suitably be completed "… and learn to ignore it".

Works Cited

Acampora, D., Avantaggiato, V., Tuorto, F., and Simeone, A. (1997). Genetic control of brain morphogenesis through Otx gene dosage requirement. Development *124*, 3639–3650.

Anderson, L.A., Izquierdo, M.A., Antunes, F.M., and Malmierca, M.S. (2009). A monosynaptic pathway from dorsal cochlear nucleus to auditory cortex in rat. Neuroreport *20*, 462–466.

Aristotle (330 BCE / 1906 AD). On Dreams, in Parva Naturalia. In The Works of Aristotle, (Oxford: Clarendon Press), p.

Arnegard, M.E., and Carlson, B.A. (2005). Electric organ discharge patterns during group hunting by a mormyrid fish. Proc. R. Soc. Lond. B Biol. Sci. *272*, 1305–1314.

Arshavsky, Y.I., Berkinblit, M.B., Fukson, O.I., Gelfand, I.M., and Orlovsky, G.N. (1972). Origin of modulation in neurones of the ventral spinocerebellar tract during locomotion. Brain Res. *43*, 276–279.

Arshavsky, Y.I., Gelfand, I.M., and Orlovsky, G.N. (1983). The cerebellum and control of rhythmical movements. Trends Neurosci. *6*, 417–422.

Auerbach, B.D., Osterweil, E.K., and Bear, M.F. (2011). Mutations causing syndromic autism define an axis of synaptic pathophysiology. Nature *480*, 63.

Azim, E., Jiang, J., Alstermark, B., and Jessell, T.M. (2014). Skilled reaching relies on a V2a propriospinal internal copy circuit. Nature *508*, 357–363.

Bacelo, J., Engelmann, J., Hollmann, M., Emde, G. von der, and Grant, K. (2008). Functional foveae in an electrosensory system. J. Comp. Neurol. *511*, 342–359.

Barash, S., Bracewell, R.M., Fogassi, L., Gnadt, J.W., and Andersen, R.A. (1991). Saccade-related activity in the lateral intraparietal area. II. Spatial properties. J. Neurophysiol. *66*, 1109–1124.

Barlow, H. (1990). Conditions for versatile learning, Helmholtz's unconscious inference, and the task of perception. Vision Res. *30*, 1561–1571.

Bastian, J. (1986). Gain control in the electrosensory system mediated by descending inputs to the electrosensory lateral line lobe. J. Neurosci. *6*, 553–562.

Bastian, J. (1993). The role of amino acid neurotransmitters in the descending control of electroreception. J. Comp. Physiol. A *172*, 409–423.

Bastian, J. (1995). Pyramidal-cell plasticity in weakly electric fish: a mechanism for attenuating responses to reafferent electrosensory inputs. J. Comp. Physiol. A *176*, 63–78.

Bastian, J. (1996). Plasticity in an electrosensory system. I. General features of a dynamic sensory filter. J. Neurophysiol. *76*, 2483–2496.

Bastian, J., and Bratton, B. (1990). Descending control of electroreception. I. Properties of nucleus praeeminentialis neurons projecting indirectly to the electrosensory lateral line lobe. J. Neurosci. *10*, 1226–1240.

Bastian, J., and Nguyenkim, J. (2001). Dendritic Modulation of Burst-Like Firing in Sensory Neurons. J. Neurophysiol. *85*, 10–22.

Battaglini, P., Galletti, C., Aicardi, G., Squatrito, S., and Maioli, M. (1986). Effect of fast moving stimuli and saccadic eye movements on cell activity in visual areas V1 and V2 of behaving monkeys. Arch. Ital. Biol. *124*, 111–119.

Battaglini, P.P., Galletti, C., and Fattori, P. (1996). Cortical mechanisms for visual perception of object motion and position in space. Behav. Brain Res. *76*, 143–154.

Bear, M.F., and Malenka, R.C. (1994). Synaptic plasticity: LTP and LTD. Curr. Opin. Neurobiol. *4*, 389–399.

Bell, C.C. (1981). An Efference Copy Which is Modified by Reafferent Input. Science *214*, 450–453.

Bell, C.C. (1982). Properties of a modifiable efference copy in an electric fish. J. Neurophysiol. *47*, 1043–1056.

Bell, C.C. (1989). Sensory coding and corollary discharge effects in mormyrid electric fish. J. Exp. Biol. *146*, 229–253.

Bell, C.C. (2001). Memory-based expectations in electrosensory systems. Curr. Opin. Neurobiol. *11*, 481–487.

Bell, C.C. (2002). Evolution of Cerebellum-Like Structures. Brain. Behav. Evol. *59*, 312–326.

Bell, C., and Szabo, T. (1986). Electroreception in mormyrid fish: central anatomy. Electroreception 375–421.

Bell, C.C., and Russell, C.J. (1978). Effect of electric organ discharge on ampullary receptors in a mormyrid. Brain Res. *145*, 85–96.

Bell, C., Finger, T., and Russell, C. (1981). Central connections of the posterior lateral line lobe in mormyrid fish. Exp. Brain Res. *42*, 9–22.

Bell, C., Bodznick, D., Montgomery, J., and Bastian, J. (1997a). The Generation and Subtraction of Sensory Expectations within Cerebellum-Like Structures. Brain. Behav. Evol. *50*, 17–31.

Bell, C.C., Grant, K., and Serrier, J. (1992a). Sensory processing and corollary discharge effects in the mormyromast regions of the mormyrid electrosensory lobe. I. Field potentials, cellular activity in associated structures. J. Neurophysiol. *68*, 843–858.

Bell, C.C., Grant, K., and Serrier, J. (1992b). Sensory processing and corollary discharge effects in the mormyromast regions of the mormyrid electrosensory lobe. I. Field potentials, cellular activity in associated structures. J. Neurophysiol. *68*, 843–858.

Bell, C.C., Caputi, A., Grant, K., and Serrier, J. (1993). Storage of a Sensory Pattern by Anti-Hebbian Synaptic Plasticity in an Electric Fish. Proc. Natl. Acad. Sci. U. S. A. *90*, 4650–4654.

Bell, C.C., Han, V.Z., Sugawara, Y., and Grant, K. (1997b). Synaptic plasticity in a cerebellum-like structure depends on temporal order. Nature *387*, 278–281.

Bell, C.C., Caputi, A., and Grant, K. (1997c). Physiology and plasticity of morphologically identified cells in the mormyrid electrosensory lobe. J. Neurosci. *17*, 6409–6423.

Bell, C.C., Han, V., and Sawtell, N.B. (2008). Cerebellum-Like Structures and Their Implications for Cerebellar Function. Annu. Rev. Neurosci. *31*, 1–24.

Belmeguenai, A., and Hansel, C. (2005). A role for protein phosphatases 1, 2A, and 2B in cerebellar long-term potentiation. J. Neurosci. *25*, 10768–10772.

Berger, E.H., Neitzel, R., and Kladden, C.A. (2006). Noise navigator TM sound level database with over 1700 measurement values. Univ. Wash. Dep. Environ. Occup. Health Sci. Seattle Avarilable Httpwww Ear CompdfhearingconsNoiseNav Xls Accessed *8*, 20.

Berman, N.J., and Maler, L. (1998). Distal versus proximal inhibitory shaping of feedback excitation in the electrosensory lateral line lobe: implications for sensory filtering. J. Neurophysiol. *80*, 3214–3232.

Berman, N., Dunn, R.J., and Maler, L. (2001). Function of NMDA receptors and persistent sodium channels in a feedback pathway of the electrosensory system. J. Neurophysiol. *86*, 1612–1621.

Berman, R.A., Cavanaugh, J., McAlonan, K., and Wurtz, R.H. (2016). A circuit for saccadic suppression in the primate brain. J. Neurophysiol. *117*, 1720–1735.

Berrebi, A.S., Morgan, J.I., and Mugnaini, E. (1990). The Purkinje cell class may extend beyond the cerebellum. J. Neurocytol. *19*, 643–654.

Blaxter, J. (1988). 1 Pattern and Variety in Development. In Fish Physiology, (Elsevier), pp. 1–58.

Bleckmann, H., and von der Emde, G. (1998). Finding food: senses involved in foraging for insect larvae in the electric fish gnathonemus petersii. J. Exp. Biol. *201*, 969–980.

Bodznick, D., and Montgomery, J. (2005). The physiology of low-frequency electrosensory systems. In Electroreception, (Springer), pp. 132–153.

Bodznick, D., and Montgomery, J.C. (1992). Suppression of Ventilatory Reafference in the Elasmobranch Electrosensory System: Medullary Neuron Receptive Fields Support a Common Mode Rejection Mechanism. J. Exp. Biol. *171*, 127–137.

BODZNICK, D., and MONTGOMERY, J.C. (1992). Suppression of Ventilatory Reafference in the Elasmobranch Electrosensory System: Medullary Neuron Receptive Fields Support a Common Mode Ejection Mechanism. J. Exp. Biol. *171*, 127–137.

Bodznick, D., Hjelmstad, G., and Bennett, M. (1993). Accommodation to maintained stimuli in the ampullae of Lorenzini: how an electroreceptive fish achieves sensitivity in a noisy world. Jpn. J. Physiol. *43*, S231–7.

Bodznick, D., Montgomery, J.C., and Carey, M. (1999). Adaptive mechanisms in the elasmobranch hindbrain. J. Exp. Biol. *202*, 1357–1364.

Bol, K., Marsat, G., Harvey-Girard, E., Longtin, A., and Maler, L. (2011). Frequency-tuned cerebellar channels and burst-induced LTD lead to the cancellation of redundant sensory inputs. J. Neurosci. *31*, 11028–11038.

Brooks, J.X., Carriot, J., and Cullen, K.E. (2015). Learning to expect the unexpected: rapid updating in primate cerebellum during voluntary self-motion. Nat. Neurosci. *18*, 1310.

Bruce, C.J., and Goldberg, M.E. (1985). Primate frontal eye fields. I. Single neurons discharging before saccades. J. Neurophysiol. *53*, 603–635.

Budinger, E., and Scheich, H. (2009). Anatomical connections suitable for the direct processing of neuronal information of different modalities via the rodent primary auditory cortex. Hear. Res. *258*, 16–27.

Bullock, T.H. (1988). The comparative neurology of expectation: stimulus acquisition and neurobiology of anticipated and unanticipated input. In Sensory Biology of Aquatic Animals, (Springer), pp. 269–284.

Bullock, T.H., and Northcutt, R.G. (1982). A new electroreceptive teleost:<Emphasis Type="Italic">Xenomystus nigri</Emphasis> (Osteoglossiformes: Notopteridae). J. Comp. Physiol. *148*, 345–352.

Bullock, T.H., Bodznick, D.A., and Northcutt, R.G. (1983). The Phylogenetic Distribution of Electroreception: Evidence for Convergent Evolution of a Primitive Vertebrate Sense Modality. Brain Res. Rev. *6*, 25–46.

Cant, N.B. (1992). The cochlear nucleus: neuronal types and their synaptic organization. Mamm. Audit. Pathw. Neuroanat. 66–116.

Cavanaugh, J., Berman, R.A., Joiner, W.M., and Wurtz, R.H. (2016). Saccadic Corollary Discharge Underlies Stable Visual Perception. J. Neurosci. *36*, 31–42.

Celesia, G.G. (2012). Alcmaeon of Croton's Observations on Health, Brain, Mind, and Soul. J. Hist. Neurosci. *21*, 409–426.

Chabrol, F.P., Arenz, A., Wiechert, M.T., Margrie, T.W., and DiGregorio, D.A. (2015). Synaptic diversity enables temporal coding of coincident multisensory inputs in single neurons. Nat Neurosci *18*, 718–727.

Chacron, M.J. (2006). Nonlinear Information Processing in a Model Sensory System. J. Neurophysiol. *95*, 2933–2946.

Chacron, M.J., Doiron, B., Maler, L., Longtin, A., and Bastian, J. (2003). Non-classical receptive field mediates switch in a sensory neuron's frequency tuning. Nature *423*, 77.

Chacron, M.J., Maler, L., and Bastian, J. (2005). Feedback and feedforward control of frequency tuning to naturalistic stimuli. J. Neurosci. *25*, 5521–5532.

Chadderton, P., Margrie, T.W., and Häusser, M. (2004). Integration of quanta in cerebellar granule cells during sensory processing. Nature *428*, 856.

Chen, L., House, J.L., Krahe, R., and Nelson, M.E. (2005). Modeling signal and background components of electrosensory scenes. J. Comp. Physiol. A *191*, 331–345.

Corbet, P.S. (1961). The food of non-cichlid fishes in the lake victoria basin, with remarks on their evolution and adaptation to lacustrine conditions. Proc. Zool. Soc. Lond. *136*, 1–101.

Crapse, T.B., and Sommer, M.A. (2008a). Corollary discharge across the animal kingdom. Nat. Rev. Neurosci. *9*, 587–600.

Crapse, T.B., and Sommer, M.A. (2008b). Corollary discharge circuits in the primate brain. Curr. Opin. Neurobiol. *18*, 552–557.

Crawford, T., Haeger, B., Kennard, C., Reveley, M., and Henderson, L. (1995). Saccadic abnormalities in psychotic patients. I. Neuroleptic-free psychotic patients. Psychol. Med. *25*, 461–471.

Creutzfeldt, O., Ojemann, G., and Lettich, E. (1989). Neuronal activity in the human lateral temporal lobe. Exp. Brain Res. *77*, 451–475.

Cullen, K.E. (2004). Sensory signals during active versus passive movement. Curr. Opin. Neurobiol. *14*, 698–706.

Czech-Damal, N.U., Liebschner, A., Miersch, L., Klauer, G., Hanke, F.D., Marshall, C., Dehnhardt, G., and Hanke, W. (2011). Electroreception in the Guiana dolphin (Sotalia guianensis). Proc. R. Soc. Lond. B Biol. Sci. rspb20111127.

Davis, K.A., Ding, J., Benson, T.E., and Voigt, H.F. (1996). Response properties of units in the dorsal cochlear nucleus of unanesthetized decerebrate gerbil. J Neurophysiol *75*, 1411–1431.

Dayan, P., and Abbott, L.F. (2001). Theoretical neuroscience (Cambridge, MA: MIT Press).

Dean, P., Porrill, J., Ekerot, C.F., and Jörntell, H. (2010). The cerebellar microcircuit as an adaptive filter: experimental and computational evidence. Nat Rev Neurosci *11*, 30–43.

Delcomyn, F. (1977). Corollary discharge to cockroach giant interneurones. Nature *269*, 160.

Derbin, C. (1974). Ultrastructure of the ampullary receptor organs in a mormyrid fish, Gnathonemus petersii. III. J. Ultrastruct. Res. *46*, 254–267.

Diamond, M.R., Ross, J., and Morrone, M.C. (2000). Extraretinal Control of Saccadic Suppression. J. Neurosci. *20*, 3449–3455.

Diño, M.R., and Mugnaini, E. (2008). Distribution and phenotypes of unipolar brush cells in relation to the granule cell system of the rat cochlear nucleus. Neuroscience *154*, 29–50.

Doiron, B., Chacron, M.J., Maler, L., Longtin, A., and Bastian, J. (2003). Inhibitory feedback required for network oscillatory responses to communication but not prey stimuli. Nature *421*, 539.

Duhamel, J.-R., Colby, C.L., and Goldberg, M.E. (1992). The Updating of the Representation of Visual Space in Parietal Cortex by Intended Eye Movements. Sci. Wash. *255*, 90.

Dupont, J.-L., Gardette, R., and Crepel, F. (1987). Postnatal development of the chemosensitivity of rat cerebellar Purkinje cells to excitatory amino acids. An in vitro study. Dev. Brain Res. *34*, 59–68.

Duysens, J., Trippel, M., Horstmann, G.A., and Dietz, V. (1990). Gating and reversal of reflexes in ankle muscles during human walking. Exp. Brain Res. *82*.

Edwards, D.H., Heitler, W.J., and Krasne, F.B. (1999). Fifty years of a command neuron: the neurobiology of escape behavior in the crayfish. Trends Neurosci. *22*, 153–161.

Eliades, S.J., and Wang, X. (2003). Sensory-motor interaction in the primate auditory cortex during self-initiated vocalizations. J Neurophysiol *89*, 2194–2207.

Eliades, S.J., and Wang, X. (2008). Neural substrates of vocalization feedback monitoring in primate auditory cortex. Nature *453*, 1102–1106.

Emde, G. von der (2013). Electroreception. In Neurosciences - From Molecule to Behavior: A University Textbook, (Springer Spektrum, Berlin, Heidelberg), pp. 409–425.

von der Emde, G. (1994). Active electrolocation helpsGnathonemus petersii to find its prey. Sci. Nat. *81*, 367–369.

von der Emde, G., and Bell, C.C. (1996). Nucleus preeminentialis of mormyrid fish, a center for recurrent electrosensory feedback. I. Electrosensory and corollary discharge responses. J. Neurophysiol. *76*, 1581–1596.

Engelmann, J., Gertz, S., Goulet, J., Schuh, A., and von der Emde, G. (2010). Coding of Stimuli by Ampullary Afferents in Gnathonemus petersii. J. Neurophysiol. *104*, 1955–1968.

Enikolopov, A.G. (2018). Back of an envelope.

Farris, S.M. (2011). Are mushroom bodies cerebellum-like structures? Arthropod Struct. Dev. *40*, 368–379.

Feinberg, I. (1978). Efference Copy and Corollary Discharge: Implications for Thinking and Its Disorders. Schizophr. Bull. *4*, 636–640.

Fischer, B., Boch, R., and Bach, M. (1981). Stimulus versus eye movements: Comparison of neural activity in the striate and prelunate visual cortex (A17 and A19) of trained rhesus monkey. Exp. Brain Res. *43*, 69–77.

Floris, A., Diño, M., Jacobowitz, D.M., and Mugnaini, E. (1994). The unipolar brush cells of the rat cerebellar cortex and cochlear nucleus are calretinin-positive: a study by light and electron microscopic immunocytochemistry. Anat. Embryol. (Berl.) *189*, 495–520.

Ford, J.M., and Mathalon, D.H. (2005). Corollary discharge dysfunction in schizophrenia: Can it explain auditory hallucinations? Int. J. Psychophysiol. *58*, 179–189.

Ford, J.M., Mathalon, D.H., Heinks, T., Kalba, S., Faustman, W.O., and Roth, W.T. (2001a). Neurophysiological Evidence of Corollary Discharge Dysfunction in Schizophrenia. Am. J. Psychiatry *158*, 2069–2071.

Ford, J.M., Mathalon, D.H., Kalba, S., Whitfield, S., Faustman, W.O., and Roth, W.T. (2001b). Cortical Responsiveness During Inner Speech in Schizophrenia: An Event-Related Potential Study. Am. J. Psychiatry *158*, 1914–1916.

Fu, Y., Tucciarone, J.M., Espinosa, J.S., Sheng, N., Darcy, D.P., Nicoll, R.A., Huang, Z.J., and Stryker, M.P. (2014). A Cortical Circuit for Gain Control by Behavioral State. Cell *156*, 1139–1152.

Fujino, K., and Oertel, D. (2003). Bidirectional synaptic plasticity in the cerebellum-like mammalian dorsal cochlear nucleus. Proc Natl Acad Sci Usa *100*, 265–270.

Fujita, M. (1982). Adaptive filter model of the cerebellum. Biol. Cybern. *45*, 195–206.

Gabbiani, F., Metzner, W., Wessel, R., and Koch, C. (1996). From stimulus encoding to feature extraction in weakly electric fish. Nature *384*, 564.

Godfrey, D.A., Lee, A.C., Hamilton, W.D., Benjamin, L.C., Vishwanath, S., Simo, H., Godfrey, L.M., Mustapha, A.I.A.A., and Heffner, R.S. (2016). Volumes of cochlear nucleus regions in rodents. Hear. Res. *339*, 161–174.

Godin, A.J. (1964). A review of the literature on the mountain beaver (US Fish and Wildlife Service).

Grant, K., Sugawara, Y., Gómez, L., Han, V.Z., and Bell, C.C. (1998a). The Mormyrid Electrosensory Lobe In Vitro: Physiology and Pharmacology of Cells and Circuits. J. Neurosci. *18*, 6009–6025.

Grant, K., Sugawara, Y., Gómez, L., Han, V.Z., and Bell, C.C. (1998b). The mormyrid electrosensory lobe in vitro: physiology and pharmacology of cells and circuits. J. Neurosci. *18*, 6009–6025.

Gross, C.G. (1999). The Fire That Comes from the Eye. The Neuroscientist *5*, 58–64.

Grüsser, O.-J. (1986). Interaction of efferent and afferent signals in visual perception a history of ideas and experimental paradigms. Acta Psychol. (Amst.) *63*, 3–21.

Grüsser, O.-J. (1995). On the history of the ideas of efference copy and reafference. In Essays in the History of the Physiological Sciences: Proceedings of a Network Symposium of the European Association for the History of Medicine and Health Held at the University Louis Pasteur, Strasbourg, on March 26-27th, 1993, (Rodopi), p. 35.

Guthrie, B.L., Porter, J.D., and Sparks, D.L. (1983). Corollary discharge provides accurate eye position information to the oculomotor system. Science *221*, 1193–1195.

Haenggeli, C.A., Pongstaporn, T., Doucet, J.R., and Ryugo, D.K. (2005). Projections from the spinal trigeminal nucleus to the cochlear nucleus in the rat. J Comp Neurol *484*, 191–205.

Hall, N.J., and Colby, C.L. (2011). Remapping for visual stability. Philos. Trans. R. Soc. B Biol. Sci. *366*, 528–539.

Hall, C., Bell, C., and Zelick, R. (1995). Behavioral evidence of a latency code for stimulus intensity in mormyrid electric fish. J. Comp. Physiol. A *177*, 29–39.

Han, V.Z., Bell, C.C., Grant, K., and Sugawara, Y. (1999). Mormyrid electrosensory lobe in vitro: morphology of cells and circuits. J. Comp. Neurol. *404*, 359–374.

Han, V.Z., Grant, K., and Bell, C.C. (2000a). Reversible Associative Depression and Nonassociative Potentiation at a Parallel Fiber Synapse. Neuron *27*, 611–622.

Han, V.Z., Grant, K., and Bell, C.C. (2000b). Reversible associative depression and nonassociative potentiation at a parallel fiber synapse. Neuron *27*, 611–622.

Hancock, K.E., and Voigt, H.F. (2002). Intracellularly labeled fusiform cells in dorsal cochlear nucleus of the gerbil. I. Physiological response properties. J Neurophysiol *87*, 2505–2519.

Harvey-Girard, E., and Maler, L. (2013). Dendritic SK channels convert NMDA-R-dependent LTD to burst timing-dependent plasticity. J. Neurophysiol. *110*, 2689–2703.

Harvey-Girard, E., Lewis, J., and Maler, L. (2010). Burst-induced anti-Hebbian depression acts through short-term synaptic dynamics to cancel redundant sensory signals. J. Neurosci. *30*, 6152–6169.

Hebb, D.O. (1949). The Organization of Behavior: A neuropsychological theory (New York: John Wiley & Sons).

Heffner, R.S., and Heffner, H.E. (1988). Sound localization in a predatory rodent, the northern grasshopper mouse (Onychomys leucogaster). J. Comp. Psychol. *102*, 66.

Heffner, R.S., and Heffner, H.E. (1990). Vestigial hearing in a fossorial mammal, the pocket gopher (Geomys bursarius). Hear. Res. *46*, 239–252.

Heiligenberg, W. (1969). The effect of stimulus chirps on a cricket's chirping (<Emphasis Type="Italic">Acheta domesticus</Emphasis>). Z. Für Vgl. Physiol. *65*, 70–97.

von Helmholtz, H. (1925). Treatise on Physiological Optics (Rochester, NY: The Optical Society of America).

von Holst, E. (1954). Relations between the central Nervous System and the peripheral organs. Br. J. Anim. Behav. *2*, 89–94.

von Holst, E., and Mittelstaedt, H. (1950). Das Reafferenzprinzip (Wedlselwirkungen zwischen Zentrainervensystem und Peripherie) [The Principle of Reafference: Interactions Between the Central Nervous System and the Peripheral Organs]. Naturwissenschaften *37*, 464–476.

Hosoya, T., Baccus, S.A., and Meister, M. (2005). Dynamic predictive coding by the retina. Nature *436*, 71–77.

Huang, C.C. (2013). Convergence of pontine and proprioceptive streams onto multimodal cerebellar granule cells. Elife *2*, e00400.

Ibbotson, M., and Krekelberg, B. (2011). Visual perception and saccadic eye movements. Curr. Opin. Neurobiol. *21*, 553–558.

Ishikawa, T., Shimuta, M., and Häusser, M. (2015). Multimodal sensory integration in single cerebellar granule cells in vivo. Elife *4*, e12916.

Jeannerod, M. (1985). The brain machine: The development of neurophysiological thought (Cambridge, MA: Harvard University Press).

Jörntell, H., and Hansel, C. (2006). Synaptic memories upside down: bidirectional plasticity at cerebellar parallel fiber-Purkinje cell synapses. Neuron *52*, 227–238.

Kalmijn, A.J. (1974). The Detection of Electric Fields from Inanimate and Animate Sources Other Than Electric Organs. In Electroreceptors and Other Specialized Receptors in Lower Vertrebrates, (Springer, Berlin, Heidelberg), pp. 147–200.

Kalmijn, A.J. (1982). Electric and Magnetic Field Detection in Elasmobranch Fishes. Science *218*, 916–918.

Kalmijn, A.J. (1988). Detection of weak electric fields. In Sensory Biology of Aquatic Animals, (Springer), pp. 151–186.

Kanold, P.O., and Young, E.D. (2001). Proprioceptive information from the pinna provides somatosensory input to cat dorsal cochlear nucleus. J Neurosci *21*, 7848–7858.

Kawasaki, M. (2005). Physiology of tuberous electrosensory systems. In Electroreception, (Springer), pp. 154–194.

Keller, C.H. (2004). Electroreception: Strategies for Separation of Signals from Noise. In The Senses of Fish, G. von der Emde, J. Mogdans, and B.G. Kapoor, eds. (Dordrecht: Springer Netherlands), pp. 330–361.

Kennedy, A., Wayne, G., Kaifosh, P., Alviña, K., Abbott, L.F., and Sawtell, N.B. (2014). A temporal basis for predicting the sensory consequences of motor commands in an electric fish. Nat. Neurosci. *17*, 416–422.

Kim, A.J., Fitzgerald, J.K., and Maimon, G. (2015). Cellular evidence for efference copy in Drosophila visuomotor processing. Nat. Neurosci. *18*, 1247–1255.

Kim, A.J., Fenk, L.M., Lyu, C., and Maimon, G. (2017). Quantitative Predictions Orchestrate Visual Signaling in Drosophila. Cell *168*, 280-294.e12.

Kirk, M.D., and Wine, J.J. (1984). Identified interneurons produce both primary afferent depolarization and presynaptic inhibition. Science *225*, 854–856.

Knapen, T., Swisher, J.D., Tong, F., and Cavanagh, P. (2016). Oculomotor Remapping of Visual Information to Foveal Retinotopic Cortex. Front. Syst. Neurosci. *10*.

Koch, C., and Segev, I. (2000). The role of single neurons in information processing. Nat. Neurosci. *3*, 1171.

Koch-Rose, M., Reddy, K., and Chanton, J. (1994). Factors controlling seasonal nutrient profiles in a subtropical peatland of the Florida Everglades. J. Environ. Qual. *23*, 526–533.

Krahe, R., and Gabbiani, F. (2004). Burst firing in sensory systems. Nat. Rev. Neurosci. *5*, 13–23.

Krasne, F.B., and Bryan, J.S. (1973). Habituation: Regulation through Presynaptic Inhibition. Science *182*, 590–592.

Krekelberg, B. (2010). Saccadic suppression. Curr. Biol. *20*, R228–R229.

Krock, R.M., and Moore, T. (2014). The Influence of Gaze Control on Visual Perception: Eye Movements and Visual Stability. Cold Spring Harb. Symp. Quant. Biol. *79*, 123–130.

Lauer, A.M., Slee, S.J., and May, B.J. (2011). Acoustic Basis of Directional Acuity in Laboratory Mice. J. Assoc. Res. Otolaryngol. *12*, 633–645.

Leinweber, M., Ward, D.R., Sobczak, J.M., Attinger, A., and Keller, G.B. (2017). A Sensorimotor Circuit in Mouse Cortex for Visual Flow Predictions. Neuron *95*, 1420-1432.e5.

Li, W.-C., Soffe, S.R., and Roberts, A. (2002). Spinal Inhibitory Neurons that Modulate Cutaneous Sensory Pathways during Locomotion in a Simple Vertebrate. J. Neurosci. *22*, 10924–10934.

Lingenhöhl, K., and Friauf, E. (1994). Giant neurons in the rat reticular formation: a sensorimotor interface in the elementary acoustic startle circuit? J Neurosci *14*, 1176–1194.

Llinas, R.R., Walton, K.D., and Lang, E.J. (2004). Ch. 7: Cerebellum. In The Synaptic Organization of the Brain., G.M. Shepherd, ed. (New York: Oxford University Press), p.

Lorente de Nó, R. (1933). Anatomy of the eighth nerve: III.—General plan of structure of the primary cochlear nuclei. The Laryngoscope *43*, 327–350.

Lorente de Nó, R. (1979). Central representation of the eighth nerve. Ear Dis. Deaf. Dizziness 64–86.

Lundberg, A. (1971). Function of the ventral spinocerebellar tract a new hypothesis. Exp. Brain Res. *12*.

Luo, F., Wang, Q., Farid, N., Liu, X., and Yan, J. (2009). Three-dimensional tonotopic organization of the C57 mouse cochlear nucleus. Hear Res *257*, 75–82.

Ma, W.L., and Brenowitz, S.D. (2012). Single-neuron recordings from unanesthetized mouse dorsal cochlear nucleus. J Neurophysiol *107*, 824–835.

Malmierca, M.S., Merchán, M.A., Henkel, C.K., and Oliver, D.L. (2002). Direct projections from cochlear nuclear complex to auditory thalamus in the rat. J Neurosci *22*, 10891–10897.

Malpeli, J.G., and Schiller, P.H. (1979). A method of reversible inactivation of small regions of brain tissue. J. Neurosci. Methods *1*, 143–151.

Manis, P.B., and Molitor, S.C. (1996). N-methyl-D-aspartate receptors at parallel fiber synapses in the dorsal cochlear nucleus. J. Neurophysiol. *76*, 1639–1656.

Manis, P.B., Spirou, G.A., Wright, D.D., Paydar, S., and Ryugo, D.K. (1994). Physiology and morphology of complex spiking neurons in the guinea pig dorsal cochlear nucleus. J Comp Neurol *348*, 261–276.

Marcoux, C.M., Clarke, S.E., Nesse, W.H., Longtin, A., and Maler, L. (2015). Balanced ionotropic receptor dynamics support signal estimation via voltage-dependent membrane noise. J. Neurophysiol. *115*, 530–545.

Marsat, G., and Maler, L. (2011). Preparing for the unpredictable: adaptive feedback enhances the response to unexpected communication signals. J. Neurophysiol. *107*, 1241–1246.

Martinez, S., Crossley, P.H., Cobos, I., Rubenstein, J.L., and Martin, G.R. (1999). FGF8 induces formation of an ectopic isthmic organizer and isthmocerebellar development via a repressive effect on Otx2 expression. Development *126*, 1189–1200.

Matthews, P.B.C. (1982). Where Does Sherrington's "Muscular Sense" Originate? Muscles, Joints, Corollary Discharges? Annu. Rev. Neurosci. *5*, 189–218.

May, B.J. (2000). Role of the dorsal cochlear nucleus in the sound localization behavior of cats. Hear. Res. *148*, 74–87.

Meek, J., and Grant, K. (1994). The role of motor command feedback in electrosensory processing. Eur. J. Morphol. *32*, 225–234.

Mehaffey, W.H., Fernandez, F.R., Maler, L., and Turner, R.W. (2007). Regulation of burst dynamics improves differential encoding of stimulus frequency by spike train segregation. J. Neurophysiol. *98*, 939–951.

Merzenich, M.M., Kitzes, L., and Aitkin, L. (1973). Anatomical and physiological evidence for auditory specialization in the mountain beaver (aplodontia rufa). Brain Res. *58*, 331–344.

Metzen, M.G., Engelmann, J., Bacelo, J., Grant, K., and Emde, G. von der (2008). Receptive field properties of neurons in the electrosensory lateral line lobe of the weakly electric fish, <Emphasis Type="Italic">Gnathonemus petersii</Emphasis>. J. Comp. Physiol. A *194*, 1063–1075.

Metzner, W., Koch, C., Wessel, R., and Gabbiani, F. (1998). Feature extraction by burst-like spike patterns in multiple sensory maps. J. Neurosci. *18*, 2283–2300.

Miall, R.C., and Wolpert, D.M. (1996). Forward Models for Physiological Motor Control. Neural Netw. *9*, 1265–1279.

Mikami, Y., Yoshida, T., Matsuda, N., and Mishina, M. (2004). Expression of zebrafish glutamate receptor δ2 in neurons with cerebellum-like wiring. Biochem. Biophys. Res. Commun. *322*, 168–176.

Mohr, C., Roberts, P.D., and Bell, C.C. (2003). The mormyromast region of the mormyrid electrosensory lobe. I. Responses to corollary discharge and electrosensory stimuli. J. Neurophysiol. *90*, 1193–1210.

Moller, P., Serrier, J., Belbenoit, P., and Push, S. (1979). Notes on ethology and ecology of the Swashi River mormyrids (Lake Kainji, Nigeria). Behav. Ecol. Sociobiol. *4*, 357–368.

Montgomery, J.C. (1984a). Noise cancellation in the electrosensory system of the thornback ray; common mode rejection of input produced by the animal's own ventilatory movement. J. Comp. Physiol. A *155*, 103–111.

Montgomery, J.C. (1984b). Noise cancellation in the electrosensory system of the thornback ray; common mode rejection of input produced by the animal's own ventilatory movement. J. Comp. Physiol. A Neuroethol. Sens. Neural. Behav. Physiol. *155*, 103–111.

Montgomery, J.C., and Bodznick, D. (1993a). Hindbrain Circuitry Mediating Common Mode Suppression of Ventilatory Reafference in the Electrosensory System of the Little Skate Raja Erinacea. J. Exp. Biol. *183*, 203–216.

Montgomery, J.C., and Bodznick, D. (1993b). Hindbrain circuitry mediating common mode suppression of ventilatory reafference in the electrosensory system of the little skate Raja erinacea. J. Exp. Biol. *183*, 203–216.

Montgomery, J., Coombs, S., Conley, R., and Bodznick, D. (1995). Hindbrain sensory processing in lateral line, electrosensory, and auditory systems: a comparative overview of anatomical and functional similarities. Aud Neurosci *1*, 207–231.

Mugnaini, E., Warr, W.B., and Osen, K.K. (1980). Distribution and light microscopic features of granule cells in the cochlear nuclei of cat, rat, and mouse. J Comp Neurol *191*, 581–606.

Mugnaini, E., Sekerková, G., and Martina, M. (2011). The unipolar brush cell: A remarkable neuron finally receiving deserved attention. Brain Res. Rev. *66*, 220–245.

Müller-Preuss, P., and Ploog, D. (1981). Inhibition of auditory cortical neurons during phonation. Brain Res. *215*, 61–76.

Muniak, M.A. (2013). 3D model of frequency representation in the cochlear nucleus of the CBA/J mouse. J Comp Neurol *521*, 1510–1532.

Murray, R.W. (1960). Electrical Sensitivity of the Ampullæ of Lorenzini. Nature *187*, 957.

Musicant, A.D., Chan, J.C., and Hind, J.E. (1990). Direction-dependent spectral properties of cat external ear: New data and cross-species comparisons. J. Acoust. Soc. Am. *87*, 757–781.

Nakamura, K., and Colby, C.L. (2002). Updating of the visual representation in monkey striate and extrastriate cortex during saccades. Proc. Natl. Acad. Sci. *99*, 4026–4031.

Nelson, S.B. (2004). Hebb and anti-Hebb meet in the brainstem. Nat. Neurosci. *7*, 687.

Nelson, A., Schneider, D.M., Takatoh, J., Sakurai, K., Wang, F., and Mooney, R. (2013). A Circuit for Motor Cortical Modulation of Auditory Cortical Activity. J. Neurosci. *33*, 14342–14353.

Neupane, S., Guitton, D., and Pack, C.C. (2016). Two distinct types of remapping in primate cortical area V4. Nat. Commun. *7*, 10402.

New, J.G., and Bodznick, D. (1990). Medullary electrosensory processing in the little skate. J. Comp. Physiol. A *167*, 295–307.

Nowak, R., and Paradiso, J. (1999). Walker's Mammals of the World. (Baltimore, MD: Johns Hopkins University Press).

Oertel, D., and Young, E.D. (2004). What's a cerebellar circuit doing in the auditory system? Trends Neurosci. *27*, 104–110.

Ohlrogge, M., Doucet, J.R., and Ryugo, D.K. (2001). Projections of the pontine nuclei to the cochlear nucleus in rats. J Comp Neurol *436*, 290–303.

Okedi, J. (1965). The biology and habits of the Mormyrid fishes: Gnathonemus longibarbis, G. victoriae, Marcusenius grahami, M. nigricans, Petrocephalus catostoma. J Appl Ecol *2*, 408–409.

O'Leary, N.A., Wright, M.W., Brister, J.R., Ciufo, S., Haddad, D., McVeigh, R., Rajput, B., Robbertse, B., Smith-White, B., Ako-Adjei, D., et al. (2016). Reference sequence (RefSeq) database at NCBI: current status, taxonomic expansion, and functional annotation. Nucleic Acids Res. *44*, D733–D745.

Oswald, A.-M.M., Chacron, M.J., Doiron, B., Bastian, J., and Maler, L. (2004). Parallel processing of sensory input by bursts and isolated spikes. J. Neurosci. *24*, 4351–4362.

Otazu, G.H., Tai, L.-H., Yang, Y., and Zador, A.M. (2009). Engaging in an auditory task suppresses responses in auditory cortex. Nat. Neurosci. *12*, 646–654.

Peters, R., and Bretschneider, F. (1972). Electric phenomena in the habitat of the catfishIctalurus nebulosus LeS. J. Comp. Physiol. *81*, 345–362.

Petralia, R.S., Wang, Y.-X., Zhao, H.-M., and Wenthold, R.J. (1996). Ionotropic and metabotropic glutamate receptors show unique postsynaptic, presynaptic, and glial localizations in the dorsal cochlear nucleus. J. Comp. Neurol. *372*, 356–383.

Piochon, C., Irinopoulou, T., Brusciano, D., Bailly, Y., Mariani, J., and Levenes, C. (2007). NMDA Receptor Contribution to the Climbing Fiber Response in the Adult Mouse Purkinje Cell. J. Neurosci. *27*, 10797–10809.

Portfors, C.V., and Roberts, P.D. (2007). Temporal and frequency characteristics of cartwheel cells in the dorsal cochlear nucleus of the awake mouse. J Neurophysiol *98*, 744–756.

Post, N., and von der Emde, G. (1999). The "novelty response" in an electric fish: response properties and habituation. Physiol. Behav. *68*, 115–128.

Poulet, J. f. a., and Hedwig, B. (2003). A Corollary Discharge Mechanism Modulates Central Auditory Processing in Singing Crickets. J. Neurophysiol. *89*, 1528–1540.

Poulet, J.F., and Hedwig, B. (2002). A corollary discharge maintains auditory sensitivity during sound production. Nature *418*, 872–876.

Poulet, J.F.A., and Hedwig, B. (2006). The Cellular Basis of a Corollary Discharge. Science *311*, 518–522.

Poulet, J.F.A., and Hedwig, B. (2007). New insights into corollary discharges mediated by identified neural pathways. Trends Neurosci. *30*, 14–21.

Rao, R.P.N., and Ballard, D.H. (1999). Predictive coding in the visual cortex: a functional interpretation of some extra-classical receptive-field effects. Nat. Neurosci. *2*, 79–87.

Reep, R.L., Corwin, J.V., Hashimoto, A., and Watson, R.T. (1987). Efferent Connections of the Rostral Portion of Medial Agranular Cortex in Rats. Brain Res. Bull. *19*, 203–221.

Reiss, L.A.J. (2005). Spectral Edge Sensitivity in Neural Circuits of the Dorsal Cochlear Nucleus. J. Neurosci. *25*, 3680–3691.

Requarth, T., and Sawtell, N.B. (2011). Neural mechanisms for filtering self-generated sensory signals in cerebellum-like circuits. Curr. Opin. Neurobiol. *21*, 602–608.

Requarth, T., and Sawtell, N.B. (2014). Plastic Corollary Discharge Predicts Sensory Consequences of Movements in a Cerebellum-Like Circuit. Neuron *82*, 896–907.

Rhode, W.S. (1999). Vertical cell responses to sound in cat dorsal cochlear nucleus. J Neurophysiol *82*, 1019–1032.

Rice, J.J., May, B.J., Spirou, G.A., and Young, E.D. (1992). Pinna-based spectral cues for sound localization in cat. Hear. Res. *58*, 132–152.

Richmond, B.J., and Wurtz, R.H. (1980). Vision during saccadic eye movements. II. A corollary discharge to monkey superior colliculus. J. Neurophysiol. *43*, 1156–1167.

Roberts, B., and Russell, I. (1972). The activity of lateral-line efferent neurones in stationary and swimming dogfish. J. Exp. Biol. *57*, 435–448.

Roberts, P.D., and Bell, C.C. (2000a). Computational Consequences of Temporally Asymmetric Learning Rules: II. Sensory Image Cancellation. J. Comput. Neurosci. *9*, 67–83.

Roberts, P.D., and Bell, C.C. (2000b). Computational consequences of temporally asymmetric learning rules: II. Sensory image cancellation. J. Comput. Neurosci. *9*, 67–83.

Ross, J., Morrone, M.C., Goldberg, M.E., and Burr, D.C. (2001). Changes in visual perception at the time of saccades. Trends Neurosci. *24*, 113–121.

Rotem, N., Sestieri, E., Cohen, D., Paulin, M., Meiri, H., and Yarom, Y. (2007). The functional architecture of the shark's dorsal-octavolateral nucleus: an in vitro study. J. Exp. Biol. *210*, 2730–2742.

Roy, J.E., and Cullen, K.E. (2001). Selective processing of vestibular reafference during self-generated head motion. J Neurosci *21*, 2131–2142.

Rummell, B.P., Klee, J.L., and Sigurdsson, T. (2016). Attenuation of responses to self-generated sounds in auditory cortical neurons. J Neurosci *36*, 12010–12026.

Sawtell, N.B. (2010). Multimodal integration in granule cells as a basis for associative plasticity and sensory prediction in a cerebellum-like circuit. Neuron *66*, 573–584.

Sawtell, N.B. (2017). Neural Mechanisms for Predicting the Sensory Consequences of Behavior: Insights from Electrosensory Systems. Annu. Rev. Physiol. *79*, 381–399.

Sawtell, N.B., and Bell, C.C. (2013). Cerebellum-Like structures. In Handbook of the Cerebellum and Cerebellar Disorders, (Springer), pp. 1257–1277.

Sawtell, N.B., and Williams, A. (2008). Transformations of Electrosensory Encoding Associated with an Adaptive Filter. J. Neurosci. *28*, 1598–1612.

Sawtell, N.B., Williams, A., and Bell, C.C. (2007). Central Control of Dendritic Spikes Shapes the Responses of Purkinje-Like Cells through Spike Timing-Dependent Synaptic Plasticity. J. Neurosci. *27*, 1552–1565.

Scheich, H., Langner, G., Tidemann, C., Coles, R.B., and Guppy, A. (1986). Electroreception and electrolocation in platypus. Nature *319*, 401.

Schneider, D.M., Nelson, A., and Mooney, R. (2014). A synaptic and circuit basis for corollary discharge in the auditory cortex. Nature *513*, 189–194.

Shadmehr, R., Smith, M.A., and Krakauer, J.W. (2010). Error Correction, Sensory Prediction, and Adaptation in Motor Control. Annu. Rev. Neurosci. *33*, 89–108.

Shannon, C.E. (1948). A Mathematical Theory of Communication. Bell Syst. Tech. J. *27*, 379–423, 623–656.

Shannon, C.E., and Weaver, W. (1949). The Mathmatical Theory of Information (Urbana: University of Illinois Press).

Sherrington, C.G. (1900). The Muscular Sense. In Text-Book of Physiology, E.A. Schäfer, ed. (Edinburgh & London: Young J. Pentland), pp. 1002–1025.

Shore, S.E., and Zhou, J. (2006). Somatosensory influence on the cochlear nucleus and beyond. Hear Res *216–217*, 90–99.

Shore, S.E., Roberts, L.E., and Langguth, B. (2016). Maladaptive plasticity in tinnitus—triggers, mechanisms and treatment. Nat. Rev. Neurol. *12*, 150.

Sillar, K.T., and Roberts, A. (1988). A neuronal mechanism for sensory gating during locomotion in a vertebrate. Nature *331*, 262–265.

Singla, S. (2016). A Cerebellum-like Circuit in the Auditory System Cancels Self-Generated Sounds.

Singla, S., Dempsey, C., Warren, R., Enikolopov, A.G., and Sawtell, N.B. (2017). A cerebellum-like circuit in the auditory system cancels responses to self-generated sounds. Nat. Neurosci. *20*, 943–950.

Sommer, M.A., and Wurtz, R.H. (2002). A Pathway in Primate Brain for Internal Monitoring of Movements. Science *296*, 1480–1482.

Sommer, M.A., and Wurtz, R.H. (2006). Influence of the thalamus on spatial visual processing in frontal cortex. Nature *444*, 374–377.

Sperry, R.W. (1950). Neural basis of the spontaneous optokinetic response produced by visual inversion. J. Comp. Physiol. Psychol. *43*, 482–489.

Sugawara, Y., Grant, K., Han, V., and Bell, C.C. (1999). Physiology of electrosensory lateral line lobe neurons in Gnathonemus petersii. J. Exp. Biol. *202*, 1301–1309.

Sun, L.D., and Goldberg, M.E. (2016). Corollary Discharge and Oculomotor Proprioception: Cortical Mechanisms for Spatially Accurate Vision. Annu. Rev. Vis. Sci. *2*, 61–84.

Sutherland, D.P., Glendenning, K.K., and Masterton, R.B. (1998). Role of acoustic striae in hearing: discrimination of sound-source elevation. Hear Res *120*, 86–108.

Szabo, T. (1965). Sense organs of the lateral line system in some electric fish of the Gymnotidae, Mormyridae and Gymnarchidae. J. Morphol. *117*, 229–249.

Szamier, R.B., and Bennett, M.V.L. (1974). Special cutaneous receptor organs of fish. VII. Ampullary organs of mormyrids. J. Morphol. *143*, 365–383.

Turner, R.W., Lemon, N., Doiron, B., Rashid, A.J., Morales, E., Longtin, A., Maler, L., and Dunn, R.J. (2002). Oscillatory burst discharge generated through conditional backpropagation of dendritic spikes. J. Physiol.-Paris *96*, 517–530.

Tzounopoulos, T., Kim, Y., Oertel, D., and Trussell, L.O. (2004). Cell-specific, spike timing-dependent plasticities in the dorsal cochlear nucleus. Nat Neurosci *7*, 719–725.

Tzounopoulos, T., Rubio, M.E., Keen, J.E., and Trussell, L.O. (2007). Coactivation of pre- and postsynaptic signaling mechanisms determines cell-specific spike-timing-dependent plasticity. Neuron *54*, 291–301.

Umeno, M.M., and Goldberg, M.E. (2001). Spatial Processing in the Monkey Frontal Eye Field. II. Memory Responses. J. Neurophysiol. *86*, 2344–2352.

Walker, M.F., Fitzgibbon, E.J., and Goldberg, M.E. (1995). Neurons in the monkey superior colliculus predict the visual result of impending saccadic eye movements. J. Neurophysiol. *73*, 1988–2003.

Warburton, K. (1990). The use of local landmarks by foraging goldfish. Anim. Behav. *40*, 500–505.

Warren, R., and Sawtell, N.B. (2016). A comparative approach to cerebellar function: insights from electrosensory systems. Curr. Opin. Neurobiol. *41*, 31–37.

Westby, G.M. (1988). The ecology, discharge diversity and predatory behaviour of gymnotiforme electric fish in the coastal streams of French Guiana. Behav. Ecol. Sociobiol. *22*, 341–354.

Wigderson, E., Nelken, I., and Yarom, Y. (2016). Early multisensory integration of self and source motion in the auditory system. Proc. Natl. Acad. Sci. *113*, 8308–8313.

Wilkens, L.A., and Hofmann, M.H. (2005). Behavior of animals with passive, low-frequency electrosensory systems. In Electroreception, (Springer), pp. 229–263.

Wurtz, R.H. (1969). Comparison of effects of eye movements and stimulus movements on striate cortex neurons of the monkey. J. Neurophysiol. *32*, 987–994.

Wurtz, R.H., and Goldberg, M.E. (1972). Activity of superior colliculus in behaving monkey. 3. Cells discharging before eye movements. J. Neurophysiol. *35*, 575–586.

Yawata, S., Tsuchida, H., Kengaku, M., and Hirano, T. (2006). Membrane-proximal region of glutamate receptor δ2 subunit is critical for long-term depression and interaction with protein interacting with C kinase 1 in a cerebellar Purkinje neuron. J. Neurosci. *26*, 3626–3633.

Young, E.D. (1980). Identification of response properties of ascending axons from dorsal cochlear nucleus. Brain Res *200*, 23–37.

Young, E.D., and Brownell, W.E. (1976). Responses to tones and noise of single cells in dorsal cochlear nucleus of unanesthetized cats. J Neurophysiol *39*, 282–300.

Young, E.D., and Davis, K.A. (2002). Circuitry and function of the dorsal cochlear nucleus. In Integrative Functions in the Mammalian Auditory Pathway, (Springer), pp. 160–206.

Young, E.D., Rice, J.J., and Tong, S.C. (1996). Effects of pinna position on head-related transfer functions in the cat. J. Acoust. Soc. Am. *99*, 3064–3076.

Yuzaki, M. (2003). The δ2 glutamate receptor: 10 years later. Neurosci. Res. *46*, 11–22.

Zaretsky, M., and Rowell, C.H.F. (1979). Saccadic suppression by corollary discharge in the locust. Nature *280*, 583–585.

Zhang, S., and Oertel, D. (1993). Cartwheel and superficial stellate cells of the dorsal cochlear nucleus of mice: intracellular recordings in slices. J Neurophysiol *69*, 1384–1397.

Zhao, Y., and Tzounopoulos, T. (2011). Physiological activation of cholinergic inputs controls associative synaptic plasticity via modulation of endocannabinoid signaling. J Neurosci *31*, 3158–3168.

Zhou, J., and Shore, S. (2004). Projections from the trigeminal nuclear complex to the cochlear nuclei: a retrograde and anterograde tracing study in the guinea pig. J Neurosci Res *78*, 901–907.

Zipser, B., and Bennett, M.V. (1976). Interaction of electrosensory and electromotor signals in lateral line lobe of a mormyrid fish. J. Neurophysiol. *39*, 713–721.